Boston University Theses & Dissertations

2022

A biomaterials science and engineering approach to developing SPION-based lipid nanoparticle systems for rare immune cell isolation

BOSTON UNIVERSITY

COLLEGE OF ENGINEERING

Thesis

A BIOMATERIALS SCIENCE AND ENGINEERING APPROACH TO DEVELOPING SPION-BASED LIPID NANOPARTICLE SYSTEMS FOR RARE IMMUNE CELL ISOLATION

by

MARISSA L. McPHILLIPS

S.B., Massachusetts Institute of Technology, 2020

Submitted in partial fulfillment of the

requirements for the degree of

Master of Science

2022

Approved by

First Reader

Joyce Y. Wong, Ph.D.
Professor of Biomedical Engineering
Professor of Materials Science and Engineering

Second Reader

John T. Ngo, Ph.D.
Assistant Professor of Biomedical Engineering

Third Reader

Xuemei Zhong, Ph.D.
Founder & CEO
HOE Holistic Wellness LLC

Fourth Reader

Allison M. Dennis, Ph.D.
Assistant Professor of Biomedical Engineering
Assistant Professor of Materials Science and Engineering

DEDICATION

I would like to dedicate this work to:

My mom, who has been my rock from the very beginning

My dad, who never fails to make me laugh

And my sister, who keeps me grounded, curious, and smiling

ACKNOWLEDGEMENTS

This thesis would not have been possible without the help of so many of my peers, mentors, family members, and friends. To all who provided guidance, support, and advice over the last two years, thank you.

First, I would like to thank and acknowledge my advisors, Drs. Joyce Wong and Xuemei Zhong. I am so grateful to have been mentored by two incredible women and will always value my time working with them. Joyce is an incredible resource, providing technical insight and connecting me with many others in the biomedical and materials science community for support. Her emphasis on collaboration within the field (likely influenced by the culture of our shared alma matter, MIT!) elevated every aspect of my master's experience. Additionally, Joyce always found a way to redirect my thinking to the bigger picture, keeping in mind the motivation and long-term goals of the project when designing new experiments. Her enthusiasm, for anything from scientific progress to new local restaurants, is infectious, and she brings such positive energy to every meeting and interaction. Xuemei has taught me so much about detail-oriented experimental design, effectively communicating my results, and connecting it back to our motivation. She is an amazing communicator, both technically and otherwise, and frequently donated extra time to help me design and execute many cell assays in this work. I cannot thank her enough for her time and patience throughout my time at Boston University.

I also want to thank and acknowledge Dr. Jin Yu, who developed the initial lipid nanoparticle formulation and cell isolation protocols in this thesis. Jin graciously donated so much of her time to guiding me through time-intensive syntheses and characterization protocols while working full time, getting married and moving across the country. I greatly appreciate her time and patience over the last two years, as her insights and experience has been invaluable to this work.

I would like to thank my additional committee members, Chair Dr. John Ngo and Dr. Allison Dennis, for graciously dedicating their time and expertise towards my master's project.

I would like to thank Dr. Jo Ann Buczek-Thomas for her constant unwavering support and honesty throughout my thesis. Any questions I had, I knew could direct to Jo Ann, who provided detailed and clear answers every time. I greatly appreciate her technical expertise and empathy during my time at BU, and I will greatly miss chatting with her in the Wong Lab office.

I would like to thank Dr. Joerg Werner for his incredible technical support, especially regarding synthesis, characterization, and polymer selection for SLNP and SPION formulations. When we hit a major roadblock in the thesis, Joerg was able to identify the cause of the issue and potential solutions. His insights drove later SLNP formulation changes that became instrumental to the outcome of my thesis.

Over the course of my work, I also had tremendous support collecting and analyzing data. I would like to thank Dr. Joel Henderson and Dr. Hui Chen for coordinating and collecting transmission electron microscopy images of all nanoparticle samples. I would like to thank Dr. Jena Goodman for helping collect stimulated emission depletion microscopy images of SLNPs. I would like to thank the O'Shea Lab at Boston University and Eric Dubois for providing access to their fluorescent microscope to image SLNP samples. I would like to thank Dr. Paul Ralifo for teaching me to use nuclear magnetic resonance (NMR), and for his assistance analyzing my oleylamine NMR samples. I would also like to thank Dr. Jon Nagy for his assistance analyzing my oleylamine NMR samples.

I would like to thank Dr. Laura Lewis and Criss Zhang at Northeastern University for their time and assistance in developing an external magnetic setup to maximize cell isolation. Although I was unable to explore their suggestions in my time at BU, I believe their insights will be instrumental in designing a robust and effective future magnetic isolation setup.

I would like to thank all members of the Joyce Wong Lab for their constant support, technical advice, constructive criticism, and humor over the last two years. I am so grateful to have been part of a brilliant and diverse group of scientists and will miss my time with you all. A few lab members have contributed to this thesis work, and so, I would like to acknowledge and thank Belle Ye, Isabella Claure, Dr. Joanna Chiu, Dr. Catherine Gormley, Dr. Gwen Hoffman, Victoria Doheny, Sydney Marchando, and Colleen McCarthy for their assistance.

I would like to acknowledge and thank Dr. Xin Brown, who not only trained me on many characterization techniques outlined in this thesis, but also acted as a mentor and guide while I was a teaching assistant for a sophomore-level introductory wet lab course. I cannot thank her enough for her guidance and the opportunity to work with students, igniting my passion for teaching/mentorship which I hope to do more of in the future.

I would also like to thank Dr. Wenda Gao for helping Xuemei and I conduct several experiments at Antagen Biosciences, Inc.

I would also like to thank my past mentors for providing technical experience, support, and mentorship prior to my studies at BU. Dr. James Moore, Dr. Simon Freeman, Dr. Steven Kennedy, and all MIT Biological Engineering faculty who provided incredible opportunities to learn and connect with the scientific community.

Lastly, I would like to thank my friends and family members who for the last two years have listened (and endured) conversations about SPIONs, lipid nanoparticles, and magnets when they ask about my project. In particular, I would like to thank my roommates Aisha, Elise and Sheridan, whose friendships kept me grounded in the uncertain times of a pandemic and starting graduate school. I would also like to thank my partner, Brian, who has been by my side since we met. Another grounding force, Brian has continued to remind me of what is important and kept me laughing even in the toughest times. I would also like to thank my family for continuing to support me in any way possible — for encouraging me to challenge myself and get back up when I fail. Their unconditional support, encouragement, and humor though a stressful, pandemic-riddled master’s degree helped me push forward. To my loved ones, thank you for being there through it all.

A BIOMATERIALS SCIENCE AND ENGINEERING APPROACH

TO DEVELOPING SPION-BASED LIPID NANOPARTICLE SYSTEMS

FOR RARE IMMUNE CELL ISOLATION

MARISSA L. McPHILLIPS

ABSTRACT

Natural IgM producing phagocytic B cells (NIMPABs) are a rare population of immune cells that can produce antibodies to broadly target and eliminate cancer cells via phosphatidylcholine (PtC)-specific phagocytosis. A novel, dual-labeled lipid-shelled superparamagnetic iron oxide nanoparticle (SPION)-based (SLNP) system was developed to trigger specific phagocytotic behavior in and subsequent enrichment of NIMPABs for a potential immunotherapy. Here we propose the design of an *in vitro* model to assess cell-SLNP interactions with J774A.1 monocyte cell line and the optimization of SLNP formulation. First, we developed and examined the morphology, size, concentration, purification, sterilization, and storage conditions of oleylamine-coated SPIONs and SLNPs using various microscopy methods, spectroscopy, dynamic light scattering, and zeta potential. Our data confirmed SPIONs are magnetic and 7-8 nm in diameter. SLNPs containing SPIONs retained the magnetic property, and are typically measured between 100-120 nm in diameter, and had a positive zeta potential. Fluorescence labeling of the SLNPs did not affect their properties. Second, we examined cytotoxicity and phagocytosis of SLNPs with J774A.1 cells. Our preliminary data showed that significant percentage of phagocytosis can be observed as early as 2 hours. However, longer than 2 hour incubation resulted in significant cytotoxic effects. The source of SLNP cytotoxicity was examined

with transmission electron microscopy and characterization techniques, identifying high un-encapsulated free oleylamine-coated SPION content in SLNP samples contributing to a positive zeta potential for these samples. Simplified SLNPs with oleic acid-coated SPIONs were synthesized and resulting examined particles had a negative zeta potential, reduced free SPION content and improved SPION incorporation into SLNP cores. Based on these findings, SLNP criteria, characterization techniques, and cell assays were revised to establish a rigorous, standardized workflow essential for determining the optimal SLNP formulation. Future work must continue to modify SLNP formulation with information obtained from all characterization techniques and cellular assays outlined in the *in vitro* model. Once optimized, selective SLNP-mediated isolation of NIMPAB cells can be validated *ex vivo* with murine peritoneal cavity washout cells and then human peripheral blood samples.

TABLE OF CONTENTS

LIST OF TABLES

LIST OF FIGURES

LIST OF ILLUSTRATIONS

LIST OF ABBREVIATIONS

AAS……………………………………………………atomic absorption spectroscopy

AF488 ………………………………………………………………...alexa fluor 488

AF594………………………………………………………………alexa fluor 594

C ……………………………………………………………………...…Celsius

CO_2 ………………………………………………………………carbon dioxide

DI ……………………………………………………………………...deionized

DLS ………………………………………………………dynamic light scattering

DMF……………………………………………………………..dimethylformamide

DMSO ……………………………………………………………dimethyl sulfoxide

DPPE………………………………1,2-Dipalmitoyl-sn-glycero-3-phosphoethanolamine

DSPE……………………………...1, 2-Distearoyl-sn-glycero-3-phosphoethanolamine

DSPE-PEG…...1, 2-Distearoyl-sn-glycero-3-phosphoethanolamine-Poly(ethylene glycol)

FITC……………………………………………………fluorescein isothiocyanate

HCl……………………………………………………………hydrochloric acid

MW ……………………………………………………………molecular weight

MWCO …………………………………………………...molecular weight cut off

NHS ………………………………………………………… succinimidyl ester

nIgMs ………………………………………………...natural IgM antibodies

NIMPABs ...……………………………………natural IgM-producing phagocytic B cells

NMR…………………………………………………..nuclear magnetic resonance

NPs…………………………………………………………….. nanoparticles

OAm……………………………………………………………………..… oleylamine

OA ……………………………………………………………………………… oleic acid

PE ……...phosphatidylethanolamine, 1,2-distearyl-sn-glycero-3-phosphoethanolamine-N

PEG………………………………………………………………poly(ethylene glycol)

PES……………………………………………………………………. polyethersulfone

PVDF…………………………………………………………polyvinylidene difluoride

PS ……………………………………………………………………………..polystyrene

PtC…………………………………………………………………phosphatidylcholine

RPMI …………………………………………………....Roswell Park Memorial Institute

SAXS ………………………………………………………small angle X-ray scattering

SLNP ……………………………………………………..SPION-lipid nanoparticles

SPIONs……………………………………… superparamagnetic iron oxide nanoparticles

STED ………………………………………stimulated emission depletion (microscopy)

TEM ……………………………………………... transmission electron microscopy

TGA………………………………………………………thermogravimetric analysis

TLC ……………………………………………………….thin layer chromatography

TRITC…………………………………………………………….tetramethylrhodamine

UV Vis……………………………………………………ultraviolet-visible spectroscopy

ZP ……………………………………………………………………….... zeta potential

CHAPTER ONE: BACKGROUND AND SIGNIFICANCE

1.1 Challenge and Potential Solution

Cancer metastasis is characterized by uncontrolled cell growth, resulting in migration of cancerous cells to healthy tissues (Krøigård et al.). Though many cellular mechanisms exist to detect, eliminate, and prevent the metastasis of cancer, many cancerous cells can evade these checks. Current cancer treatment strategies display limited effectiveness due to the disease's complexity, challenge in targeting tumor sites, and difficulty in preventing recurrence (Arruebo et al., Esfahani et al.).

To overcome these limitations of conventional cancer therapies, nanomedicine-based strategies have been designed to target tumor cells. Nanoparticles (NPs), which possess useful physiochemical properties, can be engineered to interact with cells, molecules, and/or atoms to enhance drug delivery, diagnosis, and imaging. Specific nano-bio interactions like NP half-life, biodistribution, tumor accumulation, tumor microenvironment distribution, and cell internalization can be tailored through NP formulation and synthesis methods (Shi et al.).

Cancer immunotherapy, which harnesses a patient's immune system to treat malignant neoplasms, has recently demonstrated promising results in treating various types of cancer. In particular, the "immunological surveillance system" has gained attention as a potential immunotherapy as it naturally removes cancer cells and other dysfunctional host cells to maintain a healthy environment (X. Zhong). By targeting and enriching the endogenous immune system components that select for and eliminate cancerous cells, a potent therapy could be developed.

Natural IgM-producing B cells (NIMPABS), a subset of B1 B cells discovered by Dr. Xuemei Zhong in her lab at Boston University, produce low affinity, high avidity, polyreactive natural IgM (nIgM) antibodies to clear cancerous and dysfunctional host cells (Zhong et al., Shibad et al.). nIgM antibodies could be studied as a broad-targeting cancer immunotherapy, helping combat cancer cell's evasion mechanisms by binding to a pattern of cancerous surface antigens. A strategy to enrich NIMPABs and mass-produce nIgM antibodies via NIMPAB hybridoma cells or from cloning and translating extracted genetic material is required to study the immunotherapeutic potential of these proteins (Dorai). However, NIMPAB cells are rare and challenging to isolate. NIMPAB cells share cell surface markers with many other immune cell types, making it difficult to use conventional surface marker-dependent isolation mechanisms like flow cytometry (Yu).

Zhong's group discovered that NIMPAB cells exhibit selective macrophage-like phagocytic behavior in the presence of phosphatidylcholine-coated magnetic beads compared to uncoated beads (Vo et al.). Based on these results, Dr. Zhong, Dr. Joyce Wong, and Dr. Jin Yu developed a nanomedicine-based approach for a novel, function-specific cell isolation technique to selectively enrich NIMPAB cells. Magnetic lipid-based nanoparticle systems composed of a superparamagnetic iron oxide nanoparticle (SPION)-containing core and phosphatidylcholine (PtC) shell were engineered to selectively induce phagocytic behavior in NIMPAB cells for future isolation by an external magnetic field. This thesis extends this work and focuses on optimizing the SLNP formulation and characterization methods by using an *in vitro* model to validate cell-SLNP interaction, with the long-term goal of applying the finalized SLNP formulation towards magnetic isolation of NIMPAB cells *ex vivo*.

1.2 Magnetic Properties of Superparamagnetic Iron Oxide Nanoparticle (SPION) Systems

Superparamagnetic iron oxide nanoparticles (SPIONs) exhibit magnetic field alignment when in range of an external magnetic field, or superparamagnetism. Single crystal SPIONs are typically 10-100 nm in diameter to exhibit superparamagnetic behavior and are used for a variety of therapeutic and diagnostic uses (Wahajuddin and Arora, Yu). Superparamagnetic properties were harnessed to create magnetic SPION clusters in SLNP cores to isolate a target cell population with an external magnetic field. Yu calculated the total magnetic moment of each SLNP based on several parameters: SPION saturation of magnetization of 70 emu/g and measured magnetic field strength of the cell isolation setup. The following equations were used to calculate magnetic forces of SLNPs and drag forces of surrounding fluid:

$$F_{magnetic} = \nabla(\vec{m}\vec{B}) = m(LNPs\ per\ cell) \cdot \frac{dB}{dL} \tag{Eq. 1}$$

m = magnetic moment
B = magnetic field
dL = distance between two measurements of magnetic field strength

$$\boldsymbol{F_{drag} = 6\pi\eta R\Delta V} \tag{Eq. 2}$$

η = viscosity
R = particle diameter
ΔV = difference in cell and fluid velocities

Based on Yu's calculations, $F_{magnetic}$ was greater than maximum F_{drag} by one order of magnitude, suggesting SLNPs can isolate target cell populations successfully. Intra-

SLNP SPION content, number of SLNPs phagocytosed per cell, and external magnetic field will dictate the magnetic force exerted by SLNPs on cells. Properties of the surrounding fluid will increase or decrease the drag force needed to overcome to effectively attract and separate cells. Ultimately, maximizing SPION content in the SLNP core would contribute towards maximizing the magnetic strength for SLNP-mediated cell isolation.

1.3 Colloidal Stability of Superparamagnetic Iron Oxide Nanoparticle (SPION) Systems

The colloidal stability of both SPION and SPION-based lipid nanoparticle systems (SLNPs) are addressed in this thesis. Collision frequency (due to Brownian motion, hydrodynamic flow, and concentration) and external forces NPs experience (van der Waals forces, electrostatic forces, steric forces) contribute to colloidal stability. Tailoring colloidal stability can help prevent unwanted aggregation of NPs, which can affect SPION encapsulation and phagocytosis of SLNPs. Yu's work focused on tuning SPION concentration, steric repulsion, electrostatic forces and van der Waals attraction forces to establish SPION synthesis protocols primarily for NMR/MRI contrast agents and SLNPs to isolate NIMPAB cells (Yu).

In this thesis, we utilized Yu's methods to synthesize both oleylamine and oleic acid coated SPIONs for the magnetic core of SLNPs. Oleylamine (OAm), a fatty amine group often used as a SPION coating and stabilizer, is composed of a long hydrocarbon chain capped by a methyl and amine group (Gaspar et al.). Oleic acid, an omega-3 fatty acid also used as a SPION coating and stabilizer, shares the same hydrocarbon structure as oleylamine but is capped with a carboxyl group instead of an amine group (Lai et al., Ill.

1). Though these coatings both promote SPION colloidal stability, they possess different pKa values (OAm ~ 10.7, OA ~ 9.85) which can affect the zeta potential of coated SPIONs and subsequent synthesis of SLNPs.

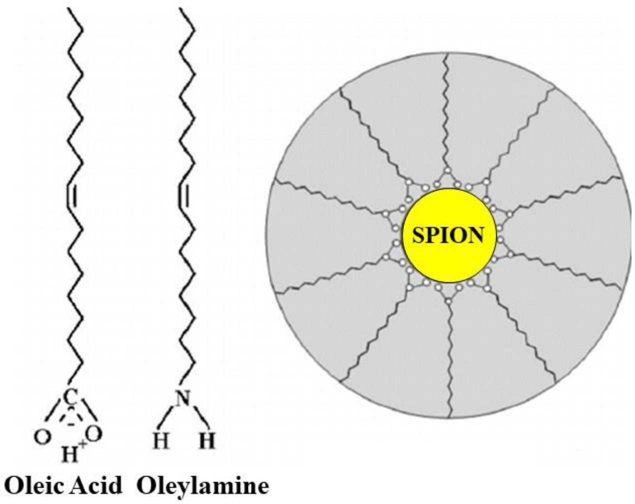

Illustration 1: Oleic acid (OA) and oleylamine (OAm) structure. Schematic of SPION capped with either OA or OAm.

SLNPs, synthesized by the nanoemulsion of hydrophobic and hydrophilic layers and subsequent self-assembly of micelles, were also tuned for colloidal stability in Yu's work (Yu). Micelle energy is proportional to the parameter (α) described by Eq. 3 while concentration of lipid monomer for formation of micelles (critical micelle concentration) is exponentially proportional to α.

$$\alpha \approx \frac{4\pi R^2 \gamma}{kT} \qquad \text{(Eq. 3)}$$

R = diameter of micelle
γ = interfacial free energy/unit area
k = Boltzmann constant
T = temperature

SLNP synthesis and resulting SLNP stability depends on the surface energies for the hydrophobic and hydrophilic layers, initial lipid concentration, and resulting concentration emulsion energy, which can impact intra-particle structure detailed in Sheth et al. (Yu, Sheth et al.). These relationships informed the formulation and synthesis of SLNPs in Yu's studies (Chiu, Yu).

1.4 Design of SPION-Lipid Nanoparticle (SLNP)

A SPION-based lipid nanoparticle (SLNP) system was designed to selectively target and magnetically isolate NIMPABs without the need of surface cell markers, using (1) PtC-specific phagocytic behavior of NIMPAB cells and (2) SPIONs' ability to align with an external magnetic field to inform the final design (Vo et al., Yu).

SLNPs were composed of a hydrophobic layer with SPIONs and hydrophilic lipid layer that were emulsified to induce lipid micelle formation (Yu, Chiu). The hydrophobic layer, which provides magnetic properties via SPIONs-OAm, was modified with polystyrene for structural stability and to ensure SPIONs are incorporated into the SLNP core. The hydrophilic shell was composed primarily of lipids selected to induce NIMPAB-specific phagocytic behavior and reduce colloidal instability. Previous studies have demonstrated that in addition to "professional" phagocytes, B1 B lymphocytes (including NIMPABs) specifically phagocytose phosphatidylcholine (PtC)-coated particles and beads (Zhong et al.; X. Zhong; Yu; Vo et al.). Therefore, PtC was the primary lipid used to form the hydrophilic shell of SLNP. Previous work has demonstrated distearyl phosphatidylethanolamine polyethylene glycol (DSPE-PEG)-coated lipid micelles can be designed to target specific cell types and encapsulate a variety of drugs to suit each application (Gill et al.). PEG also prevents protein corona formation, which can destabilize SLNPs, induce agglomeration and limit the efficacy of the SLNP targeting strategy, and was added to the SLNP hydrophilic shell composition (Chinen et al.). Intracellular localization of SLNPs can be tracked by labeling particles with pH-dependent fluorophores, which fluoresce only in an acidic environment as pH drops below 7.0 like in the cytosol and lysozyme (Lee et al.). SLNP diameter was limited to 200-600nm to avoid non-specific endocytosis or potential cytotoxic effects (Vo et al., Yameen et al.). In addition, B1 B cells are smaller in size compared to professional phagocytes, like macrophages. Based on these prior findings, SLNP design criteria and solutions were summarized in the table below, establishing a standard set of requirements for Yu's SLNP formulation (Tbl. 1).

	Design Criteria	Design Solution
SLNP core	Highly magnetically responsive compared to existing magnetic beads	Clustered SPIONs
SLNP coating	Prevent aggregation and protein binding	PEG lipid
	Efficiently target NIMPAB cells in < 6 hours	PtC-lipid coating
SLNP stability	Stable for 3 days during cell experiments	Polymer in core to provide structural integrity
SLNP size	Does not trigger non-specific endocytosis	Size should be ≤ 500nm
Verify targeting abilities	Track location of SLNPs	pHrodo-red-fluorescence marker

Table 1: Design criteria and proposed solutions for SLNP formulation to target and magnetically isolate NIMPAB cells. Modified from Yu, Table 18.

1.5 Project Aims

Zhong et al. demonstrated PtC-coated magnetic beads were selectively phagocytosed by B1 B cells over uncoated magnetic beads, inspiring current SLNP designs (Vo et al.). The initial SLNP formulation designed by Dr. Joyce Wong, Zhong, and Yu was able to increase B1 B cell purity by 25% after magnetic isolation from mouse peritoneal cavity washouts *ex vivo* (Yu). Optimizing the SLNP formulation is essential for increasing the efficiency of SLNP-mediated phagocytic and magnetic isolation of the target cell type. However, since NIMPAB cells are rare, obtaining a large quantity for cell-SLNP studies and optimization is challenging and difficult. An i*n vitro* platform using a phagocytosing cell line would be a more accessible alternative.

The **overall objective** of this thesis was to establish an *in vitro* experimental workflow to test, optimize, and standardize a magnetic lipid nanoparticle (SLNP) formulation to enrich the target cell type. The **central hypothesis** of this work is that a standardized SLNP formulation can be used to efficaciously and reproducibly isolate phagocytosing cells *in vitro*. The **rationale** behind this hypothesis is that previous work established magnetic isolation of target cell types could be executed using magnetic beads. Additionally, previous magnetic SLNP formulations developed by Yu demonstrated success in isolating B1 B cells in mouse peritoneal washout cells. The **long-term goal** of the project is to use magnetic SLNPs designed to selectively induce NIMPAB-specific phagocytosis to isolate and amplify target cells for future immune-oncology studies. The central hypothesis was tested with the following specific aims:

Specific Aim 1: Design, synthesize, characterize, and optimize SPION-based lipid nanoparticles (SLNP) to determine consistency and reproducibility of formulations. SLNPs were synthesized by a nano emulsion of magnetic SPION-containing layers with lipid shell. Key SLNP parameters (prior to this thesis work) include nanoparticle size, aggregation, morphology, and (pH-dependent) fluorescence. These properties can be optimized by tailoring various reagents prior to emulsion, with the goal of fulfilling design requirements detailed in Tbl. 1. Updating the formulation and desired parameters can improve the stability, consistency, and eventually scalability of SLNPs.

Specific Aim 2: Design an experimental *in vitro* model to study the effects of SLNPs on natively phagocytosing cells. SLNP design can be more easily assessed in an *in vitro* model than using rare and challenging-to-access NIMPAB cells. SLNP formulations can then be optimized to maximize future magnetic isolation and be retested in the *in vitro* model. Cell-SLNP interactions can be determined and used to influence the next SLNP iteration to fulfill the following sub-aims:

Sub-aim 1: Determine and minimize cytotoxicity of SLNPs in vitro. SLNP cytotoxic effects should be negligible over the course of 24 hours, as cells must stay intact to phagocytose SLNPs and be magnetically isolated for future studies. *Sub-aim 2: Determine and maximize phagocytosis of SLNPs in vitro*. SLNPs should be maximally phagocytosed to increase the magnetic strength of each cell and likelihood of successful isolation when in the presence of an external magnetic field.

CHAPTER 2:

MATERIALS AND METHODS

2.1 NANOPARTICLE SYNTHESIS

2.1.1 Synthesis of Oleylamine-Coated SPIONs (SPIONs-OAm)

Oleylamine-coated SPIONs (SPIONs-OAm) were synthesized using a thermal decomposition synthesis method established in Xu et al., Sun et al., Pan et al., and modified by Yu (Xu et al., Sun et al., Park et al., Yu). In short, iron oxide nanoparticles were synthesized by mixing tris(acetylacetonato)iron(III) ($Fe(acac)_3$) (Sigma Aldrich, CAS 14024-18-1, Lot# MKCK7101, St. Louis, MO), oleylamine (OAm) (Sigma Aldrich, CAS 112-90-3, St. Louis, MO), and benzyl ether (Acros Organics, CAS 103-50-4, Lot# A0408202, Geel, Belgium) at a high temperature.

Material	**Mass or Volume**	**Moles (mmol)**
$Fe(acac)_3$ (≥97%)	1059.51 mg	3
Oleylamine (≥98%)	15 mL	0.0456
Benzyl Ether (≥99%)	15 mL	-
Hexane	40 mL	-
200 pf Ethanol	≥ 100 mL	excess

Table 2: Mass or volume and moles of reagents required for thermal decomposition reaction to make monodisperse SPIONs-OAm from Yu's Table 3 (Yu). Benzyl ether and ethanol were chosen as solvents to dissolve materials for the desired reaction rate and wash the resulting product, respectively.

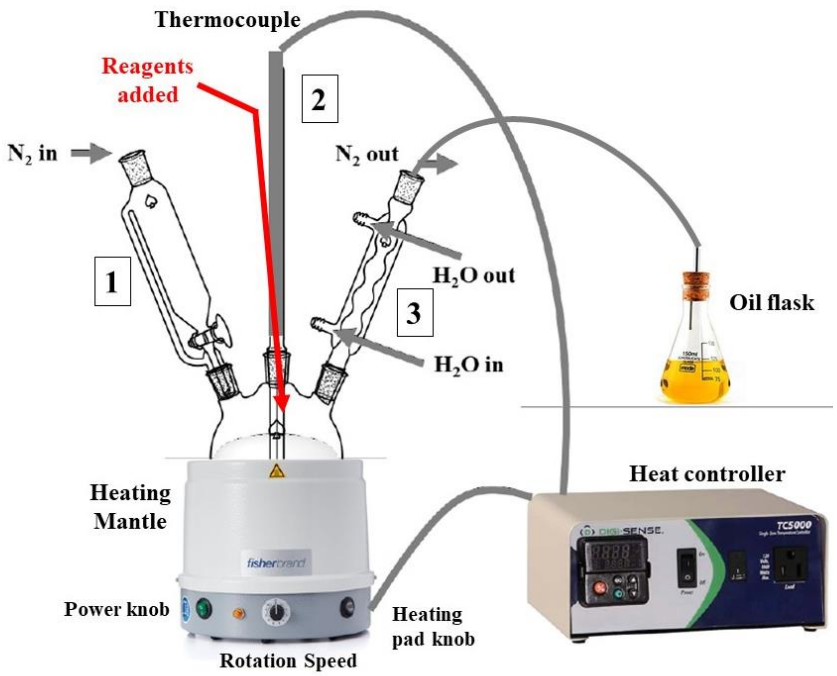

Figure 1: Thermal decomposition synthesis reaction setup in Fisherbrand™ Metal-Housed Magnetic Stirring Heating Mantle (Fisher Scientific, Waltham, MA) consisted of a 300 mL three-neck round bottom flask (24/40): 1) the left neck was connected to a pressure equalizing cylindrical funnel to allow nitrogen gas to flow; 2) the middle neck was connected to a thermocouple to measure the temperature of the reaction; 3) the right neck was connected to an Allihn condenser to control the temperature of the reaction with cold water flow. The reaction was kept under a nitrogen environment, which is monitored via oil bubbling in a flask connected to the Allihn condenser. A heat controller (Oakton Temp 9500 Advanced Multiparameter Controller, Oakton Instruments, Vernon Hills, IL) is connected to the heating mantle and the thermocouple, which senses and controls the temperature of the reaction. Modified from Fig. 2 in Yu (Yu).

Nitrogen gas was flowed through the reaction setup for at least 15 minutes prior to adding reagents and a magnetic stir bar to the round bottom flask. After clearing gas from the setup with nitrogen flow, 1059.51 mg of tris(acetylacetonato)iron(III), 15 mL of oleylamine (OAm), and 15 mL of benzyl ether were transferred to the round bottom flask via a funnel in the middle neck and mixed thoroughly for 10-15 minutes using a magnetic stir bar (moderate rpm) at room temperature (Tbl 2, Fig. 1). Once the materials were thoroughly mixed, the thermocouple was placed in the middle neck and adjusted so that it was submerged in the solution but did not disrupt the magnetic stir bar. The heating controller was turned on, set to the following profile, and allowed to run:

1. Increase temperature at 2°C per minute to 110°C.
2. Dehydrate reaction materials for 1 hour at 110°C.
3. Increase temperature at 20°C per minute to final temperature at 300°C for 10 minutes.
4. Hold 300°C isotherm for 1 hour.
5. Cool to 40°C (or less).

The heating mantle control knobs (heating pad and heating power) were adjusted depending on the goal temperature. Insulating electric heat tape was used during the heating steps to help control the temperature of the reaction.

Once the reaction had cooled, the magnetic stir bar was removed and at least 50 mL of 200 proof ethanol was added to the reaction materials. The resulting solution was transferred to a Griffin beaker and allowed to precipitate overnight on a magnet in the fume hood. The following day, excess ethanol was removed by vacuum aspiration, 30-50 mL of 200 proof ethanol was added to the beaker, gently mixed, allowed to precipitate on the magnet for a few minutes, and removed by aspiration again. These steps were repeated three times to wash the iron oxide NPs. The washed iron oxide NP precipitate was dissolved in 40 mL of hexane (Fisher Chemical, H292-4, Lot#211840, Waltham, MA), transferred to a 50 mL centrifuge tube, and centrifuged at 2880 g for 10 minutes to separate particles ≤ 10 nm from larger particles (AccuSpin 400 Benchtop Centrifuge, Fisher Scientific, Waltham, MA). The supernatant was transferred to another Griffin beaker via a Pasteur pipette. Ethanol was added in excess once more and the solution was allowed to precipitate on a magnet for 10-15 minutes. Excess ethanol and hexane were aspirated, and remaining particles were placed in a vacuum oven (no heat, pressure ~ 15-25 Hg vac) overnight to evaporate remaining solvents (VWR SHEL-LAB, Sheldon Manufacturing, Model 1410, Cornelius, OR).

Dried, powdery particles were removed from the Griffin beaker using a static gun and scraper and transferred to a pre-weighed 20 mL scintillation vial for bench storage. Yield was determined by measuring the scintillation vial with SPIONs-OAm and subtracting the mass of the empty scintillation vial.

2.1.2 Synthesis of Oleic Acid-Coated SPIONs (SPIONs-OA)

Oleic acid coated SPIONs (SPIONs-OA) were synthesized using a similar thermal decomposition method outlined in section 2.1.1 with slightly different reagents and heating profile (Yu). In this protocol, 2.826 g of tris(acetylacetonato)iron(III), 9.216 g of 1,2 tetradecanediol (Sigma Aldrich, 260290, Lot# STBH8150, St. Louis, MO), 7.60 mL of oleic acid (Sigma Aldrich, CAS 112-80-1, Lot# MKCM4892, St. Louis, MO) , 7.90 mL of oleylamine, and 80 mL of benzyl ether were mixed using the reaction setup and protocol detailed in section 2.1.1 (Tbl 3).

Material	**Mass or Volume**	**Moles (mmol)**
$Fe(acac)_3$	2.826 g	8
1,2 tetradecanediol (≥90%)	9.216 g	40
Oleic Acid (≥90%)	7.60 mL	24
Oleylamine (≥98%)	7.90 mL	24
Benzyl Ether (≥99%)	80 mL	-
Hexane	40 mL	-
Ethanol	≥ 160 mL	excess

Table 3: Mass/volume and moles of reagents required for thermal decomposition reaction to make monodisperse OA-coated SPIONs from Table 1 in Yu (Yu). Like section 2.1.1,

benzyl ether and ethanol were chosen as solvents to dissolve materials for the desired reaction rate and wash the resulting product, respectively.

The following heating profile was implemented:

1. Increase temperature at 2°C per minute to 100°C.
2. Hold 100°C isotherm for 45 minutes.
3. Increase temperature at 2°C per minute to 180°C.
4. Hold 180°C isotherm for 2 hours.
5. Increase temperature at 10°C per minute to 280°C.
6. Hold 280°C isotherm for 1 hour.
7. Cool to 40°C (or less).

The same precipitation, washing, and drying steps for synthesis of SPIONs-OAm in section 2.1.1 were conducted for synthesis of SPIONs-OA.

2.1.3 Synthesis of Lipid Nanoparticles (SLNPs)

SPION-lipid nanoparticles (SLNPs) were synthesized using an emulsion method inspired by Dr. Joanna Chiu and modified by Yu (Chiu, Yu). The hydrophobic core was composed of 18 mg of SPIONs-OAm synthesized via thermal decomposition outlined in section 2.1.1, 21 mg of polystyrene (Sigma Aldrich, M_w = 280K, CAS 9003-53-6, batch#15702JB, St. Louis, MO), 3 mL of toluene (Fisher Chemical, T324-1, CAS 108-88-3, Waltham, MA), and 0.5 mL of chloroform (Fisher Chemical, C298-4, CAS 67-66-3, Waltham, MA), which were transferred to a 20 mL scintillation vial and sonicated for 5 minutes in a bath sonicator (1510 Branson Ultrasonic Cleaner, Brookfield, CT). The hydrophilic shell was composed of 0.34 mg DPSE-PEG(2K) (Nancocs, PG1-DS-2K, Lot#18060H, Boston, MA) and 0.74 mg 95% lecithin (soy) (Avanti Polar Lipids, CAS97281-47-5, Alabaster, AL), which were measured in a scintillation vial and dissolved in 3 mL of 4% ethanol in deionized (DI) water (pH 7.5-8.0) using a magnetic stir bar and hot plate (<80°C). In a separate scintillation vial with 9 mL of DI water (pH 7.5-8.0), 3 mL of the hydrophilic layer was added dropwise, mixed by pipetting up and down, quickly followed by the addition of 1 mL of the hydrophobic layer. The resulting solution was first mixed by shaking the vial, then by a tip sonicator (Branson 450 Digital Sonifier, Brookfield, CT or Sonics VibraCell VCX 750, Newtown, CT with 1/8” tip) set to 30% amplitude for 1 minute. The sonicated solution was placed in a vacuum oven overnight to eliminate any organic solvents remaining.

Following overnight evaporation, the SLNP solution was transferred to the top compartment of a 100K MWCO or 10K MWCO ultracentrifugation tube (MilliporeSigma™ Amicon™ Ultra Centrifugal Filter Units, Fisher Scientific, Cat# UFC910024 or UFC901024, Waltham, MA) and centrifuged at 2880 g for 10 minutes. The solution collected in the bottom compartment of the centrifuge tube was discarded. Then 6 mL of DI water (pH 7.5-8.0) was added to the top compartment, mixed by pipetting up and down, and centrifuged at 2880 g for 3 minutes. The solution collected in the bottom compartment of the centrifuge tube was discarded, and 5 mL of DI water (pH 7.5-8.0) was added to the top compartment, mixed by trituration, and centrifuged at 2880 g for 3 minutes. This last step was repeated once more. The solution retained in the top compartment of the centrifuge was emptied into a new 20 mL scintillation vial, rinsed with 2 mL of DI water (pH 7.5-8.0), and the final solution was diluted with another 5 mL of DI water (pH 7.5-8.0) before storage at 4°C. If SNLPs are fluorescent, the scintillation vial should be covered with tinfoil before storing at 4°C.

2.1.3.i Addition of Fluorophores to SLNPs

pHrodo-red-1,2-Dipalmitoyl-sn-glycero-3-phosphoethanolamine (pHrodo-red-DPPE):

To validate phagocytosis, intracellular and extracellular SLNPs can be distinguished by using a pH-sensitive probe like pHrodo-red, which only fluoresces when pH of the surrounding solution is less than 7.0 (as in the acidic environment of endosome and lysosome) (Lee et al.). pHrodo-red-DPPE was synthesized according to the protocol detailed in section 2.1.3.iii Lyophilized pHrodo-red-DPPE was dissolved in chloroform at a concentration of 1.9 mg/mL. While synthesizing the hydrophobic layer of SLNPs (section 2.3), 100 uL of pHrodo-red-DPPE dissolved in chloroform was added in place of 100 uL of the total volume of chloroform. The concentration of pHrodo-red-DPPE in chloroform can vary if needed, but 0.19 mg of pHrodo-red-DPPE must be added in accordance with the 90:10 molar ratio of pHrodo-red-DPPE with the hydrophilic layer established in Yu's protocol (Yu).

1,2-dioleoyl-sn-glycero-3-phosphoethanolamine-N-Alexa Fluor 488 (AF488-PE):

A pH-insensitive fluorophore was added as a positive control to show both intracellular and extracellular NPs. AF488-PE in chloroform was purchased from Avanti Polar Lipids (18:0 PE-TopFluor® AF488, 810386C-250 ug, CAS2410280-01-0, Alabaster, AL). While synthesizing the hydrophobic layer of lipid nanoparticles (according to section 2.1.3), 397.7 uL (or 99.42 ug) of AF488 in chloroform was added in place of 397.7 uL of the total volume of chloroform (1:6 ratio with hydrophilic layer).

<u>1,2-dioleoyl-sn-glycero-3-phosphoethanolamine-N-Alexa Fluor 594 (AF594-PE):</u>

With guidance from Dr. Jena Goodman at Boston University, AF594-PE was used to label SLNPs for STED microscopy due to the microscope's current laser setup. AF594-PE in chloroform was purchased from Avanti Polar Lipids (18:1 PE-TopFluor® AF594, 810387C-250 ug, CAS 2315262-12-3, Alabaster, AL). While synthesizing the hydrophobic layer of lipid nanoparticles (according to section 2.1.3), 151.1 uL (37.78 ug) of AF594 in chloroform was added in place of 151.1 uL of the total volume of chloroform (2:90 ratio with hydrophilic layer).

<u>1, 2-Distearoyl-sn-glycero-3-phosphoethanolamine-Poly(ethylene glycol)-fluorescein isothiocynate (FITC-DPSE-PEG)</u>:

FITC-DPSE-PEG was utilized as an alternative pH insensitive probe and was purchased from Creative PEGWorks™ (DSPE-PEG-FITC, M_W 3.4k, PLS-9928-50 mg, Durham, NC). While synthesizing the hydrophilic layer of lipid nanoparticles (according to section 2.1.3), 0.34 mg of FITC-DPSE-PEG (3.4k) replaced 0.34 mg of unlabeled DPSE-PEG (2k) to be dissolved in 3 mL of 4% ethanol in DI water (pH 7.5-8.0) with 0.74 mg lecithin.

2.1.3.ii Dialysis of SLNPs

Dialysis was used as a gentler alternative to wash, purify and retain a higher yield of SLNP samples compared to centrifugation. To prepare for dialysis, a 2 L Griffin beaker was filled with pH-balanced DI water of pH 7.5-8.0 and placed on a magnetic stir plate. A 5–6-inch length of 10K MWCO SnakeSkin Dialysis Tubing (Thermofisher Scientific, Lot#W6319708, Waltham, MA) was "pre-wet" in pH-balanced DI water and clamped on one end with a polypropylene dialysis tubing clamp (Spectrum Medical Industries, Cat#08-700-241, Chester, PA). After overnight evaporation in a vacuum oven (~15-25 Hg vac), SLNP samples were transferred to the clamped dialysis tubing through the open end via pipetting. Once all the SLNP sample was fully transferred, the open end of the dialysis tubing was clamped with another dialysis clamp and a float buoy (Slide-A-Lyzer™ Cassette Float Buoys, ThermoFisher Scientific, Cat#66430, Waltham, MA). A magnetic stir bar, which was spun at a moderate rpm, and SLNP-containing dialysis tubing were placed in the 2 L Griffin beaker of DI water, which was covered in tin foil to prevent photo-bleaching of the fluorophores. SLNPs were spun for 1 hour, then DI water was replaced with fresh DI water (pH > 7.0). SLNPs were spun for another 1-2 hours, and DI water was replaced again before spinning overnight. After an overnight dialysis, SLNPs were removed from the dialysis tubing via pipette and transferred to a 20 mL scintillation vial.

2.1.3.iii pHrodo-red-DPPE-Preparation

pHrodo-red-succinimidyl ester (Invitrogen™, pHrodo™ Red, SE P36600, Waltham, MA) was purchased and used to synthesize pHrodo-red-DPPE using a column chromatography method outlined in Kemmer et al. and modified by Yu. In an aluminum-covered brown vial, 2.2 mg 1,2-Dipalmitoyl-sn-glycero-3-phosphoethanolamine (97% DPPE P1348, Sigma Aldrich, CAS 923-61-5, Lot#BCBW6848, Waltham, MA), 1 mg pHrodo-red-succinimidyl ester, 60 uL trimethylamine (T2268, TCI America, CAS 75-50-3, Lot#CN48E-D8, Toyko, Japan), 300 uL dimethyl sulfoxide (DMSO) (D128-500, Fisher Chemical, Lot#163913, Waltham, MA), 400 uL N,N dimethylformamide (DMF) (D119-1, Fisher Chemical, CAS 68-12-2, Lot#128010, Waltham, MA), and 140 uL chloroform were vortexed for 1 hour (Fisher Scientific Pulsing Vortex Mixer, Fisher Scientific, Waltham, MA). Silica gel was created by mixing silica beads with thin layer chromatography (TLC) solvent of 90:50:7 chloroform: methanol: ammonium hydroxide) and was used to create a gel chromatography column for pHrodo-red-DPPE separation detailed in Fig. 2.

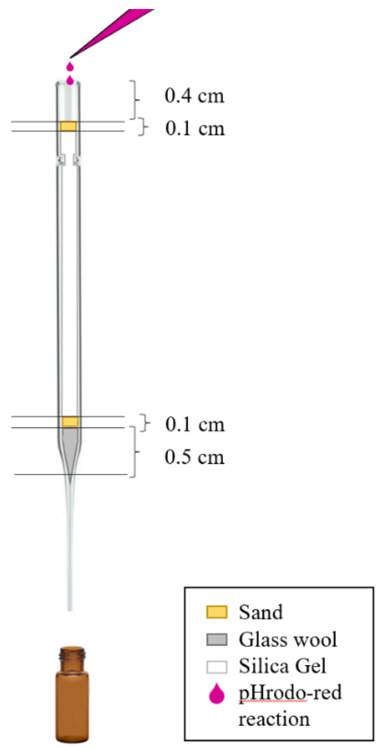

Figure 2: pHrodo-red-DPPE reaction setup. A gel chromatography column was prepared using a 5.75" Pasteur pipette suspended using a ring stand and clamp above an empty brown vial of known mass. The column was constructed with the following layers of vertical heights above the base of the pipette: 1) 0.5 cm of glass wool (Sigma Aldrich, CAS 65997-17-3, Waltham, MA); 2) 0.1 cm quartz silicon dioxide (sand) (Sigma Aldrich, CAS 14808-60-7, Waltham, MA); 3) silica gel up to 0.5 cm from the top of the Pasteur pipette; and 4) 0.1 cm sand. pHrodo-red reaction solution was loaded at the top of the chromatography column

Once vortexed, the pHrodo-red reaction solution was dissolved in a small amount of TLC solvent via pipetting up and down and loaded in the top of the gel chromatography column in small volumes (Fig. 2). The final product of the reaction, pHrodo-red-DPPE, traveled down the column as the first layer and was collected in the brown vial below the column. TLC solvent was added periodically to prevent the silica gel from drying and cracking.

Once all the pHrodo-red reaction solution passed through the column, the first layer collected in the brown vial was prepared for lyophilization. The brown vial was capped with a Kim wipe secured by an elastic band, submerged in liquid nitrogen, and lyophilized overnight (SP Scientific Benchtop Pro Lyophilizer, Warminster, PA). Mass of lyophilized pHrodo-red-DPPE was measured and suspended in the appropriate volume of chloroform for a concentration of 1.9 mg/mL in preparation for protocols detailed in section 2.1.3.i.

2.1.4 Synthesis of Polystyrene-Based Nanoparticles (PS-NPs)

2.1.4.i Polystyrene Nanoparticles

Polystyrene nanoparticles were synthesized using an emulsion method inspired by lipid nanoparticle synthesis methods by Chiu and Yu (Chiu, Yu). The hydrophobic layer consisted of 21 mg PS in 3 mL of toluene and 0.5 mL chloroform and was sonicated for 5 minutes with a bath sonicator. The hydrophilic layer consisted of 0.74 mg lecithin dissolved in 3 mL of 4% ethanol in DI water (pH 7.5-8.0) via magnetic stir bar and hot plate. In a separate scintillation vial with 9 mL of DI water (pH 7.5-8.0), 3 mL of the hydrophilic layer was added dropwise and mixed by pipetting up and down. Quickly, 1 mL of the hydrophobic layer was added. The resulting solution was first mixed by shaking the vial, then by a tip sonicator (1/8” tip) set to 30% amplitude for 1 minute. The sonicated solution was placed in a vacuum oven overnight to eliminate any organic solvents remaining. Following overnight evaporation, the SLNP solution was transferred to the top compartment of a 100K MWCO ultracentrifugation centrifuge tube and centrifuged at 2880 g for 10 minutes. The remaining solution was transferred to another 20 mL scintillation vial for storage at 4°C.

2.1.4.ii Polystyrene Nanoparticles with OAm

Another batch of PS-NPs was synthesized using the same protocol detailed in section 2.1.4.i with an addition of 0.1 mL OAm in the hydrophobic phase. In addition to the 10-minute centrifugation step in section 2.1.4.i, an additional 3-minute centrifugation at 2880 g was conducted after emptying the bottom compartment of the ultracentrifugation tube and adding 5 mL of DI water (pH 7.5-8.0) to the top compartment. The remaining solution was transferred to another 20 mL scintillation vial for storage at 4°C.

2.1.4.iii SPION-OA Encapsulating Polystyrene Nanoparticles

SPION-OA encapsulating PS-NPs were synthesized using the same protocol detailed in section 2.1.4.i with a modified hydrophobic layer: 18 mg PS and 9 mg of SPIONs-OA (synthesized by methods described in section 2.1.2) were sonicated in 3 mL chloroform in a bath sonicator for 5 minutes. Either 0.1 mL OAm or 0.1 mL OA was added to the hydrophobic layer to produce PS/SPIONs-OA/OAm and PS/SPIONs-OA/OA respectively. The remaining solution was transferred to another 20 mL scintillation vial for storage at 4°C.

2.2 CHARACTERIZATION OF NANOPARTICLES

2.2.1 Dynamic Light Scattering (DLS)

Dynamic Light Scattering (DLS), or photo correlation spectroscopy, is used to study the diffusion behavior of macromolecules and colloids based on their size and shape.

DLS uses a monochromatic laser beam source as the incident light with wavelength, λ, and wave function described by Eqs. 4 and 5.

$$\boldsymbol{E_i}(\boldsymbol{r},t) = \boldsymbol{n_i} E_0 e^{-i[\boldsymbol{k_i}\cdot\boldsymbol{r} - \varpi_i t]} \qquad \text{(Eq. 4)}$$

i = incident light	ω_i = frequency
r = direction	$\mathbf{n_i}$ = polarization vector
t = time	E_0 = amplitude
	k_i = wave vector

$$\boldsymbol{k_i} = \frac{\omega_i}{c}\widehat{\boldsymbol{k_\iota}} \qquad \text{(Eq. 5)}$$

$\hat{\boldsymbol{k}}_{\boldsymbol{t}}$ = unit wave vector

DLS analyzes both the incident wave function from a monochromatic laser beam source and the wave function after it has passed through the sample. The incident light wave is scattered by the medium with colloidal dispersion, which has a dielectric function of **ε**(r,t). The scattered wave function is described by Eq. 6 and collected by the appropriate detector at distance R from scattering volume *V*:

$$E_f(\boldsymbol{R},t) = \frac{E_0}{4\pi R\varepsilon_0} \exp ikR \int_V d^3r \; exp\; i(\boldsymbol{q}\cdot\boldsymbol{r} - \omega_i t)[\boldsymbol{n_f}\cdot[\boldsymbol{k_f}\times\big(\boldsymbol{k_f}\times(\delta\boldsymbol{\varepsilon}(\boldsymbol{r},t)\cdot\boldsymbol{n_i})\big]] \qquad \text{(Eq. 6)}$$

f = post-scattering
n_f = polarization vector after scattering
k_f = wave vector after scattering
$\mathbf{q} = \mathbf{k_i} - \mathbf{k_f}$, scattering vector

A photocount correlation function C(t) is correlated to the diffusion coefficient, D (Eq. 7), which can be used to estimate a nanoparticle's hydrodynamic diameter R based on the Stokes Einstein relation (Eq. 8) (Stetefeld et al., Berne et al.).

$$C(t) = [1 + \gamma \times \exp(-qDt)] \qquad \text{(Eq. 7)}$$

γ = constant depending on instrument (ideally = 1; often < 1)
q = scattering vector

$$D = k_B T / (6 \pi \eta R) \quad \text{(Eq. 8)}$$

k_B = Boltzmann's constant
T = temperature
η = dynamic viscosity
R = radius of particle

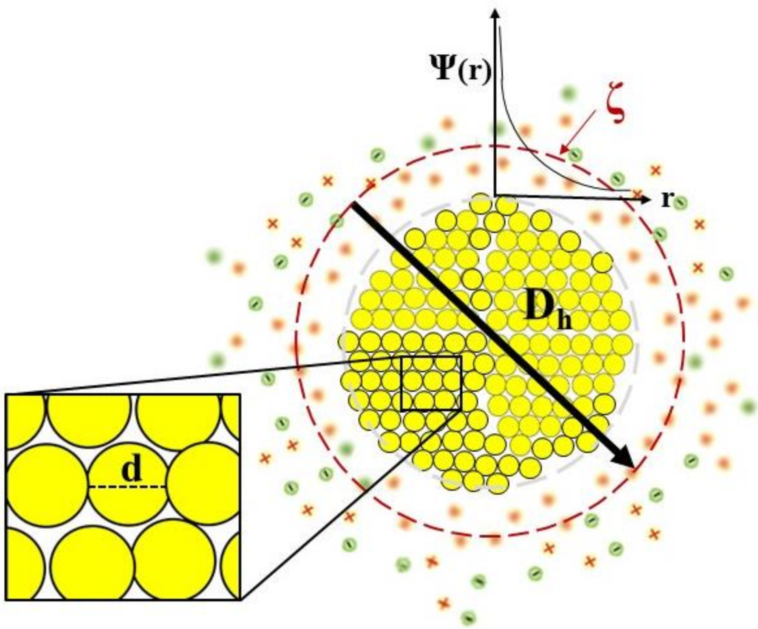

Illustration 2: Parameters measured to characterize SPION and SLNP samples. Hydrodynamic diameter, D_h; single particle diameter, d; zeta potential, ζ; electrostatic potential, $\psi(r)$; distance from colloid, r; single colloids, yellow spheres; slipping plane, red dashed line.

For both SPION and various NP samples, effective/hydrodynamic diameter (D_h) and polydispersity index (pdi) were measured and recorded to determine size and stability of colloidal dispersions. SPION-OAm samples were prepared by dissolving dry SPIONs-OAm in toluene using a bath sonicator to a final concentration of 0.2 mg/mL. The solution was aliquoted in quartz cuvettes in 2 mL volumes for DLS analysis with the NanoBrook Omni Series (Brookhaven Instruments, Holtsville, NY). Stability of SPION-OAm in toluene was studied by taking DLS measurements every 30 minutes for 2 hours after sonicating the solution, with more stable dispersions resulting in static DLS measurements over time. SPION-OA samples were prepared by dissolving dry SPIONs-OA in chloroform using a bath sonicator to a final concentration of 0.1 mg/mL. The solution was aliquoted in square quartz cuvettes in 2 mL volumes for DLS analysis with the NanoBrook Omni Series (five measurements per sample).

Estimated SPION-OAm aggregation size was calculated using hydrodynamic diameter and average single particle diameter (Eq. 9):

$$N_{SPIONs} = D_h / d \quad \text{(Eq. 9)}$$

N_{SPIONs} = number of particles in aggregate
D_h = hydrodynamic diameter (DLS)
d = single particle diameter (TEM)

Aqueous samples (SLNPs, PS-NPs) were prepared in 2 mL volumes at a 1:4 dilution in DI water (pH 7.5–8.0) in square plastic cuvettes (Brookhaven Instruments Corporation 100 Plastic Cells/Caps 2.2, NC9968046). SLNP and PS-NP size was measured with DLS (five measurements per sample) immediately after completing synthesis. Additional stability studies are outlined in section 2.2.5.

2.2.2 Zeta potential (ZP)

Zeta potential (ZP) describes the electrical potential at the slipping plane, the region which separates the mobile fluid from fluid attached to the surface. For colloidal dispersions, ZP describes the electrokinetic potential and quantifies the magnitude of the charge at the interface between the solid particle/colloid and the liquid medium (Clogston & Patri) (Ill. 2). Additionally, stability of colloidal dispersions is correlated with the absolute magnitude of ZP, with larger ZP (≥ ±30 mV) indicating a resistance to particle aggregation (Shao et al.).

Samples for zeta potential were prepared using the same techniques in 2.6.1, except volume of samples in cuvettes were reduced to 1.6 mL. For hydrophobic samples (SPIONs), the SR-751 electrode was used while for hydrophilic samples (SLNPs, PS-NPs), the BI-ZEL electrode was used. The Phase Analysis Light Scattering (PALS) ZP setting was used to collect data (five measurements with ten cycles per measurement for each sample) with the NanoBrook Omni Series. ZP measurements were verified by confirming expected ZP of control sample, 1M potassium chloride (-53±4 mV).

2.2.3 Lyophilization of SLNPs

Known volumes of SLNPs were lyophilized to determine mass concentration (section 2.2.4) and yield of SLNP samples. Small, known volumes (< 1 mL) were pipetted into Eppendorf tubes which were opened, covered with Kim wipes secured to the tube by an elastic band, and submerged in liquid nitrogen to flash freeze. Samples were lyophilized overnight using SP Scientific Benchtop Pro Lyophilizer and mass of the dried particles was measured (Warminster, PA).

2.2.4 Ultraviolet-visible Spectroscopy Mass Concentration Curve

A characteristic mass concentration curve was determined for SLNPs by measuring absorbance at 500 nm (due to iron oxide in SPIONs) of diluted SLNP samples with a spectrometer (SpectraMax M5, Molecular Devices, San Jose, CA) (Yu). Using the known volume-to-mass ratio determined by lyophilization, the dilutions were converted to mass concentration and plotted against the average absorbance values.

2.2.5 Storage and SLNP stability

Short-term stability of SLNPs in different storage solvents was determined by measuring hydrodynamic diameter over time with DLS (section 2.2.1), focusing on particle stability in media conditions for future cell experiments. Synthesized SLNPs were placed on a magnet for 6-24 hours. The supernatant was removed and an equal volume of RPMI 1640 media (1x RPMI 1640 Medium, Gibco, Ref# 11875093, Waltham, MA) without heat-inactivated fetal bovine serum (HI-FBS, ThermoFisher Scientific, Cat#A5209501, Waltham, MA) (pH 8.0) or RPMI 1640 media with 10% HI-FBS was added to resuspend magnetically isolated SLNPs (Atlas & Snyder). The hydrodynamic diameter and zeta potential of each batch of SLNPs was measured at 0 hours, 2 hours, 4 hours, 6 hours, 18 hours, and 24 hours after synthesis. Visual observations of SLNP agglomeration were recorded if DLS measurements were not possible.

Long-term stability of SLNPs in different storage solvents was determined by measuring hydrodynamic diameter over time with DLS, focusing on optimizing storage conditions for a longer shelf-life. SLNPs were synthesized and placed on a block magnet overnight. The following day, the supernatant was removed and an equal volume of RPMI 1640 media (without HI-FBS, pH 8.0) or phosphate buffered solution (PBS without calcium and magnesium, 21-040-CV, Corning CellGro, Corning, NY) (pH 7.4) was added to resuspend magnetically isolated SLNPs. The hydrodynamic diameter of each batch of SLNPs was measured using DLS at 0 hours, 24 hours, 48 hours, 1 week, 2 weeks, 4 weeks, and 8 weeks after resuspension in the new storage solvent.

2.2.6 Brightfield/Fluorescence Microscopy

Brightfield microscopy was used to observe SLNP morphology and general size. Fluorescence microscopy was conducted to verify strength of each fluorophore and identify SLNPs that had been phagocytosed by J774A.1 cells. SLNP samples were diluted 1:10 in DI water, ~30 uL was pipetted onto a glass microscope slide (1-1.2 mm thickness), and covered in a #1 or 1.5 coverslip. pH-balanced DI water of pH < 7.0 and pH 7.5-8.0 was used to confirm pH-dependence of pHrodo-red fluorescence. FITC and AF488 both have an excitation wavelength of ~500 nm and emission wavelength of ~520 nm, whereas pHrodo-red has an excitation wavelength of ~560 nm and emission wavelength of~585 nm. Brightfield and fluorescent images were acquired using three different microscopes depending on access: IX83 Inverted microscope (Olympus, Tokyo, Japan), Axiovert S100 Inverted Phase Contrast Fluorescence Microscope (ZEISS, Oberkochen, Germany), and Keyence All-in-One Fluorescent Microscope BZ-X710 (Woburn, MA). Typically, FITC laser/filter cube and TRITC laser/filter cube were used to excite and collect emission from AF488 or FITC and pHrodo-red fluorophores respectively. Use of non-fluorescent SLNPs were imaged as negative controls to identify SLNP autofluorescence. ImageJ tools were used for image analysis.

2.2.7 Transmission Electron Microscopy (TEM) (performed by Dr. Hui Chen at Boston University School of Medicine)

TEM utilizes a beam of electrons that passes through a sample to generate images with near atomic resolution at its highest magnification (Lee et al.). A source emits electrons through a cooled vacuum environment, which pass through the sample and hit the objective lens to produce an image. All NP samples imaged with TEM were prepared on PELCO® Single Layer Graphene TEM Support Films (Ted Pella, Inc., PELCO® Single Layer Graphene TEM Support Films on Lacey Carbon, 300 Mesh Copper Grids, 21710-10, Redding, CA) which were gently cleaned with soap, DI water, and acetone and allowed to dry at least two days prior to imaging. At least one day prior to imaging, the number of cleaned and dried TEM grids needed for each sample were placed on filter paper using clean tweezers, navy-blue side of the grid facing up. SPION samples were dispersed in toluene at 0.5 mg/mL and sonicated in a bath sonicator for 5 minutes (or until dispersed). SLNP and PS-NP samples were prepared by diluting the sample 1:50 in DI water. One drop (<50 uL) of each sample solution was added to the navy-blue side of the TEM grids and allowed to dry overnight. On the day of imaging, TEM grids were loaded into the grid storage box using tweezers (Fisherbrand™ High Precision Straight Tapered Ultra Fine Point Tweezers/Forceps, Fisher Scientific, Waltham, MA) and transported to Boston University's BioSquare Research Building III. Prepared grids were examined in a JEOL JEM-1010 transmission electron microscope and digital images were collected at a range of magnifications with an Erlangshen ES100W digital camera (Gatan, Pleasanton, CA).

2.2.8 Stimulated Emission Depletion Microscopy (STED) (performed by Dr. Jena Goodman at Boston University Cellular Imaging Core at Evans Biomedical Research Center)

STED microscopy is one of several super-resolution microscopy techniques, achieving resolutions below the diffraction limit of light microscopy and allowing for sharper images at the nanoscale (Muller et al.). STED selectively deactivates fluorescence to reduce unwanted fluorophore emission when taking images. A high intensity laser generates many incident photons separated into two light beams: an excitation light beam, to excite fluorophores and generate fluorescence, and a red-shifted light beam, which confine fluorophores to their ground state via stimulated emission (Fig. 3). The target fluorescence emission and second photon emission can be separated during detection, allowing for selective activation and depletion of fluorophores to generate a desired image at high resolution. Though STED allows for super-resolution images, high intensity of incident photons can also result in photobleaching.

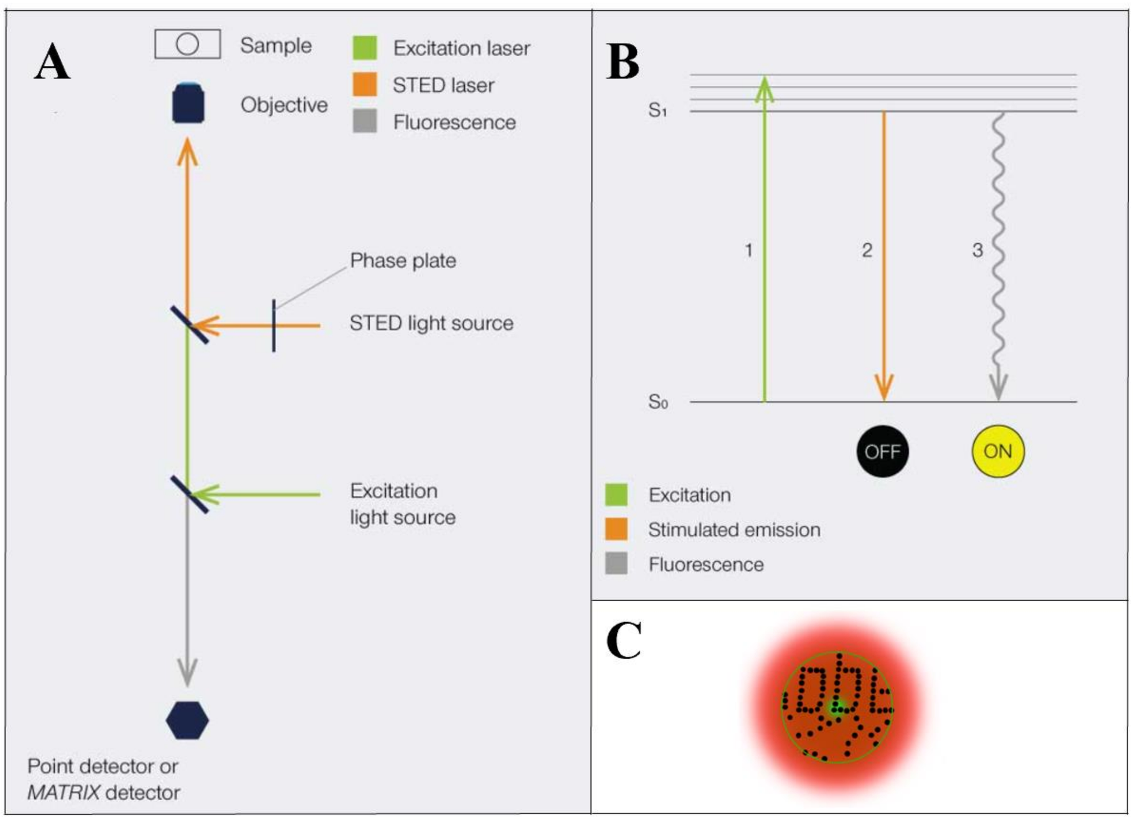

Figure 3: STED principle in Abberior microscope. A) Excitation and STED beam laser setup used to excite target fluorophores and quench off-target fluorophores determined by the phase plate. B) Jablonski diagram of STEM excitation of fluorophore, with stimulated emission and fluorescence emission producing off and on state fluorophores respectively. C) Donut-shape of laser used in STEM microscopy; excitation as green; stimulated emission as red. Figure adopted from Abberior STED (“STED”).

SLNP samples were prepared by pipetting 50 uL of the sample solution and 50 uL of embedding media (Abberior Mount Liquid Antifade, Abberior Instruments, Göttingen, Germany) onto a 35mm glass bottom dish (WillCo Wells Glass Bottom Dish, #1.5, ~0.75 μm thickness, Cat#70671-52, Amsterdam, Netherlands). The sample and embedding media were gently mixed by pipetting up and down. When imaging SLNPs with pHrodo-red-DPPE, 5-10 uL of hydrochloric acid (HCl) was added to decrease pH below 7.0 and trigger pHrodo-red fluorescence. A #1.5 (~0.17mm) coverslip was placed on top of the sample and embedding media solution. The prepared glass bottom dish was covered with tinfoil during transportation and then imaged using an Abberior INFINITY platform and STED system (Abberior Instruments, Göttingen, Germany) at Boston University's Cellular Imaging Core in the Evans Biomedical Research Center.

2.2.9 Magnetic Properties of SPIONs and SLNPs

Magnetization of SPIONs and SLNPs were verified using simple tests with neodymium disc magnets (500mm in diameter, axially magnetized), block magnets (350 mT magnetic field at surface, axially magnetized) or radial ring magnets (SuperMagnetMan N50 Neodymium Radial Ring Magnet RR0100N, Pelham AL). SPION magnetic response was near immediate when the sample was brought within appropriate distance for all magnets (neodymium, ring, block). SLNP magnetic response was tested by placing a scintillation vial containing a sample on a horizontal array of neodymium magnets (7x7) or taping an Eppendorf tube of sample in a ring magnet suspended above the benchtop with a ring stand and clamp for several hours or overnight. Separation of SLNPs from DI water storage solvent and aligned of SLNPs with magnetic fields of the magnet were observed the following day. Gravitational accumulation was tested by leaving a sample of SLNPs on the benchtop overnight with no magnet and confirmed SLNPs do not significantly settle.

When handling any magnets, safety must be prioritized. Using a separate, labeled container to store, handle, and transport strong magnets will reduce unwanted magnetic attraction and make separation of magnetic components easier, if it does occur. Before handling magnets, ferrous jewelry should be removed. Other ferrous equipment or material should be kept at a distance from the magnet as well as phones, computers, and other electronics.

2.2.10 Proton Nuclear Magnetic Resonance (^{1}H-NMR)

Purity of oleylamine (molecular weight: 267.493 g/mol) was assessed using proton nuclear magnetic resonance (^{1}H-NMR) as impurities can affect SPION coating and dispersion in the hydrophobic core of SLNPs. Samples were prepared by diluting 15 uL of oleylamine in 0.7 uL of deuterated chloroform (99.6+atom%, Acros Organics, CAS 865-49-6, Geel, Belgium) in an NMR tube ($3.95*10^{-5}$ mol). ^{1}H-NMR was conducted using the Agilent 400 MHz VNMRS (Oxford Instruments, Concord, MA) in Boston University's Chemical Instrumentation Center. Resulting ^{1}H-NMR data for oleylamine samples were analyzed with the help of Dr. Jon Nagy of NanoValent Biosciences and Dr. Paul Ralifo of Boston University Department of Chemistry.

2.1.11 Storage of Oleylamine (OAm)

For SPION-OAm and SPION-OA synthesis, oleylamine must be of high purity (≥98%) to maximize SPION coating and dispersion in the SLNP core. Proper storage of

OAm is critical for reducing oxygen-related impurities (Baranov et al.). Ideally, oleylamine should be stored under vacuum in an airtight container. In this work, 100 mL aliquots of OAm with parafilm-sealed caps were stored in a 700 mL VWR Desi-Vac Container with manual vacuum pump (Fisher Scientific, Waltham, MA) at -20 ºC. OAm was thawed inside the Desi-Vac at room temperature before any synthesis procedure. Additional purification techniques can also be useful to maintain high purity of OAm, though this option was not explored in this work.

2.3 CELL STUDIES

2.3.1 Sterilization and Preparation of SLNPs

SLNPs were sterilized using UV light from a biosafety cabinet prior to cell experiments. SLNPs stored in DI water (pH 7.5-8.0) were placed on a magnet overnight. The following day, the supernatant was removed and, in a biosafety cabinet, an equal volume of sterile, phenol-free RPMI 1640 media (Gibco™ RPMI 1640 Medium, no phenol red, 11835030, Waltham, MA) was added to resuspend SLNPs. SLNPs in phenol-free RPMI 1640 were loaded into wells of a commercial sterile 6-well plate (TC-treated, polystyrene, Costar, Cat#3506, Corning, NY) at 2-3 mL/well. The UV sterilization light of the biosafety cabinet was turned on for > 30 minutes. DLS of SLNPs before and after UV light sterilization was collected to examine changes in particle size or stability.

2.3.2 Minimize Autofluorescence

Phenol-red, which acts as a pH indicator and marker of viability in cell culture, can increase background fluorescence and interfere with fluorescence measurements. Therefore, phenol-free RPMI 1640 media was used in all cell assays in this work. (Phenol-red can have a proliferative effect on cells and was used for cell culturing prior to experiments (Wesierska-Gadek et al.)). Additionally, black-walled, glass-bottomed opaque plates were used for cell studies, as they are 2–25x more efficient than white/clear plates at reducing autofluorescence. Non-fluorescent SLNPs were used as a control to confirm proper pH-sensitive and pH-insensitive fluorescence of dual-labeled SLNPs.

2.3.3 Native Phagocytic Behavior of J774A.1 Monocyte Cells

J774A.1 monocyte cell line was selected as our phagocytosing model for *in vitro* studies of SLNP-mediated magnetic pull-down, but it was necessary to first establish the cell line's spontaneous phagocytic capabilities with a Vybrant Phagocytosis Assay (ThermoFisher Scientific Vybrant™ Phagocytosis Assay Kit, Invitrogen, Ref#V6694, Waltham, MA). J774A.1 cells were incubated at 37°C, 5% CO_2 for 3-4 days prior to collection and resuspended in phenol-free RPMI 1640 media at 10^6 cells/mL. Two identical serial dilutions of J774A.1 cells (10^5 cells to 10^3 cells) were plated in triplicate in a 96-well black/clear bottom plate (Corning™ 96-Well, Cell Culture-Treated, Flat-Bottom Microplate, 07-200-565, Corning, NY), phenol-free RPMI 1640 media was added for a total volume of 200 uL in each well, and the plate was incubated at 37°C for 1 hour. Edge/outer wells were filled with 200 uL of PBS to prevent drying of samples and edge effects when imaging. Media was removed by aspiration with a Pasteur pipette/10 uL pipette tip (to prevent accidental removal of cells), replaced with 100 uL of fluorescein-labeled bioparticles (prepared by mixing 0.5 mL of concentrated Hanks' balanced salt solution (Invitrogen, Ref#V6694B, Waltham, MA) with 5 mg of bioparticles (*Escherichia coli* (K-12 strain) Bioparticles™ fluorescein conjugate, Invitrogen, Ref#V6694A, Waltham, MA) in 4.5 mL of DI water according to the Vybrant Phagocytosis Assay manual. The plate was incubated for 2 hours at 37°C/5% CO_2 to allow for phagocytosis to occur. Bioparticles were then removed and replaced with 100 uL of trypan blue (Invitrogen, Ref#V6694C, Waltham, MA) for 1 minute. Trypan blue was removed from all wells and replaced with phenol-free RPMI 1640 media for only one set of serially diluted wells. Media only (negative), bioparticles plus trypan blue (negative), cells only (negative), and bioparticles only (positive control) were plated in triplicate as controls. Fluorescence output was measured at excitation wavelength of 480 nm and emission wavelength of 520 nm using a Fluostar Optima Spectrophotometer (BMG LabTech, Ortenberg, Germany). Percent effect of cell concentration on phagocytosis was determined by calculating the ratio of the net experimental reading (average experimental reading - average negative control reading) and net positive reading (average positive control reading) multiplied by 100%. While calculating percent effect on phagocytosis, average fluorescence readings from cell only wells were used as the negative control while the fluorescence readings from the highest concentration of cells and bioparticles were used as the positive control.

2.3.4 Phagocytosis of SLNPS (#1)

Phagocytosis of SLNPs by J774A.1 cells was initially explored while studying native phagocytosis of J774A.1 cells, and thus, used the same setup as section 2.3.2. J774A.1 cells were cultured 3-4 days in advance of each experiment. Cells were resuspended at 10^6 cells/mL in phenol-free RPMI 1640 media and 100 uL aliquots were added to three wells in a 96-well black/clear bottom plate. Phenol-free RPMI 1640 media was added to a final volume of 200 uL in each well. After 1 hour incubation, media was aspirated from each well using a Pasteur pipette/10 uL pipette tip and replaced with 195 uL of phenol-free RPMI 1640 media plus 5 uL (~30 ug) of sterilized SLNPs prepared for cell studies according to section 2.3.1. Cells and SLNPs were incubated for 2 hours at 37°C/5% CO_2, after which media was removed. In one well, 100 uL of RPMI 1640 media was added. In a second well, 100 uL of trypan blue was added for 1 minute then removed. In a third well, 100 uL of trypan blue was added for 1 minute, removed, and replaced with 100 uL of phenol-free RPMI 1640 media. Both fluorescent microscopy and fluorescence emission using FITC laser/filter cube and TRITC laser/filter cube were collected using Keyence All-in-One Fluorescent Microscope BZ-X710 (Woburn, MA) and Fluostar Optima spectrometer (BMG LabTech, Ortenberg, Germany) at Antagen Biosciences, Inc., respectively. No controls were used during this initial exploration (except for those included in section 2.3.1).

2.3.5 Phagocytosis of SLNPS (#2)

This version of the protocol focused on verifying SLNP phagocytosis using the same cell and SLNP concentrations used in section 2.3.4 and documenting results using fluorescent microscopy. However, incubation times were lengthened to allow for more potential phagocytosis to occur.

Cells were cultured 3-4 days prior to the experiment and resuspended at 10^6 cells/mL in phenol-free RPMI 1640 media. In a 96-well black/clear bottom plate, 100 uL of cells were plated in triplicate for one negative control and three experimental conditions, and 100 uL of media was added to each well for a total volume of 200 uL. Edge/outer wells were filled with 200 uL of PBS to prevent drying of samples and edge effects when imaging. SLNP incubation was conducted as a reverse time course for three experimental conditions: 1) 6-hour incubation; 2) 4.5-hour incubation; 3) 3-hour incubation. After cells were incubated in media at 37°C, 5% CO_2 for 1 hour, media was removed from one experimental condition triplicate via aspiration with a Pasteur pipette/10 uL pipette tip and replaced with 195 uL of RPMI 1640 media plus 5 uL (~30 ug) of sterilized SLNPs resuspended in RPMI 1640 media according to section 2.3.1 for the 6-hour incubation period. After 1.5 hours, media removal and replacement with 195 uL of RPMI 1640 media plus 5 uL of SLNPs was repeated in another experimental triplicate for the 4.5-hour incubation period. Lastly, after another 1.5 hours, media removal and replacement with 195 uL of RPMI 1640 media plus 5 uL of SLNPs was repeated in the last experimental triplicate for the 3-hour incubation period. Negative control wells with 100 uL of cells and 100 uL of media were not disturbed during the incubation. Upon finishing the incubation, media was aspirated from all wells and 100 uL of trypan blue was added for 1 min. Trypan blue (Gibco, Ref#15250-061, Waltham, MA) was removed and wells were imaged using Axiovert S100 Inverted Phase Contrast Fluorescence Microscope (ZEISS, Oberkochen, Germany).

2.3.6 Cytotoxicity of SLNPs

Cytotoxic effects of SLNPs were studied for 3-hour and 6-hour incubation periods with J774A.1 cells at final concentrations of 20-200 ug/mL. Cells were cultured 3-4 days prior to the experiment and resuspended at 10^6 cells/mL in RPMI 1640 media. In two 96-well black/clear bottom plates, 100 uL of cells were plated in 48 wells. Eight wells in each plate were used for cell-only negative control wells, which 50 uL of media were added to.

After determining the mass concentration calibration curve for the given sample and preparing sterile SLNPs according to sections 2.2.3, 2.2.4 and 2.3.1, the following experimental conditions (in quadruplicate) were used:

Experimental condition	Target concentration of SLNPs (ug/mL)	Volume of SLNP sample (uL)	Volume of RPMI 1640 (uL)	Mass particles/cell (ug/cell)
1	20	2.14	47.86	0.03
2	40	4.28	45.71	0.06
3	60	6.43	43.57	0.09
4	80	8.57	41.43	0.12
5	100	10.72	39.28	0.15
6	120	12.86	37.14	0.18
7	140	15.00	34.99	0.21
8	160	17.15	32.85	0.24
9	180	19.29	30.71	0.27
10	200	21.43	28.57	0.30

Table 4: SLNP volumes and concentrations for cell cytotoxicity experiment.

Appropriate volumes of SLNP and media were pipetted into corresponding wells according to Table 4 and mixed by pipetting up and down. Plates were incubated for 3 and 6 hours at 37°C/5% CO_2 in reverse time course. The cytotoxicity of SLNPs at 3 and 6 hours was determined using MTT cell proliferation assay according to manufacturer's instruction (American Type Culture Collection, Cat#30-1010K™, Manassas, VA).

2.3.7 Fluorescence Activated Cell Sorting (FACS) (performed by Belle Ye in BU Khalil Lab and/or Dr. Xuemei Zhong and Dr. Wenda Gao at Antagen Biosciences, Inc.)

Fluorescence Activated Cell Sorting (FACS) was used to quantify the percentage of J774A.1 cells that phagocytosed SLNPs. Fixed and live cells were both prepared to test and establish a reproducible protocol.

Fixed sample:

Samples were prepared by plating 2–5 million cells (suspended in phenol-free RPMI 1640 media) per condition in a 96 or 6-well plate and incubating with the appropriate volume of SLNPs for low (35 ug/mL) and high signals (155 ug/mL). Following a 3-hour or 6-hour incubation period at 37°C/5% CO_2, cells were scraped from each well and transferred to a 15 mL centrifuge tube per each experimental condition. Cells were centrifuged at 200g for 5 minutes in phenol-free RPMI 1640 media four times and fixed in 4% paraformaldehyde (PFA) (Electron Microscopy Sciences, 16%, Cat#15710, Hatfield, PA) in PBS for 20 minutes at 4°C. Fixed cells were centrifuged twice at 200g for 5 minutes and resuspended in PBS for analysis within 24 hours. Samples were analyzed with Attune® NXT Acoustic Focusing Cytometer (ThermoFisher Scientific, Waltham, MA) or FACS Calibur (Becton Dickinson, Franklin Lakes, NJ) at Antagen Biosciences, Inc.

Live sample:

Samples were prepared according to the fixed sample protocol; however, after cells were transferred to a 15 mL centrifuge tube for each experimental condition, they were centrifuged at 200g for 5 minutes in phenol-free RPMI 1640 media four times and resuspended in FACS buffer for analysis with Attune® NXT Acoustic Focusing Cytometer.

CHAPTER 3:

RESULTS AND DISCUSSION

3.1 Long-term Goal and Initial SLNP Design

Inspired by Zhong's findings, SPION-lipid nanoparticles (SLNPs) in this thesis work were designed to specifically target and isolate natural IgM-producing phagocytic B cells (NIMPABs) to study for potential cancer immunotherapy applications. With the guidance of Dr. Joyce Wong and Dr. Xuemei Xhong, Dr. Jin Yu developed a set of criteria the final SLNP design must fulfill to complete the long-term goal of magnetic isolation of NIMPABs (Tbl. 1, Ill. 3).

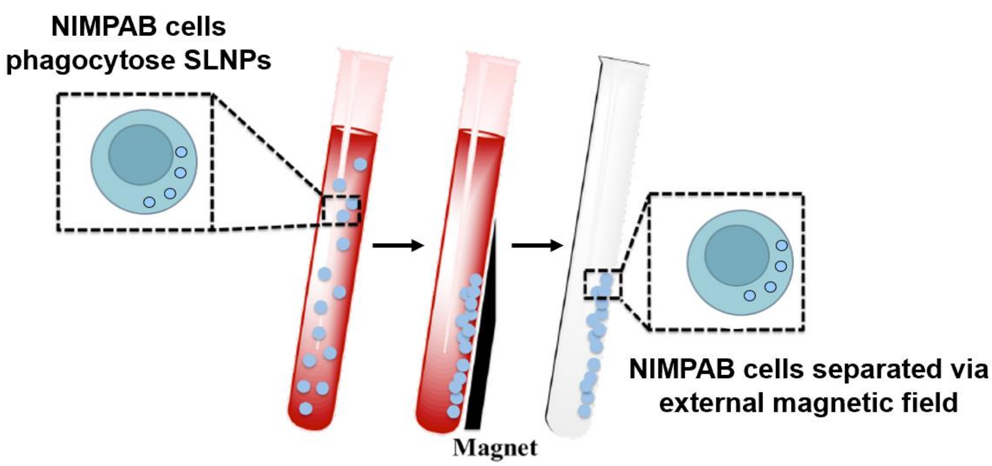

Illustration 3: Long-term goal of isolating NIMPAB cells from blood or other fluid sample with SLNPs. Modified from Yu (Yu).

To magnetically isolate cells using a function-specific targeting method, SLNPs must possess strong magnetic properties and be selective for the target cell type. Superparamagnetic iron oxide nanoparticles (SPIONs) were incorporated in Yu's design to provide magnetic properties of SLNPs, finding that SLNPs with SPION cores were magnetically separated 50% more than comparable MACS magnetic beads in a 20-minute period (Yu). To target NIMPAB cells, the SLNP lipid shell was composed primarily of phosphatidylcholine (PtC), an apoptosis marker which has demonstrated selective induction of phagocytotic behavior by B1 B cells (Vo et al.). Protein corona formation on the surface of SLNPs can cause destabilization and potentially induce agglomeration, which can decrease selective phagocytosis thus limiting the efficacy of our targeting strategy (Zhang et al.). Polyethylene glycol (PEG) was added to the hydrophilic shell of SLNPs to reduce protein corona formation and particle agglomeration. A polymer, in this case polystyrene (PS), was added in the hydrophobic core of the particle to maintain structural stability. pHrodo-red, which will only fluoresce when SLNPs have been phagocytosed and entered the acidic endosome and lysosome environment, was utilized distinguish extracellular and intracellular SLNPs. SLNP diameter was limited to 200-600nm to avoid non-specific endocytosis by off-target cell types and cytotoxic effects of larger particles (Vo et al., Yameen et al.). In Yu's work, pHrodo was added to SLNPs via pHrodo-red-DPPE detailed in sections 2.1.3 and 2.3.1.i. Yu established the pHrodo-red labeled SLNP formulation as the final design and completed remaining studies with this version of the SLNP (Fig. 4) (Yu).

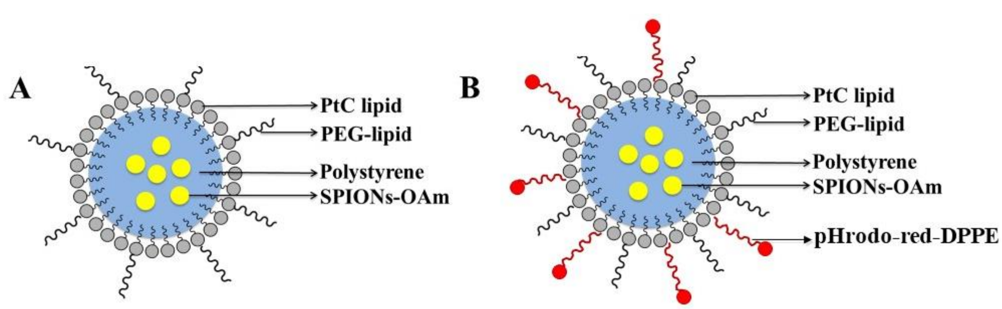

Figure 4: Lipid nanoparticle formulations from Yu consisting of a hydrophobic core of PS and SPIONs-OAm and a hydrophilic shell of PtC, DSPE-PEG, and A) no fluorescence as a control; B) pHrodo-red-DPPE to track intracellular localization of SLNPs. Figure adapted from Yu.

This thesis work focuses on:

1. Improving the current pHrodo-red labeled SLNP formulation
2. Establish a quality control protocol for batch-to-batch consistency
3. Development of an *in vitro* model to quantify cell-SLNP interactions, including cytotoxicity and phagocytosis

3.2 Synthesis and Characterization of SPIONs

Superparamagnetic iron oxide nanoparticles (SPIONs) possess unique magnetic properties, making them an excellent candidate to magnetize SLNPs. Synthesized primarily with iron oxide (Fe_3O_4) via thermal decomposition (section 2.1.1 and 2.1.2), SPIONs exhibit ferromagnetic behavior in the presence of an applied magnetic field, and superparamagnetic behavior depending on their size (10–100 nm) (Yu). During synthesis of SPIONs, oleylamine (OAm) acted as both the reducing agent and surface coating to promote dispersion of SPIONs-OAm in the hydrophobic SLNP core (section 2.1.1, 2.1.3). SPION-OAm incorporation is essential to forming magnetic SLNPs for future applied-field magnetic attraction and cell isolation.

To characterize SPION-OAm size and stability, hydrodynamic diameter (D_h) measurements were taken according to protocols outlined in section 2.2.1. Over the course of 2 hours, SPION hydrodynamic diameter was measured every 30 minutes to determine any change in aggregate size and particle stability (Fig. 5D, E). Additionally, TEM images were collected with the help of Dr. Hui Chen to examine average single SPION-OAm particle diameter which was slightly smaller than the expected superparamagnetic range of 10-100 nm (7.69 ± st. dev. 1.23 nm) (Fig. 5A-C). SPIONs-OAm dispersions remained relatively stable over time, with hydrodynamic diameter of aggregates changing by < 20 nm or ≤ 3 single SPIONs over 2 hours.

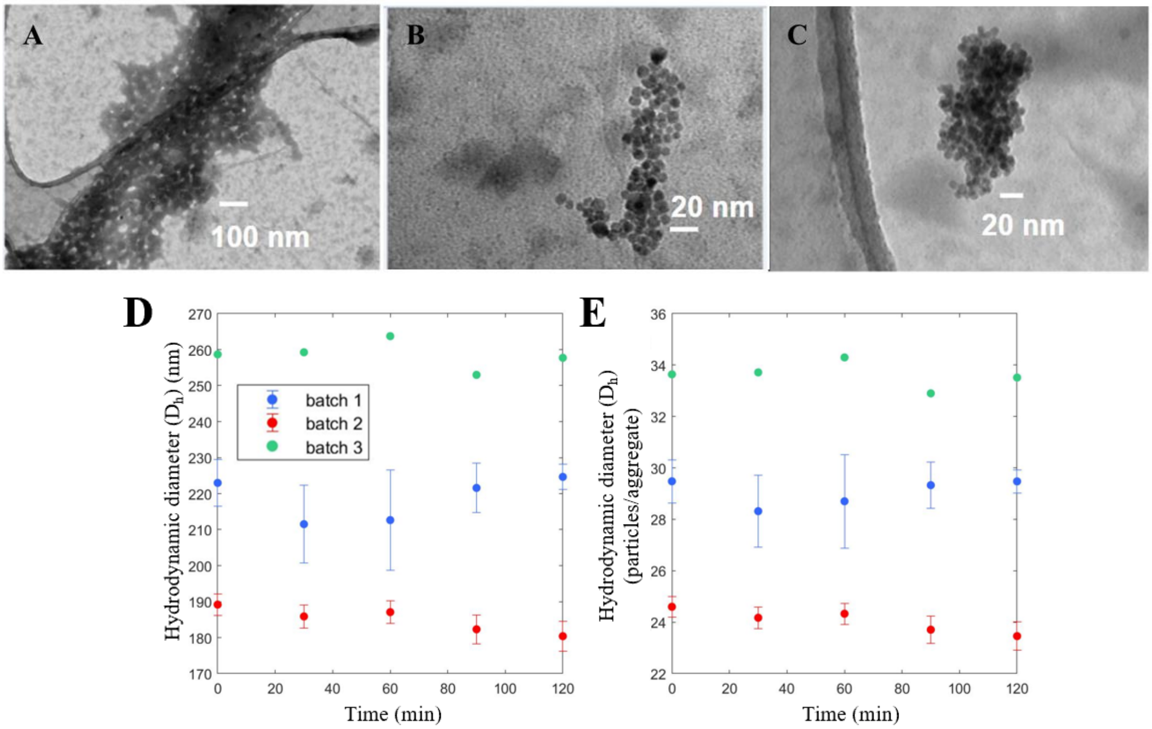

Figure 5: TEM images of SPIONs-OAm dispersed in toluene with scale bars A) 100 nm, B) 20 nm, C) 20 nm. D) Hydrodynamic diameter and E) estimated aggregation (# particles/aggregate diameter) of 0.5 mg/mL SPIONs-OAm in toluene 0, 30, 60, 90, and 120 minutes after sonication and dispersion.

SPIONs-OAm ZP was also measured, though measurements varied greatly between three separate samples of varying storage times: +50.37±87.34 mV (7 months old), +4.27±50.02 mV (5 months old), and +33.82±35.29 mV (3 months old). These data suggest SPIONs-OAm have a positive net electrical charge at the slipping plane of each colloid. OAm, which has a pKa of 10.7, should be positively charged when stored in any solvent with a pH < 10.7, thus supporting our results. However, the DLS results were unreliable for each sample due to large standard deviations. Measurements should be repeated with the proper electrode (SREL solvent-resistant electrode, Brookhaven

Instruments, Holtsville, NY) and quartz cuvette fit (BI-SCGO, Brookhaven Instruments, Holtsville, NY). Additionally, establishing ZP of each sample within 24 hours of synthesis and collecting data at later time points would allow a better understanding of SPION-OAm stability over time.

Properties of oleic acid coated SPIONs (SPIONs-OA), which were synthesized according to section 2.1.2 with the help of Sydney Marchando, were measured and compared to SPIONs-OAm as an alternative magnetic source in the SLNP core. The hydrodynamic diameter of SPIONs-OA in chloroform (prepared for DLS measurement according to section 2.2.1) was 340.80 nm with polydispersity index (pdi) of 0.002. Wulandari et al. determined single SPION-OA diameter was approximately 5.16 nm from TEM images (Walundari et al.). Using this single SPION-OA diameter and Eq. 9, estimated aggregate size was approximately 66.05 particles/aggregate. SPIONs-OA ZP was measured at -38.45 mV, which is consistent with previous research and expected charge of oleic acid at chloroform's acidic pH (OA pKa: 9.85) (Kanicky & Shah, Wulandari et al.). These results only reflect measurements from one batch of SPIONs-OA and should be repeated to confirm our results. Future investigation should also include stability studies and TEM imaging/analysis for SPIONs-OA.

Magnetic responses of SPIONs-OAm and SPIONs-OA were conducted according to section 2.2.9. SPIONs-OAm and SPIONs-OA had similar, rapid responses to external magnetic fields, as expected for iron oxide nanoparticles (Fig. 6).

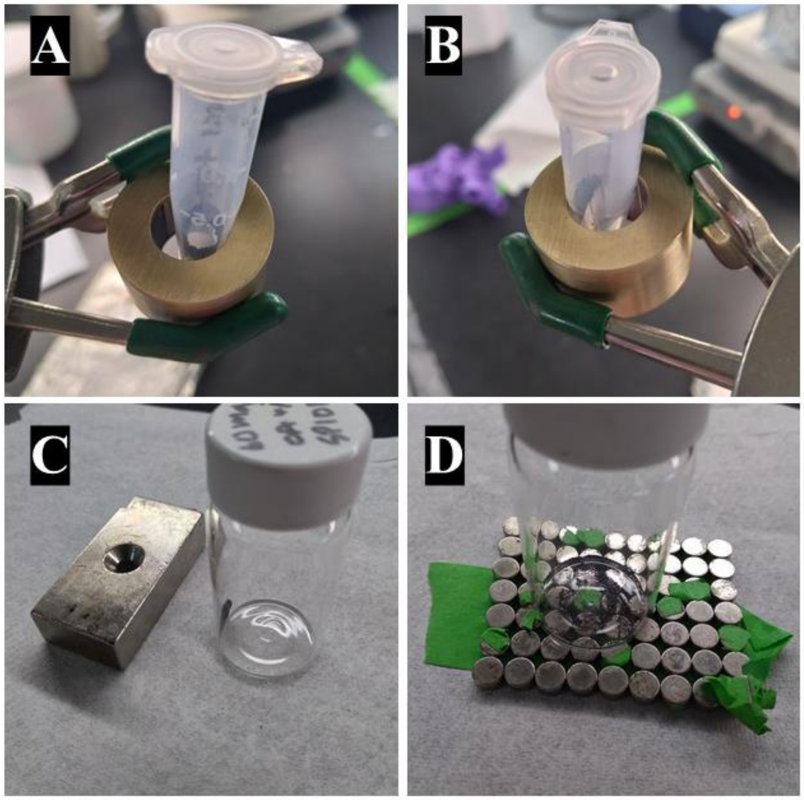

Figure 6: Magnetic testing of synthesized SPIONs-OAm using a A-B) ring magnet and SPIONs-OA using C) block magnet and D) array of neodymium magnets. SPIONs-OAm and SPIONs-OA, which appear as a black powdery substance, exhibited near immediate magnetic response to applied external fields, as expected.

Synthesis of SPIONs-OAm and SPIONs-OA require reagents of high purity (OAm ≥ 98%; OA ≥ 90%). Dispersion of SPIONs-OAm in the hydrophobic core of SLNPs relies on purity of reagent and successful coating of SPIONs. Therefore, proper storage of OAm to limit exposure to oxygen and resulting impurities is crucial for successful synthesis of both SPIONs-OAm and SLNPs (Baranov et al.). Assessing OAm purity with H^1-NMR (section 2.2.10) can identify any impurities in the sample before synthesizing SPIONs-OAm. In Figure 7, only minor impurities are present and hydrogen atoms of OAm structure are confirmed. Purity can be maintained with improved storage methods and improved with additional purification steps.

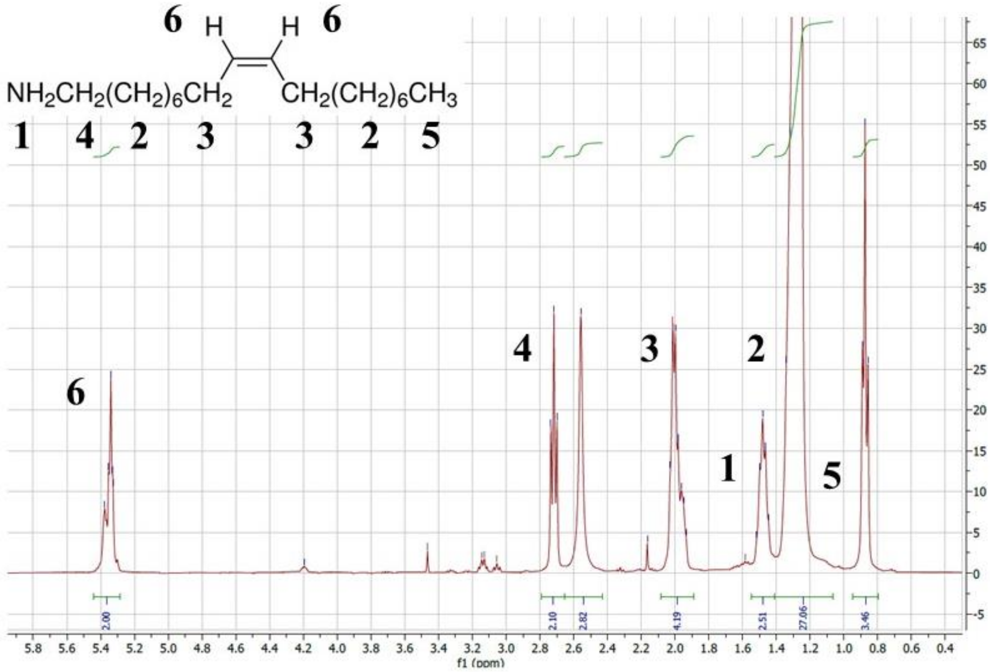

Fig. 7: ^{1}H-NMR spectrum of cis-isomer oleylamine.

3.3 Synthesis and Characterization of SLNPs

SLNPs were synthesized via nano-emulsion of hydrophobic core and hydrophilic shell according to section 2.1.3 and were fluorescently labeled with at least one fluorophore according to section 2.1.3.i. In Dr. Yu's dissertation, SLNPs with pHrodo-red-DPPE were synthesized to track phagocytosis of SLNPs and successfully isolate NIMPAB/IgM+CD19+ B cells from mouse peritoneal fluid (Yu, Lee et al.).

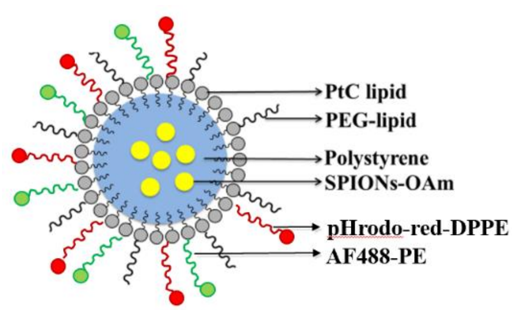

Fig. 8: AF488/pHrodo-red labeled SLNPs.

A pH-insensitive fluorophore, AF488, was added to the SLNP formulation to better track and distinguish SLNP location (Fig. 8). Differentiating intracellular and extracellular SLNPs in future cell studies can provide useful information about efficiency and efficacy of SLNP uptake by J774A.1 monocyte cells. AF488 was selected as a potential candidate due to low spectral overlap with pHrodo-red and reduced compensation required when quantifying cellular uptake of SLNPs with flow cytometry (Herzenberg, et al.). Various molar ratios of AF488-PE were added to SLNPs to achieve high fluorescence output, optimal particle size, and successful synthesis. Initial explorations of AF488 fluorophore addition began with a high AF488-PE:hydrophilic layer lipid molar ratio to maximize fluorescence output (Tbl. 5). However, the molar ratio of 20:90 (20 AF488-PE:90 hydrophilic layer lipids) resulted in unsuccessful purification; centrifugation with 100K MWCO centrifugation tubes caused significant aggregation and clogging of the filter, likely due to excessive lipid content (Fig. 9). To reduce filter clogging and low SLNP yield, the molar ratio of 10:90 (10 AF488-PE:90 hydrophilic layer lipids) was explored. Filter clogging during SLNP purification still occurred, though less than 20:90 ratio. To avoid any clogging, 2:90 molar ratio (2 AF488-PE:90 hydrophilic layer lipids) was tried. SLNP synthesis and purification was successful, but weak fluorescence output was noted during STED imaging, causing fast quenching and imaging challenges. A few more iterations were tried, and the final AF488-PE:lipid molar ratio of 6:90 was selected due to successful SLNP purification (with high yield) and sufficient fluorescence output. This final molar ratio was incorporated into the final SLNP design and used for the remainder of the thesis work (Tbl. 5).

AF488-PE:lipid molar ratio	D_h (nm)	pdi	Successful purification?	Fluorescence output?
2	61.0	0.236	Yes; no clogging	Low and easily quenchable *
5	266.0	0.192	Yes; no clogging	Good**
6	248.6±8.2	0.107±0.051	Yes; no clogging	Good, robust output 72 hrs post-synthesis**
10	-	-	No; Some clumping of lipids clogged centrifugal filter during purification, likely reduced overall yield	-
20	-	-	No; Significant clumping of lipids clogged centrifugal filter during purification, very low SLNP yield	High*

Table 5: Hydrodynamic diameter (D_h) (nm) and fluorescence output observations of SLNPs synthesized using different AF488-PE molar ratios. Certain measurements/observations were not collected due to unsuccessful synthesis/purification of SLNPs. Fluorescent output observed with *STED, **fluorescent microscopy. (DLS samples were not diluted with DI water for these measurements.) Ultimately, AF488-PE:lipid ratio of 6:90 produced samples with high yield and sufficient fluorescence and was incorporated into the SLNP synthesis procedure.

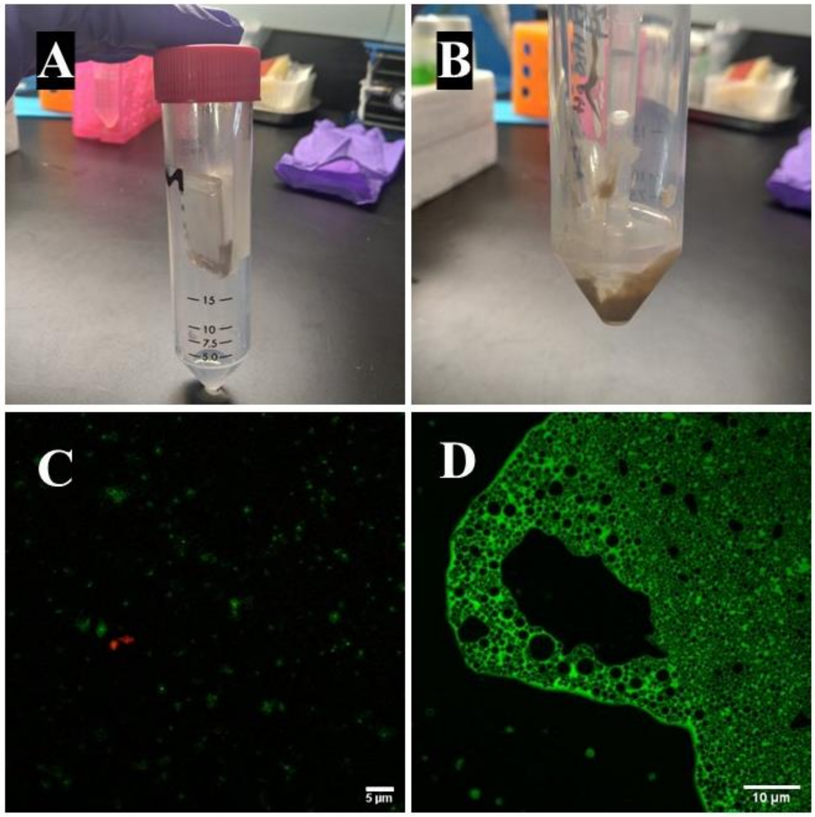

Figure 9: Results of synthesizing AF488/pHrodo-red labeled SLNPs at 20 AF488-PE: 90 hydrophilic layer lipid molar ratio. A) Clogged filter after centrifugal purification due to excessive lipid content. B) Resulting gum-like lipid material which could not be extracted for additional analysis. C) STED imaging of SLNPs collected low yield after centrifugal purification (488nm excitation laser/FITC filter cube, 560nm/585nm laser/filter cube). D) STED imaging of waste from centrifugal purification, exhibiting robust AF488 fluorescence from excessive AF488-PE. AF488, green; pHrodo-red, red.

SLNPs morphology and fluorescence were observed using brightfield/fluorescence and STED microscopy. SLNPs labeled with AF488/pHrodo-red were first imaged with fluorescence microscopy according to section 2.2.6 (Fig. 10). Fluorescent microscopy provided useful information about the general shape, morphology, and distribution of SLNPs as well as the strength of each fluorophore. Fluorophore-labeled SLNPs were also prepared and imaged in basic DI water to confirm pH-dependence of pHrodo-red. Fluorescence-free SLNPs were used as a negative control to identify SLNP autofluorescence and confirm robust fluorescence output from fluorophore-labeled SLNPs. All SLNP samples were prepared and imaged in DI water, which exhibits no autofluorescence. SLNPs exhibited Brownian motion while confined between a microscope slide and coverslip (section 2.2.6, Fig. 11).

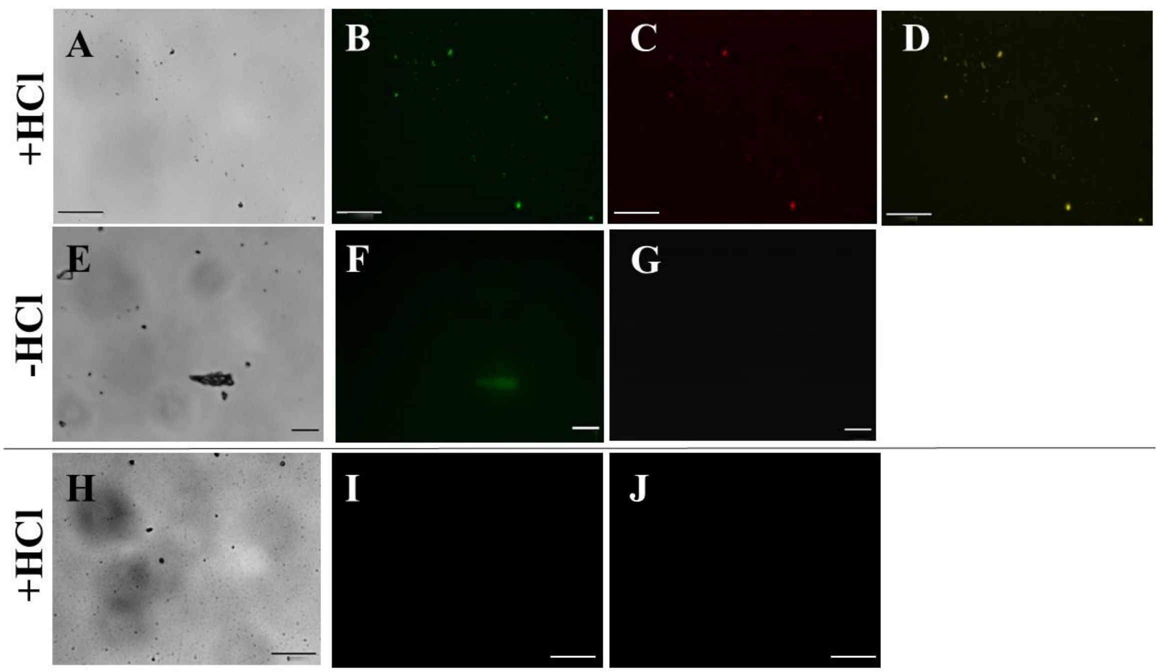

Figure 10: Images of SLNP samples prepared according to section 2.2.6 (molar ratio 6:90) and imaged with Axiovert S100 Fluorescent microscope. A) Brightfield, B) FITC laser/filter cube fluorescence, C) TRITC laser/filter cube images of SLNPs prepared in DI water of pH < 7.0, D) Composite image of A-C shows overlaps of brightfield, FITC, and TRITC-excited SLNPs. E) Brightfield, F) FITC laser/filter cube fluorescence, and G) TRITC laser/filter cube fluorescence images of SLNPs prepared in DI water of pH > 7.0. H) Brightfield, I) FITC laser/filter cube fluorescence, and J) TRITC laser/filter cube fluorescence images of unlabeled SLNPs in DI water (pH > 7.0). 63x magnification; scale bars are 5 μm.

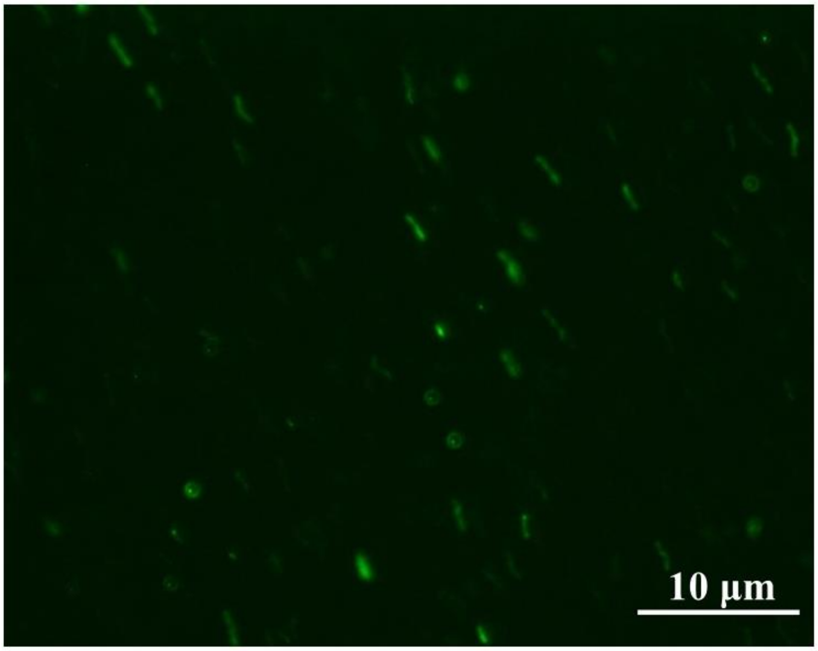

Figure 11: SLNPs imaged using FITC laser/filter cube of Axiovert S100 Fluorescent microscope for 2 second exposure time. Brownian motion of particles result in traces of fluorescence, which marks SLNP motion in DI water when exposed to excitation laser for 2 seconds. 40x magnification.

SLNPs stored in DI water with added HCl (pH < 7.0) exhibited both pH-dependent (pHrodo-red) and pH-independent (AF488) fluorescence as expected (Fig. 10 A, B, C). SLNPs stored in DI water without HCl (pH > 7.0) only exhibited pH-independent fluorescence, though in the images shown, the fluorescence is dull (Fig. 10 E, F, G). Fluorescence-free SLNPs did not fluoresce, thus confirming unlabeled SLNPs due not exhibit autofluorescence that affects pHrodo-red or AF488 output.

SLNPs were also imaged using STED microscopy with the assistance of Dr. Jena Goodman at the Cellular Imaging Core at Boston University Evans Biomedical Research Center to gain further insight into SLNP morphology (Fig. 12). SLNP samples were prepared according to section 2.2.8 and imaged for AF488 fluorescence in basic conditions (pH >7.0). Another sample of SLNPs was labeled with AF594, the optimal fluorophore for the current Abberior INFINITY STED laser configuration, for high resolution images of SLNPs.

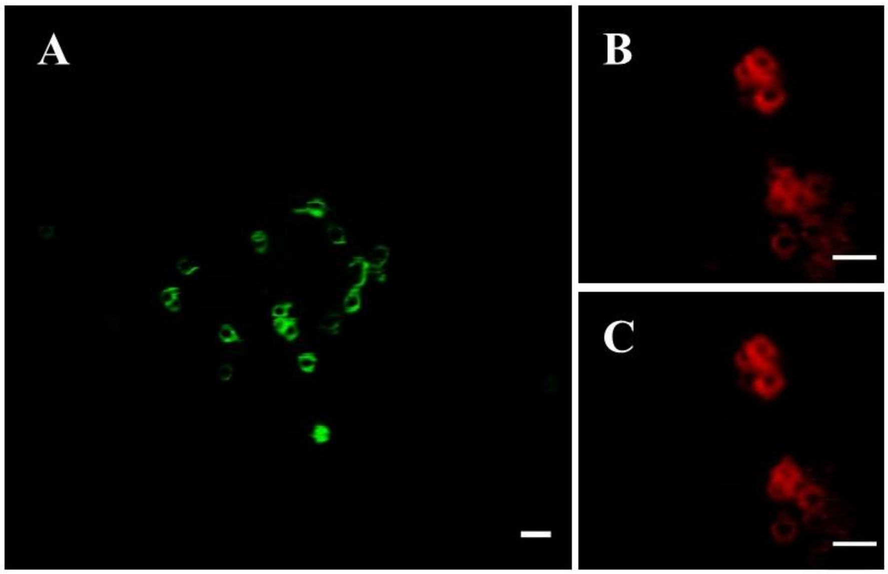

Figure 12: STED microscopy images of A) AF488/pHrodo-labeled (molar ratio 2:90) SLNPs and B-C) AF594-labeled SLNPs. All scale bars are 1 μm.

Insertion of the lipid conjugate on both AF488-PE and pHrodo-red-DPPE into the hydrophilic lipid shell of the SLNP was confirmed using the super-resolution abilities of STED microscopy. Fig. 12 suggests AF488-PE, pHrodo-red-DPPE, and AF594-PE tend to cluster in the lipid shell of the particle, producing a "halo" effect of fluorescence on the perimeter of each SLNP. Hydrodynamic diameter, measured with DLS, of AF488/pHrodo-red labeled SLNPs and AF594 labeled SLNPs was measured at 369.45 (pdi 0.260) and 222.30 (pdi 0.159), respectively.

Multiple washing and purification methods were implemented to isolate SLNPs in each sample. Either centrifugation using 100K MWCO or 10K MWCO centrifugation filters or dialysis with 10K MWCO SnakeSkin were used to retain large SLNPs and separate smaller particles and unused reagents for disposal. Centrifugation is an effective

SLNP purification method; however, it can be harsh and potentially reduce SLNP yield (Fig. 9) (Mihaila, et al.). Dialysis can also be an effective SLNP purification method and tends to be gentler than centrifugation. In this thesis, dialysis was primarily used as an alternative purification method when centrifugation units were unavailable. Hydrodynamic diameter and zeta potential were collected at 24 hours, 48 hours, 72 hours, 1 week, 2 weeks, 4 weeks, and 8 weeks post synthesis (Tbl. 6, Fig. 13). Hydrodynamic diameter, zeta potential, and sample yield for both centrifuged and dialyzed particles were comparable over 8 weeks, indicating both methods are suitable for SLNP purification.

Purification method	D_h (nm)	pdi	ZP (mV)	Yield (g)
Centrifugation	332.6±23.5	0.146±0.088	+ 30.12±16.14	3.44±0.62
Dialysis	293.5±20.6	0.212±0.064	+ 26.30±11.64	3.27±0.16

Table 6: Average hydrodynamic diameter and zeta potential (± standard deviation) were collected for centrifuged and dialyzed AF488/pHrodo labeled SLNPs over a 4-week period. Yield of centrifuged and dialyzed AF488/pHrodo-red labeled SLNPs was measured using methods described in section 2.2.4.

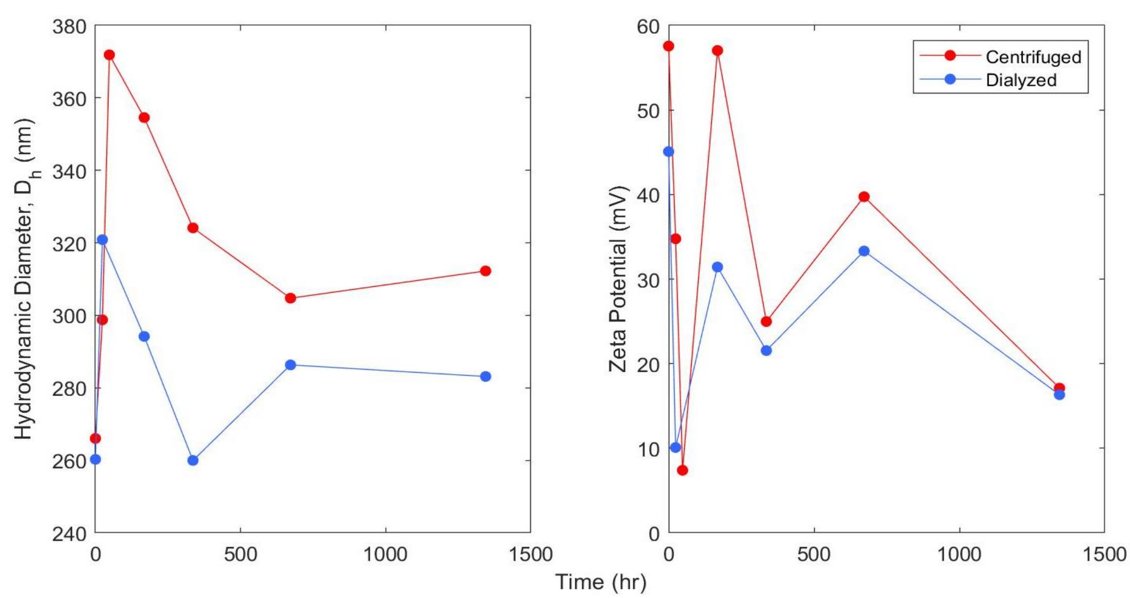

Figure 13: Hydrodynamic diameter (D_h) and zeta potential of centrifuged and dialyzed SLNPs over 8 weeks.

Mass concentration of AF488/pHrodo-red labeled SLNPs was determined by developing a UV Vis mass concentration curve. After synthesizing and purifying SLNPs, known volumes (0.5-1 mL) were separated into pre-weighed Eppendorf tubes for lyophilization according to section 2.2.3. The average concentration was calculated by dividing dried SLNP mass after lyophilization by known SLNP sample volume before lyophilization and was used to estimate the overall sample concentration. From these data, a UV Vis mass concentration curve was developed using diluted SLNP samples (section 2.2.4, Fig. 14).

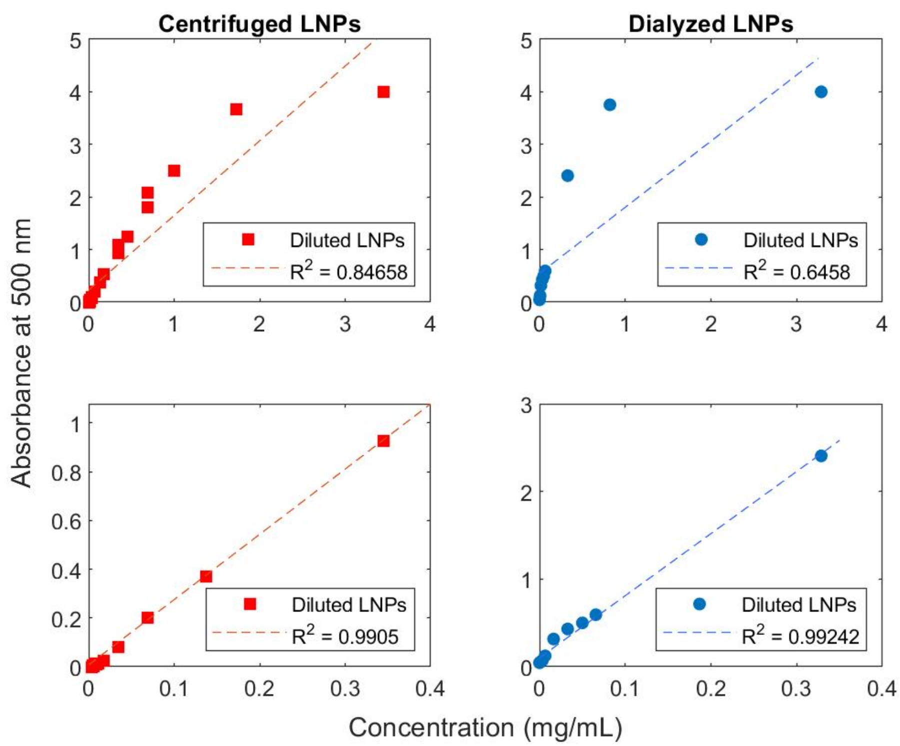

Figure 14: Mass concentration curves determined for AF488/pHrodo-red labeled SLNPs purified by centrifugation (red) and dialysis (blue). Samples were measured according to sections 2.2.3 and 2.2.4 and diluted to determine a linear calibration curve for future measurements. A) Centrifuged SLNP (y = 1.4204x + 0.2275) and B) dialyzed SLNP (y = 1.2587x + 0.5452) mass concentration curves are not linear when high concentration conditions are included. C) Centrifuged SLNP (y = 2.6772x + 0.0076) and D) dialyzed SLNP (y = 7.0916x + 0.1009) mass concentration curves are linear for more diluted samples (<0.4 mg/mL).

At high concentrations (greater than 0.4 mg/mL), SLNP mass concentration was non-linear (Fig. 14A, B). However, we expected to add low concentrations of SLNPs to cells (< 200 ug/mL). Therefore, we focused on concentrations below 0.4 mg/mL which demonstrated a linear relationship (Fig. 14C, D). These mass concentration curves were used to estimate SLNP mass concentration for all future AF488/pHrodo-red labeled samples depending on their purification technique.

Magnetic properties of SLNPs were assessed using techniques described in sections 2.2.9. SLNPs were successfully isolated after < 3 hours using the suspended ring magnet and over 24 hours using the block magnet (Fig. 15).

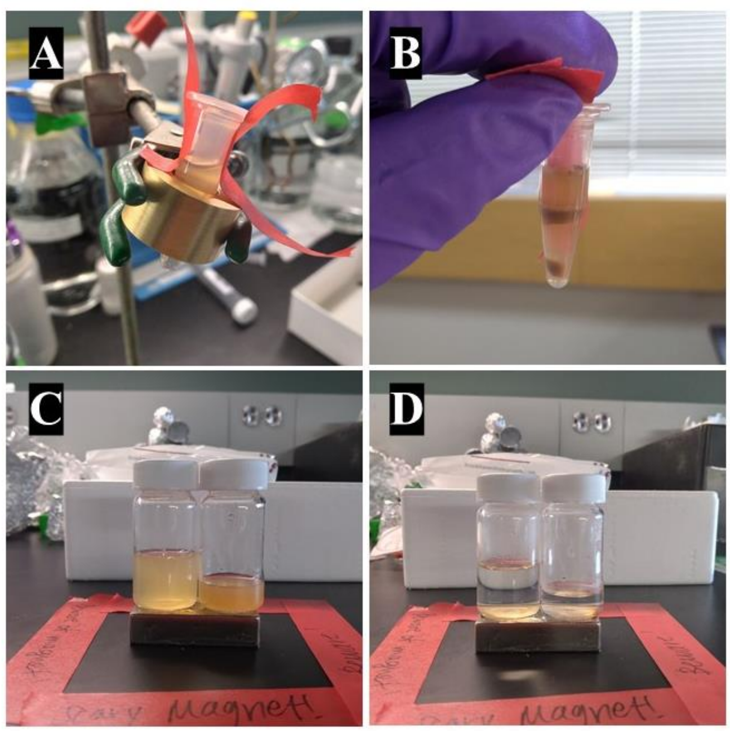

Figure 15: Magnetic properties of SLNPs determined using two different magnet types. A) Eppendorf tube of SLNPs taped to ring magnet elevated using ring clamp. B) Separation of SLNPs by ring magnet after 3 hours. Magnetic SLNPs accumulated in ring shape in Eppendorf tube in accordance with the ring's magnetic field. C) SLNP samples placed on block magnet at 0 hrs. D) Magnetic SLNPs accumulated at the bottom of the scintillation vial in accordance with the axial magnetic fields of block magnet overnight.

For both magnetic isolation methods, SLNPs could be easily resuspended after gently shaking the scintillation vial or Eppendorf tube. Additionally, a separate SLNP sample was left on a non-magnetic bench overnight to determine if gravitational accumulation influenced block magnet mediated SLNP attraction. SLNPs did not settle or separate without a magnetic field present, suggesting any accumulation seen in Fig. 15 is due to SLNPs being attracted to the external magnetic field.

Magnetically isolated SLNPs and non-magnetic SLNP "washout" were imaged with TEM to identify any morphological differences between magnetic SLNPs and non-magnetic SLNPs (Fig. 16). Magnetic SLNPs were taken from the dark, concentrated matter in Fig. 15B after the 3-hr ring magnet isolation and suspended with DI water. Non-magnetic SLNP washout was taken from the less turbid surrounding solution in Fig. 15B. Magnetic SLNPs are consistent, round, and surrounded by free SPIONs-OAm while non-magnetic SLNPs are irregular in shape and contain pores. These pores can be created when small water drops are emulsified inside toluene drops during SLNP emulsification, most likely due to an excessive amount of surfactant. Therefore, it appears there are two distinct morphologies that distinguish magnetic and non-magnetic SLNPs synthesized from the current emulsion protocol. Free SPION-OAms in dual-labeled SLNP samples and optimizing SPION-OAm/surfactant content in the SLNP synthesis protocol are further discussed in section 3.5 and 4.2.

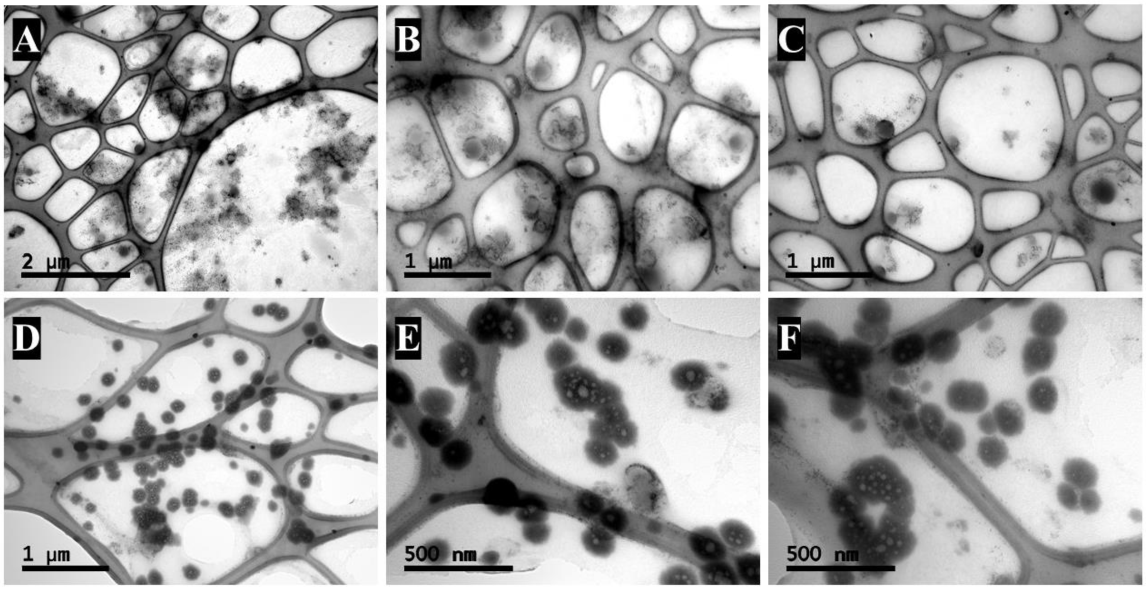

Figure 16: TEM images of A-C) magnetically isolated FITC/pHrodo-red labeled SLNPs from ring magnet setup, B) and D-F) SLNPs not magnetically isolated in remaining washout.

SLNPs should be sterilized prior to any cell work and long term storage. In previous studies, SLNPs labeled with pHrodo-red were sterilized by a 0.2 µm filter before incubating with peritoneal washout cells (Yu). Based on hydrodynamic diameter measurements of AF488/pHrodo-red labeled SLNPs (which consistently exceed 0.2 µm), a larger filter (0.45 µm) was tried. However, upon trying both polyether sulfone (PES) and polyvinylidene difluoride (PVDF) filters of 0.45 µm, sterilization of AF488/pHrodo-red labeled SLNPs (purified by dialysis) was unsuccessful due to clogging of the filter. Samples sterilized by both types of filters were lyophilized overnight with known volumes to determine loss of SLNPs after filtration, but no recoverable mass remained. These data suggest significant agglomeration of particles likely contributed to clogging in both filter types. Fig. 17 shows collection of SLNPs in each filter and differences in turbidity of SLNP samples before and after filtration. Additionally, DLS of each sample shows that larger particles/aggregates had been removed, resulting in a lower hydrodynamic diameter after filtration (Tbl. 7). Zeta potential increased slightly before and after filtration, indicating overall SLNP stability was slightly increased by PES or PVDF filtration. Despite the positives of removing large aggregates and increasing particle stability, yield was too low for filtration with 0.45 μm PES or PVDF filters to be a useful sterilization method for AF488/pHrodo-red labeled SLNPs. Previous work has acknowledged the poor recovery of NPs when sterilizing with filters, especially when particles exceed 200 nm in diameter (Tapia-Guerrero).

Filter Type (0.45 um)	Fluorescence	D_h (nm)	pdi	ZP (mV)
none	None	277–371	0.053–1.480	+37.33–40.96
PES		198–273	0.175–0.213	+40.37
none	AF488/pHrodo-red	386–455	0.215–0.336	+34.09
PES		145–149	0.138–0.192	+38.49
PVDF		120–141	0.092–0.334	-

Table 7: Hydrodynamic diameter (nm) and zeta potential (mV) of unlabeled and AF488/pHrodo-red labeled SLNPs before and after filtration by 0.45 μm PES or PVDF filters.

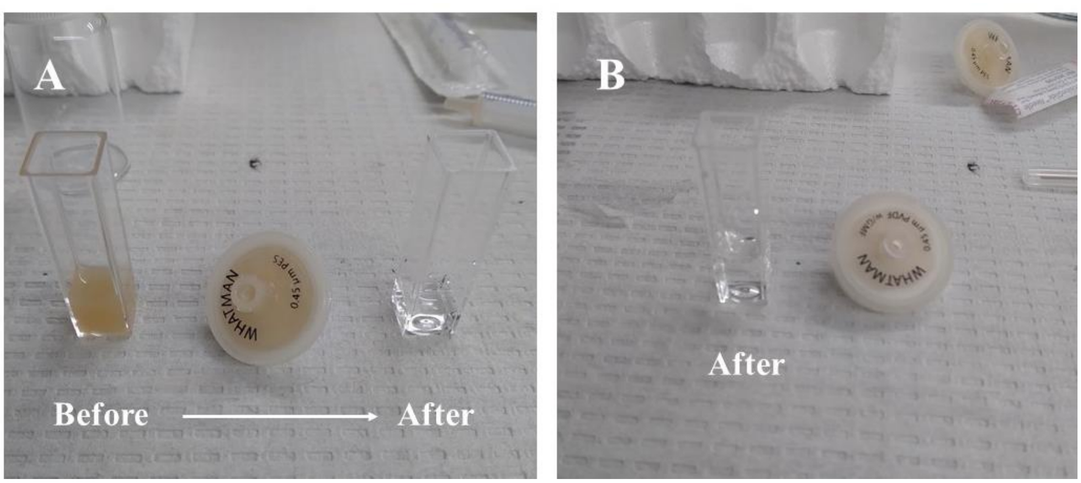

Figure 17: AF488/pHrodo-red labeled SLNP samples before and after filtration with A) 0.45 μm PES filter or B) 0.45 μm PVDF filter. Both filters appear to have stopped most SLNPs from passing through during the filtration. A transparent solution with a significantly reduced yield of SLNPs was collected post-filtration.

Therefore, an alternative sterilization method was needed to improve SLNP yield post-sterilization. UV light sterilization was selected as previous work established 30-60 minutes under UV light was sufficient to sterilize polymeric and lipid nanoparticle samples and did not significantly impact nanoparticle properties (Tapia-Guerrero, Bernal-Chavez et al.). SLNP samples in this work were prepared according to section 2.1.3 and sterilized for 30-60 minutes under the biosafety cabinet.

	Unsterilized SLNPs	UV-Sterilized SLNPs
D_h (nm)	362.0 ± 23.2	410.5 ± 47.1
pdi	0.378 ± 0.414	0.445 ± 0.511
ZP (mV)	13.27 ± 1.73	27.16 ±2.25

Table 8: Hydrodynamic diameter (nm) and zeta potential (mV) of unsterilized and UV-sterilized AF488/pHrodo-red labeled SLNPs stored in phenol-free RPMI 1640 media. SLNP hydrodynamic diameter and zeta potential both increased after 30-60 minutes of UV sterilization.

SLNP hydrodynamic diameter and zeta potential both increased after 30-60 minutes of UV radiation, though increase in size was comparable to short term stability studies in RPMI media (Fig. 18). Resulting hydrodynamic diameter data confirm observations of UV light-related impact on SLNP size, though these experiments should be repeated to determine if this increase is due to UV exposure (Bernal-Chavez et al., Tapia-Guerrero). Increase in zeta potential is significant, indicating increased SLNP stability, though additional studies would be useful to confirm this increase is due to UV sterilization.

Short- and long-term stability studies were conducted on SLNP samples to determine current shelf-life and change in nanoparticle properties over time in cell-friendly storage solvents. Yu’s work demonstrated that SLNPs were stable for at least 72 hours in pH balanced DI water (pH > 7.0), which was sufficient for the timeline of cell phagocytosis experiments (Yu). However, even a small volume of DI water (~10%), when added to cells, can be toxic. A more cell-friendly storage solvent would help reduce unwanted cytotoxic effects when incubating SLNPs with cells.

Short term stability studies were conducted for AF488/pHrodo-red labeled SLNPs in phenol-free RPMI 1640 media (with and without heat-inactivated fetal bovine serum) by measuring hydrodynamic diameter at multiple time points over 24 hours, the maximum planned incubation time of cells and SLNPs for future experiments (Fig. 18). Noticeable SLNP aggregation occurred in HI-FBS-free media within the first 2 hours which made the samples not suitable for DLS/ZP characterization, so results were not collected. In HI-FBS-containing media, changes in hydrodynamic diameter were comparable to DI water, suggesting there is little change in SLNPs stability in media and should not be a concern for cell studies. However, absolute magnitude of zeta potential of SLNPs in HI-FBS containing media was significantly lower than SLNPs in DI water, suggesting particles are less stable when stored in media. Overall, the fold change of hydrodynamic diameter and zeta potential of SLNPs stored in either solvent over time did not fluctuate significantly, suggesting SLNP size and charge remain constant over 24 hours.

Reduced aggregation of SLNPs in HI-FBS containing media compared to HI-FBS free media may be due to adsorption of HI-FBS protein on the surface of SLNPs, reducing SLNP-SLNP interactions and resulting instability (Wiogo et al.). However, previous work has demonstrated an increase in hydrodynamic diameter of PEG-coated SPIONs in 50% serum solution, likely due to protein corona formation (Meisel et al.). These studies should be repeated, potentially with a range of serum concentrations, to confirm reduced aggregation size of SLNPs in FBS-containing conditions.

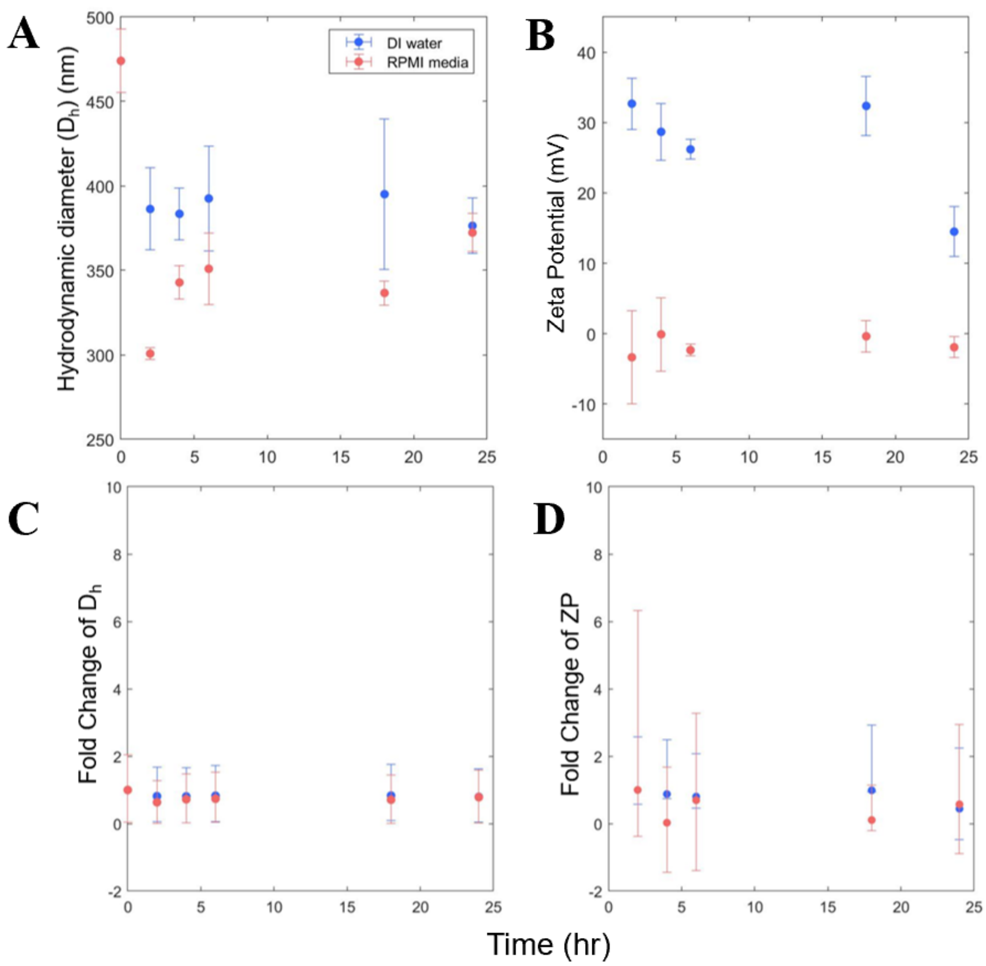

Figure 18: Short term stability studies of AF488/pHrodo-red labeled SLNPs stored in DI water (pH > 7.0) and RPMI 1640 media (with 10% HI-FBS). A) Hydrodynamic diameter and B) zeta potential of SLNPs stored in DI water and RPMI 1640 media. Fold change of C) hydrodynamic diameter and D) zeta potential of SLNPs in DI water and RPMI 1640 media.

Long term stability studies were conducted for AF488/pHrodo-red labeled SLNPs stored in pH balanced DI water (pH < 7.0), RPMI 1640 media (without HI-FBS), and 1% phosphate buffered solution (PBS) in 4 ºC or -20 ºC over an 8-week period (Fig. 19). Noticeable aggregation began to occur in both HI-FBS-free media and PBS conditions, indicating significant SLNP instability in these storage solvents (Wiogo et al.) (Fig. 19C). Noticeable aggregation began to occur for SLNPs in DI water at 4 ºC (original storage condition) as well, but only around week 4.

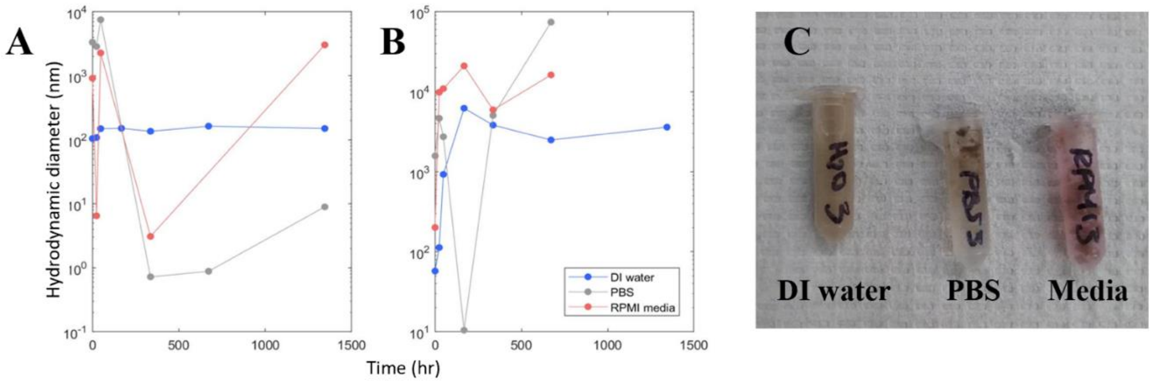

Figure 19: Hydrodynamic diameter of AF488/pHrodo-red labeled SLNPs stored in DI water (pH > 7.0), PBS, RPMI 1640 media (10% HI-FBS) in A) 4 ºC and B) -20 ºC was measured. C) SLNP samples stored in Eppendorf tubes after 24 hours in 4 ºC. Visible aggregation is present in PBS and RPMI 1640 media.

Both stability studies provided useful information about the impact of storage solvents on SLNP stability over time. Short term stability studies indicated a low impact of phenol-free, HI-FBS-containing RPMI 1640 media on SLNP stability (fold change of D_h and ZP over time) compared to the standard pH balanced DI water storage solvent over 24 hours. Long term stability studies demonstrated that out of the three solvents tried, DI water maintained SLNP stability over a longer period than PBS and HI-FBS-free media (Wiogo et al.). Additionally, long term stability studies suggest the maximum shelf life of SLNPs stored in DI water at 4 ºC is around 4 weeks.

Additional single and dual fluorophore combinations were also explored (Fig. 20). Another pH insensitive fluorophore FITC, which has a nearly identical fluorescence emission to AF488, was added to SLNPs as DSPE-PEG-FITC according to section 2.1.3.i in place of AF488 (The University of Mississippi Medical Center). SLNP hydrodynamic diameter and zeta potential measurements are detailed in Table 9.

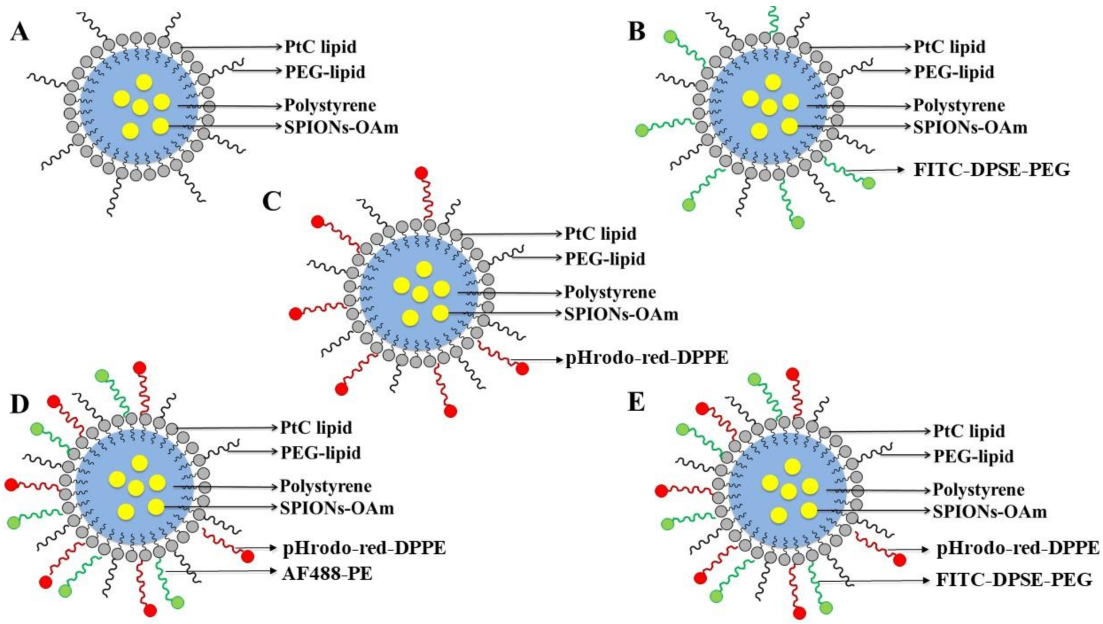

Figure 20: All fluorophore combinations for SLNPs examined. A) Fluorescence-free as negative control, B) FITC only, C) pHrodo-red only, D) AF488/pHrodo-red, and E) FITC/pHrodo-red.

Fluorophores	D_h (nm)	pdi	ZP 24 hr(mV)	ZP 1 week (mV)
None	452.2±18.4	1.860±0.939	+58.03±5.50	+14.12±1.58
pHrodo-red/FITC	379.0±25.7	1.456±1.620	+19.16±7.69	+41.20±2.75
FITC	543.5±22.6	0.191±0.132	+28.59±6.35	+53.87±2.39
pHrodo-red/AF488	248.6±8.2	0.107±0.051	+56.91±4.45	+55.49±3.31
pHrodo-red	313.5±25.7	1.572±0.735	+ 9.24±5.24	+47.92±1.43

Table 9: Hydrodynamic diameter (nm) and zeta potential (mV) of SLNPs with different fluorophore combinations at 24 hours and 1 week post synthesis.

According to the results in the table above, all SLNP formulations have varying hydrodynamic diameter and *positive* zeta potential values. These results, compared with single SLNP diameter data from TEM images of AF488/pHrodo-red SLNPs (dialyzed) in sections 3.4-3.5 demonstrate there was aggregation of samples for all fluorophore conditions. Additionally, zeta potential for all fluorophore combinations were collected 1-

week post-synthesis (stored in DI water at 4 ºC) showed fluctuations in aggregate stability. All SLNP samples (except single fluorophore pHrodo-red labeled SLNPs) had positive zeta potential values with magnitude > 10 mV at least 1-week post-synthesis, indicating high stability (especially above 30 mV) (Shao et al.).

pHrodo-red/FITC labeled particles were also imaged using fluorescent microscopy to observe their morphology, size distribution, and fluorescent strength and compare to AF488/pHrodo-red labeled SLNPs (Fig. 21). In Fig. 21A and B, a large feature with both FITC and pHrodo-red fluorescence was imaged, though it was mostly likely a collection of lipid conjugated fluorophores that have not been properly removed with dialysis.

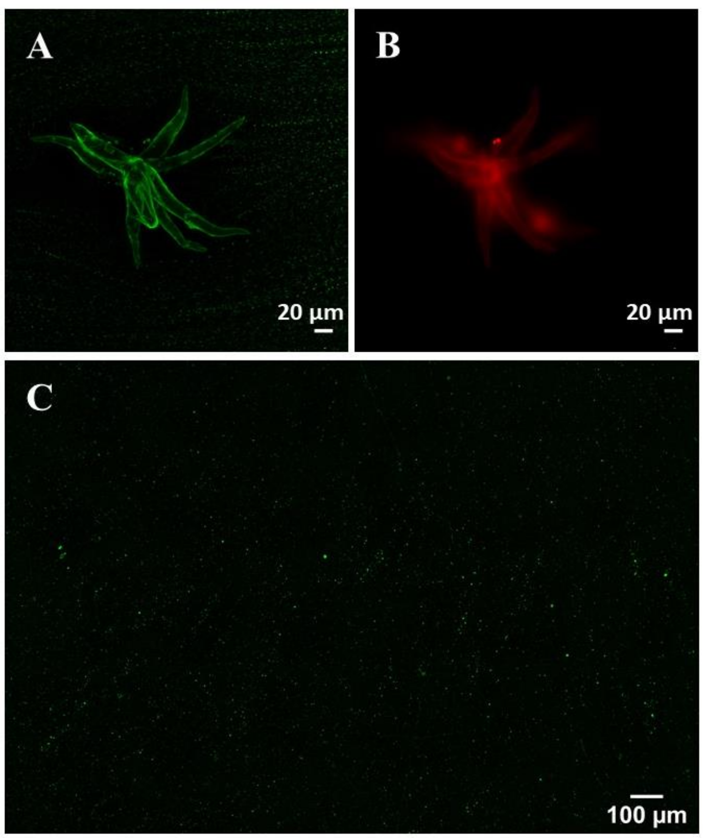

Figure 21: Fluorescent images taken with Olympus IX83 Inverted Fluorescence microscope of FITC/pHrodo-red labeled SLNPs using FITC and TRITC laser/filter cubes, including an unknown form likely created by fluorophore-labeled lipids. A) FITC

laser/filter cube fluorescence of SLNPs. B) TRITC laser/filter cube fluorescence of SLNPs. C) FITC laser/filter cube fluorescence of SLNPs.

FITC proved to be a robust fluorophore and sufficient alternative pH-insensitive marker, labeling SLNPs as well as or better than AF488. However, in this sample, pHrodo-red did not fluoresce even in acidic conditions. It's possible the pHrodo-red-DPPE was old and/or no longer robust enough to detect for nanoscale SLNPs.

3.4 J774A.1 Monocyte Cell Studies

3.4.1 Cell Line Selection

In this thesis work, we aimed to improve stability, batch consistency, and scalability of SLNP formulations and test the uptake of SLNPs with phagocytosing cells *in vitro*. Prior to designing the *in vitro* model, we needed to decide on a cell population to test with SLNPs. NIMPABs, which are the target cell type for our SLNPs, would assess the selective induction of phagocytotic behavior and efficacy of resulting cell isolation (Vo et al.). However, these cells are very rare and require *ex vivo* extraction to study (Yu). Monocyte cells, which can non-discriminately phagocytose particles, would not assess the selective induction of phagocytic behavior and subsequent isolation of the target cell type, but are much simpler to use. There are several monocyte cell lines with established protocols, making these lines easy to use and a much simpler population to work with than NIMPABs. Testing SLNP formulations on a natively phagocytosing cell line can provide insight into general cell-SLNP phagocytic success and magnetic isolation, allowing for optimization and testing of the SLNP that could be easily repeated applied to NIMPAB studies in the future. These cells can also be diluted with non-phagocytosing cells to mimic rare cell populations in future experiments (section A.2). Therefore, we selected J774A.1 mouse monocyte cells (referred to as J774 cells for the remainder of this thesis) as an *in vitro* model cell line for SLNP incubation experiments.

3.4.2 J774A.1 Phagocytic Behavior

Prior to examining SLNP uptake by J774 cells, spontaneous phagocytic behavior (no phagocytosis-stimulating reagents were added) of various cell concentrations was examined using a Vybrant Phagocytosis Assay Kit according to manufacturer's protocol (section 2.3.3). Results from the Vybrant Phagocytosis assay indicate uptake of fluorescein-labeled *Escherichia coli* (*E. coli*) by J774 cells over the 2-hour incubation period was concentration-dependent and sufficient for future SLNP studies. Cell only and media only negative controls were implemented to examine any autofluorescence of non-bioparticle materials in the experiment (Fig. 22).

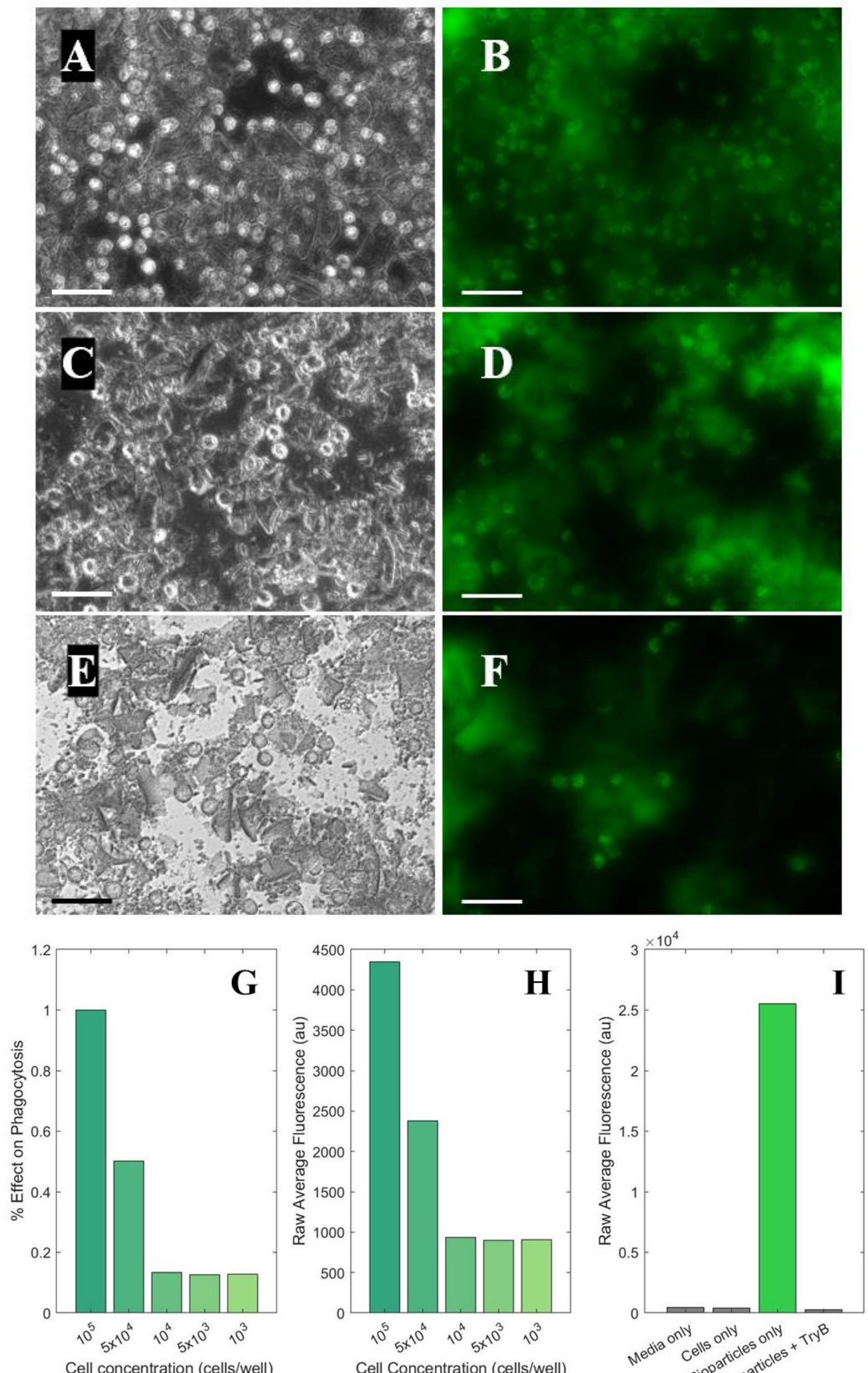

Fig. 22: Fluorescein-labeled bioparticles were phagocytosed and fluoresced in a cell concentration-dependent condition, with the highest J774 concentration displaying increased uptake and bioparticle fluorescence. Phase contrast, brightfield, and fluorescent images of Vybrant Phagocytosis Assay results taken with Keyence All-in-One Fluorescent microscope at 40x magnification. A) Phase contrast and B) fluorescent microscopy of 10^5

cells/well condition, C) phase contrast and D) fluorescent microscopy of 10^4 cells/well condition, E) brightfield and F) fluorescent microscopy of 10^3 cells/well condition. G) Percent effect on phagocytosis was calculated using Vyrbant Phagocytosis Assay protocol, with cell only results as negative control and 10^5 cell/well results as positive control. Average raw fluorescence (au) for H) experimental cell concentrations and I) negative (media only, cells only, bioparticles with trypan blue) and positive controls (bioparticles only). Scale bars, 60 μm.

Additionally, AF488/pHrodo-red labeled SLNP uptake was observed briefly during the Vybrant Phagocytosis Assay using the protocol detailed in section 2.3.4. A few experimental conditions and measurement techniques were tried to develop a standardized protocol for future SLNP phagocytosis assays (Fig. 23).

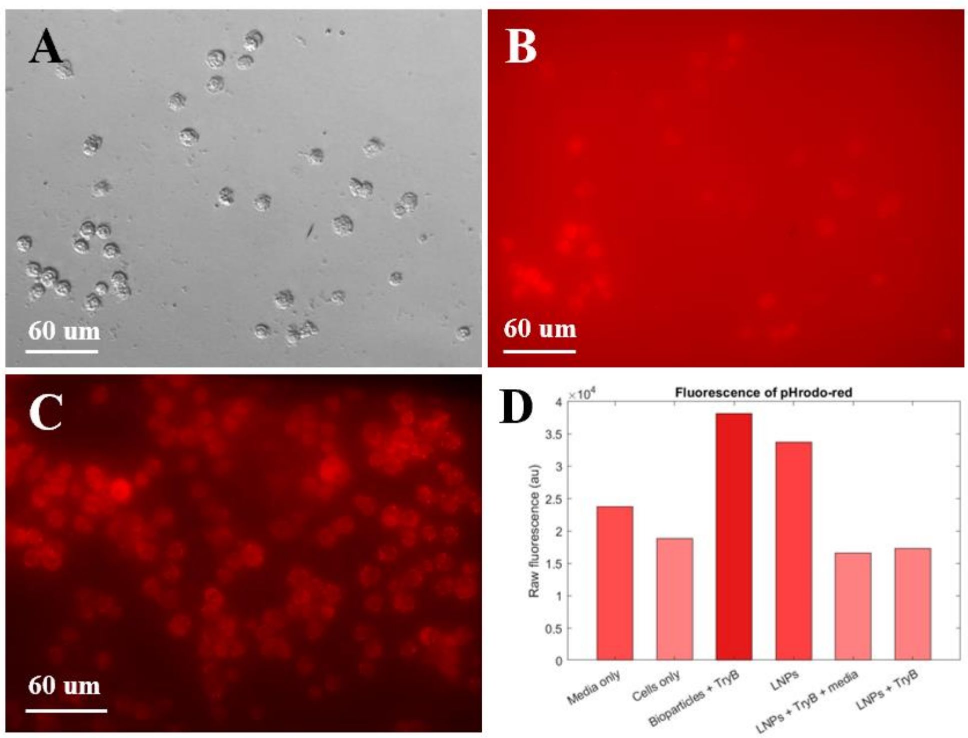

Fig. 23: AF488/pHrodo-red labeled SLNPs were phagocytosed by and fluoresced in J774 cells. SLNP phagocytosis assay was executed according to section 2.3.4. A) Brightfield and B) fluorescent microscopy images of 10^5 cells at 40x after trypan blue addition. C) Fluorescent microscope image of 10^5 cells at 40x after trypan blue addition. D) Raw fluorescence output from negative controls (phenol-free RPMI 1640 media only, cells only, fluorescein-labeled *E. coli* bioparticles + trypan blue) and experimental conditions (cells with SLNPs, SLNPs + trypan blue + media, SLNPs + trypan blue).

From these results, we determined that adding trypan blue for 1 minute after SLNP phagocytosis allowed us to better distinguish phagocytosis of SLNPs by live cells. By adding trypan blue, extracellular SLNPs would also be quenched. Therefore, we adopted this practice when conducting our next round of SLNP phagocytosis experiments (section 2.3.5). Additionally, we discovered SLNP fluorescence from pHrodo-red is likely not strong enough to be measured by a spectrometer, and focused future experiments on fluorescence microscopy driven observations and flow cytometry. However, this assay was conducted once to observe SLNP phagocytosis, analyze results, and develop a standardized, *in vitro* SLNP phagocytosis study to be repeated. Additional spectrometer readings would help determine if SLNP-mediated pHrodo-red fluorescence is consistently too low for spectrometer quantification.

The next SLNP phagocytosis assay was conducted according to the protocol detailed in section 2.3.5. AF488/pHrodo-red labeled SLNPs were incubated with J774 cells for 3, 4.5 and 6 hours at 30 ug/mL concentration in a 96-well plate, which were imaged using Axiovert S100 Fluorescent microscope (Fig. 24).

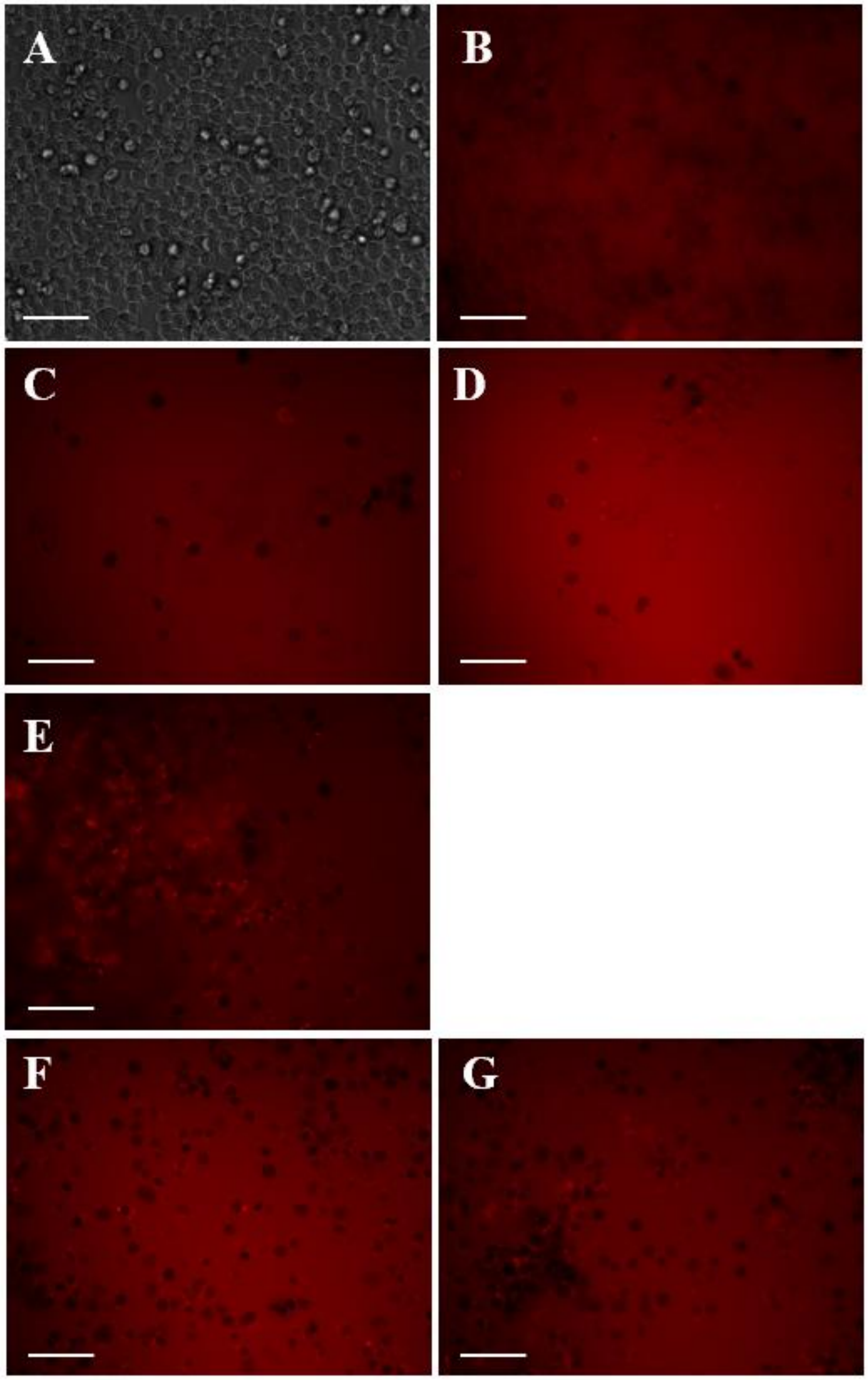

Figure 24: J774A.1 cells incubated with AF488/pHrodo-red labeled SLNPs according to the protocol outlined in section 2.3.5. A) Brightfield microscopy cells only; B) Fluorescence microscopy (with TRITC-laser/cube) of cells only. Fluorescence microscopy of cells with AF488/pHrodo-red labeled SLNPs incubate for C–D) 3 hours, E) 4.5 hours, and F–G) 6 hours.

Based on these results, there is little phagocytic uptake during 3-hour incubation but increases with 4.5- and 6-hour incubation periods. However, cell death, marked by trypan blue-filled cells, also appears to increase with increased incubation time. Though isolated cells do not need to remain alive for the long-term goal of studying immunotherapeutic potential, cells must remain alive and intact for the duration of phagocytosis and magnetic isolation (12-24 hours).

Fluorescence activated cell sorting (FACS) was used next to quantify SLNP uptake. J774 cells were incubated with SLNP conditions listed in Table 10 to quantify SLNP uptake in high concentration/long incubation (155 ug/mL; 6 hr), high concentration/short incubation (155 ug/ml; 3 hr), and low concentration/long incubation (30 ug/mL; 6 hr) conditions. Cells were fixed according to (section 2.3.7) and results were collected with the help of Belle Ye (Fig. 25, Tbl. 10). AF488 fluorescence levels were low indicating pH-insensitive fluorescence in this sample were not particularly robust. pHrodo-red did fluoresce in SLNP-containing conditions, indicating successful phagocytotic did occur in SLNP-containing conditions. However, significant cell death, marked by low cell granularity, small cell size, and major cell loss during centrifugation during preparation of samples for FACS, had occurred in all SLNP-containing samples (data not shown).

Phagocytosis conditions		Freq. of Parent		Geometric Mean	
Incubation time (hr)	SLNP Concentration (ug/mL)	Cells/GFP+	Cells/ mRuby2-A +	Cells (GFP-A)	Cells (mRuby2-A)
6	0	0.042 %	0.034 %	53.7	359
3	155	10.3 %	1.91 %	359	1416
6	30	4.04 %	2.66 %	248	1060
6	155	16.1 %	2.35 %	393	1413
	Mean	7.62 %	1.74 %	263	1062
	SD	7.06 %	1.18 %	153	498

Table 10: Results of FACS assay using fixed cell samples. GFP+ detects green fluorescence from pH-insensitive green fluorophore, mRuby2-A+ detects pH-sensitive red fluorophore.

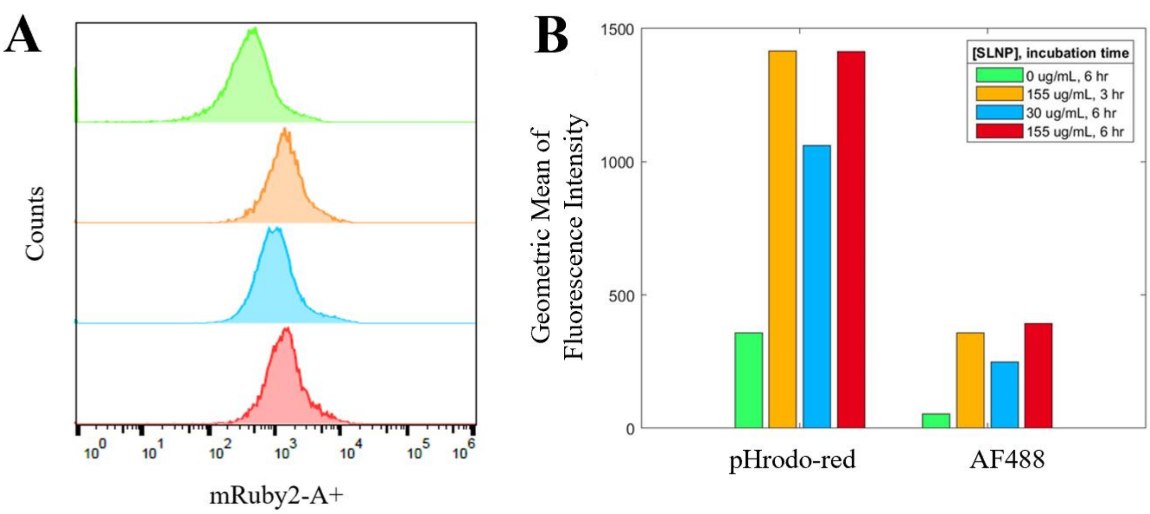

Figure 25: A) J774 cells expressing pHrodo-red (mRuby2-A+). B) Geometric mean fluorescence intensity of pHrodo-red and AF488. All conditions containing SLNPs show increased cell numbers at higher intensity of pHrodo-red fluorescence. AF488 fluorescence does not distinctly increase in fluorescence intensity in SLNP-containing conditions.

An additional FACS assay was executed under the guidance of Dr. Xuemei Zhong and Dr. Wenda Gao at Antagen Biosciences, Inc (data not shown). Three experimental conditions (155 ug/mL SLNP/3-hour incubation, 90 ug/mL SLNP/6-hour incubation, 30 ug/mL SLNP/18-hour incubation) were plated and fixed. We did notice intracellular pHrodo-red fluorescence in both 3- and 6-hour conditions. Unfixed cells stained with a monocyte cell marker exhibited high fluorescence, and the cell only negative control exhibited very low fluorescence, as expected. Again, significant cell death was detected in all SLNP-containing conditions.

These unexpected results prompted an investigation into the reversibility of pHrodo-red (due to pH increase of buffer fixed cells are stored in). Fluorescence of pHrodo-red after phagocytosis can be reversed after fixation, as cell membranes are broken and can allow the more basic solution to interact with and decrease intensity of pHrodo-red fluorescence, especially after 24-48 hours (Meena & Kimmel, Luce-Fedrow et al., Berger et al.).

With this information, we transitioned to unfixed live cell FACS quantification of SLNP uptake (section 2.3.7) to remove any adverse effects of cell fixing on cell viability and pHrodo-red fluorescence. However, cell death was still significant in these conditions, regardless of SLNP concentration or incubation time (data not collected). These assays were conducted once and likely need to be repeated to confirm the observation of high cytotoxicity and limited phagocytosis.

3.4.3 Cytotoxicity of SLNPs

To further investigate the high cytotoxicity detected in FACS assays, SLNP-induced cell death was directly examined using an MTT assay described in section 2.3.6. AF488/pHrodo-red labeled SLNPs were incubated with cells for 3 and 6 hours at 20 ug/mL – 200 ug/mL, and cytotoxicity was determined using MTT according to the manufacturer’s protocol. Yu’s work established that pHrodo-red labeled SLNPs, incubated with cells at 100:1 and 150:1 ratios, did not significantly impact cell death during 3- and 6-hour incubation periods using trypan blue exclusion assay (Yu). However, in this study, all

AF488/pHrodo-red labeled SLNP concentrations induced significant cell death over 3- and 6-hour incubation periods.

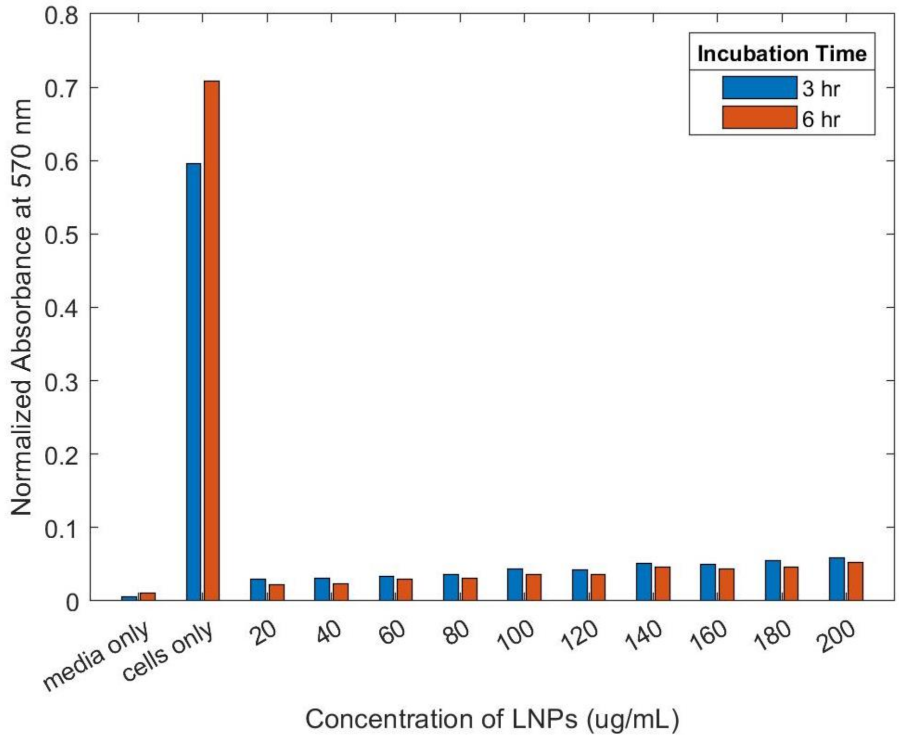

Figure 26: J774 cell viability after 3-hour or 6-hour incubation with varying concentrations of SLNPs was quantified with absorbance values at 570 nm normalized to absorbance at 670 nm according to MTT protocol. Massive cell death occurred at all SLNP concentrations and incubation periods.

3.5 Modification of SLNP Formulation

We hypothesized the significant cytotoxicity could be a result of one of the following:

1. <u>Positive zeta potential</u>: As described in section 3.3, all SLNPs, regardless of fluorophore configuration, had a positive zeta potential of high magnitude. Positively charged particles have demonstrated potent cytotoxic effects in a variety of work, suggesting a highly positive zeta potential could be the cause of J774 cell death (Shao et al., Sukhanova et al., Fröhlich).

2. <u>Concentration of SLNP sample</u>: Previous work used Nanoparticle Tracking Analysis (NTA) to determine number concentration of SLNPs for each sample (Yu). Due to access and time issues, number concentration could not be determined, and thus, a simpler method was used to quantify SLNP yield and mass concentration. Unfortunately, there was no direct relationship established between SLNP mass concentration and number concentration, and thus, replicating Yu's study was not possible. Based on prior literature, a concentration range of 20 – 200 ug/mL was selected for this initial cytotoxicity study but may have been too concentrated for J774 cells (Vo et al., Yameen et al.). Previous studies have also demonstrated increased cytotoxicity with higher NP concentrations (Shao et al.). Establishing a relationship between SLNP number and mass would help determine an optimal concentration to maximize phagocytotic uptake and minimize cytotoxicity. A known SLNP number and mass concentration ratio would also help establish a reproducible protocol regardless of access to number or mass concentration quantification techniques.
3. <u>Sterilization of SLNPs</u>: UV sterilization techniques were used to sterilize SLNPs prior to cell studies instead of filters due to significant clogging (Tapia-Guerrero, Bernal-Chavez et al.). However, more rigorous studies could be conducted to verify UV sterilization is sufficient and does not introduce cytotoxic effects compared to unsterilized or alternatively sterilized SLNPs (filtered, gamma radiation, etc.).

We began examining the first hypothesis, determining which component(s) of the SLNP contributed to positive zeta potential. Previous literature suggests PtC, PEG, AF488, PE, pHrodo-red and DPPE do not contribute to a positive zeta potential (Stillwell, Zanetti-Domingues et al., Luangtana-anan et al.). However, in this work, a pH-insensitive fluorophore, AF488, was added to the original SLNP formulation detailed by Yu. Several fluorophore configurations were synthesized, and hydrodynamic diameter and zeta potential were measured to determine if added fluorophore(s) impacted zeta potential (Tbl. 9). All fluorophore combinations produced SLNP samples with positive zeta potential, and thus, we eliminated AF488-PE as the main contributor to positive zeta potential. It is important to note that 24 hours post-synthesis, pHrodo-red only SLNPs had the lowest magnitude zeta potential, potentially reducing cytotoxic potential compared to SLNP samples with zeta potentials of higher magnitude (Shao et al.).

TEM images were captured of AF488/pHrodo-red labeled SLNPs purified by dialysis to better observe SLNP morphology than other microscopy methods and confirm SLNPs were synthesized properly.

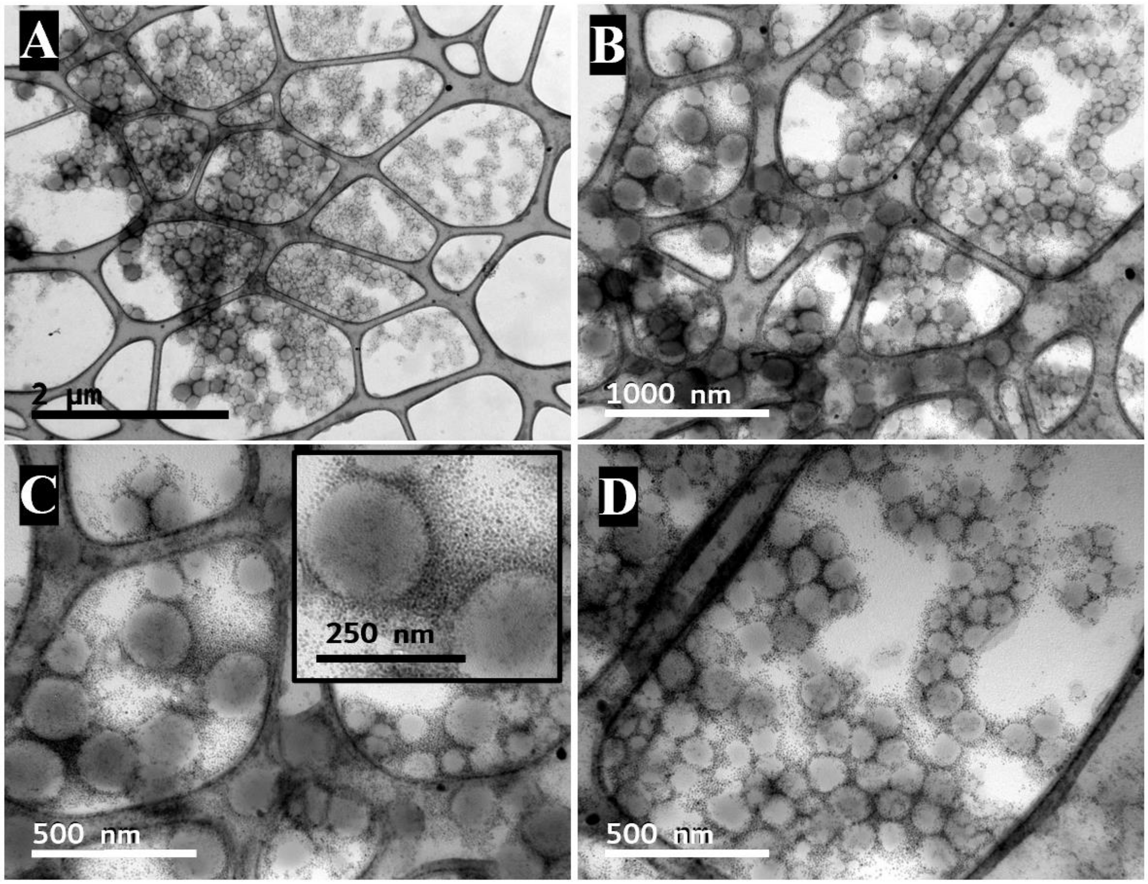

Figure 27: TEM images of AF488/pHrodo-red labeled SLNPs purified by dialysis. Both SLNPs and free SPIONs (clustered at the surface of SLNPs) were captured. Scale bars are A) 2 µm, B) 1000 nm, C) 500 nm (inset 250 nm) and D) 500 nm.

Average single particle size of 100.90nm ± 34.99nm (standard deviation) was calculated using ImageJ analysis tools on TEM images (Fig. 27). Morphology of the AF488/pHrodo-red labeled SLNPs (dialyzed) was round and consistent for each particle, indicating successful synthesis of lipid shell/polymer core. A small number of SLNPs appear to have SPIONs-OAm in their core, but it is not possible to distinguish intra-SLNP SPIONs and SPIONs on top of/under SLNPs in TEM (Sundaram). However, there were large groups of particles of 5-10 nm in size surrounding SLNPs, which were most likely SPIONs-OAm that had not been properly incorporated into or removed from synthesized

SLNPs (Fig. 25C, inset). Overnight drying of sample and solvent elimination for TEM grid preparation may cause SPION and SLNP aggregate formation, and thus, SPION clustering near the surface of SLNPs may not indicate how SPIONs aggregate with SLNPs in solution (Wulandri et al.). However, large numbers of free SPIONs-OAm exist in the dialyzed sample, indicating magnetic SLNP cores were not being synthesized properly and potentially contributing to positive, high magnitude zeta potential and resulting cytotoxic effects.

These results suggest two potential issues with the current SLNP protocol:

1) <u>Purification Method</u>: The purification method used for this sample, dialysis (section 2.1.3.ii), was not sufficient to remove free SPIONs-OAm from the surface of SLNPs.

2) <u>SPION-OAm incorporation into SLNP core</u>: SPIONs were not successfully attracted to and incorporated in the core of SLNPs, resulting in an excess of external SPIONs-OAm. This may be due to surfactant-SPION interaction and/or a non-optimal SPION-coating/polymer pair in SLNP formulation.

To understand how and why SPIONs-OAm were not being encapsulated in the SLNP core and instead remained outside the particles, both potential issues were explored with TEM. Free SPION presence due to SLNP purification method was examined by imaging AF488/pHrodo-red labeled SLNPs purified using 10K MWCO centrifugal filter (Fig. 28).

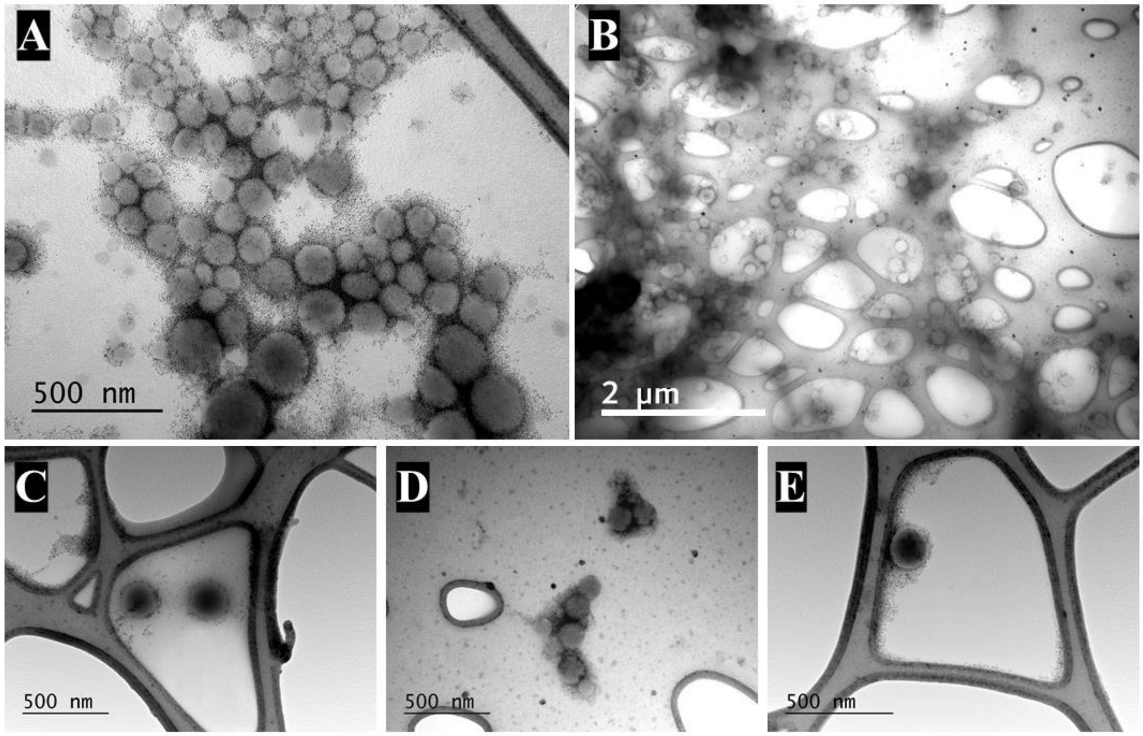

Figure 28: TEM images of A) AF488/pHrodo-red labeled SLNPs purified by dialysis and B-E) FITC/pHrodo-red labeled SLNPs purified by centrifugation. Free SPION-OAm concentration was observed to determine if one purification method better removed free SPIONs-OAm and purified SLNPs than another.

Compared to the dialyzed sample, the concentration of free SPIONs in the centrifuged sample was lower, suggesting centrifugal purification was better at removing free SPIONs from the SLNP sample than dialysis. However, there were still noticeable clusters of SPIONs around SLNPs, indicating the current centrifugation steps were not sufficient to remove free SPIONs from the sample (Fig. 28C-E). These observations are merely qualitative and should be confirmed with additional TEM studies and quantitative analyses.

SPION-OAm attraction to the hydrophobic SLNP core was likely limited due to lipid surfactants coating SPIONs-OAm, creating a second hydrophilic "shell" to make SPIONs-OAm water soluble, and/or insufficient SPION coating/polymer interaction.

When synthesizing SLNPs according to the protocol detailed in section 2.1.3, the hydrophobic layer and hydrophilic layers are sonicated together and thus all reagents are mixed at one time (Ill. 4A). This can present an opportunity for SPIONs-OAm to interact with additional lipid surfactants, which can create a bilayer around each particle, reduce the hydrophobicity of SPIONs-OAm, and limit the ability of SPIONs-OAm to stay in the SLNP core (Ill. 4B). Therefore, SPIONs-OAm may migrate to the hydrophilic layer during synthesis due to their interactions with lipid surfactants.

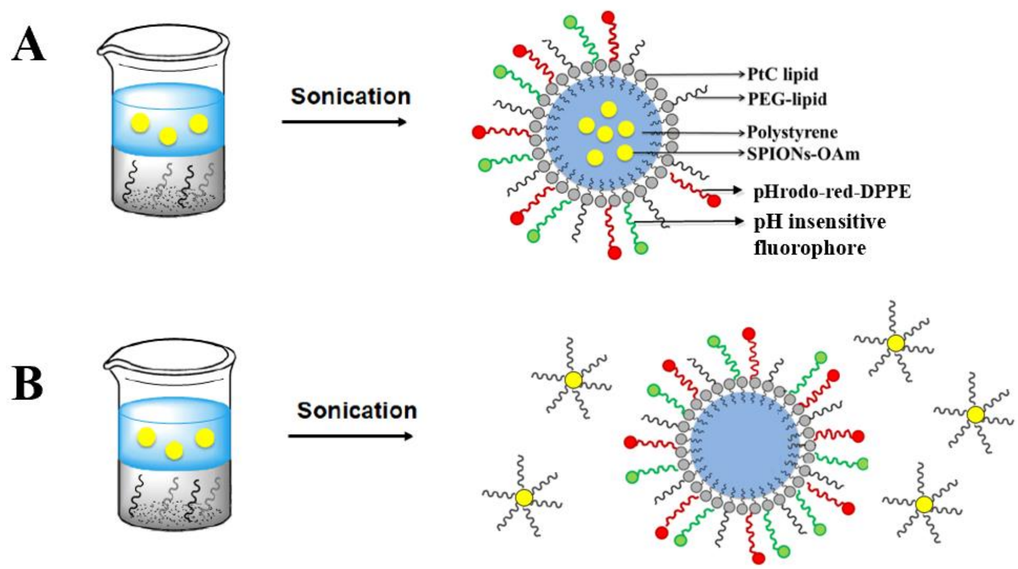

Illustration 4: Sonication of hydrophobic and hydrophilic layers of SLNP formulation can introduce SPION-OAm-surfactant interaction that reduces SPION-OAm incorporation into SLNP core.

A simple test was conducted to determine SPIONs-OAm and SPION-OA affinity for the hydrophilic phase of SLNP. SPIONs-OAm were sonicated in the hydrophobic layer of SLNPs (0.5 mL chloroform, 3 mL toluene, 0.1 mL OAm) or toluene at 6 mg/mL for 5 minutes and gently mixed with the hydrophilic layer (0.34 mg DPSE-PEG-FITC or DPSE-PEG, 0.74 mg PtC in 4% ethanol) at a 1:2 ratio. Similarly, SPIONs-OA were sonicated in chloroform at 3 mg/mL for 5 minutes and gently mixed with the hydrophilic layer at a 1:2 ratio. Samples were imaged with a phone camera before and 2 hours after gently mixing the hydrophobic and hydrophilic components.

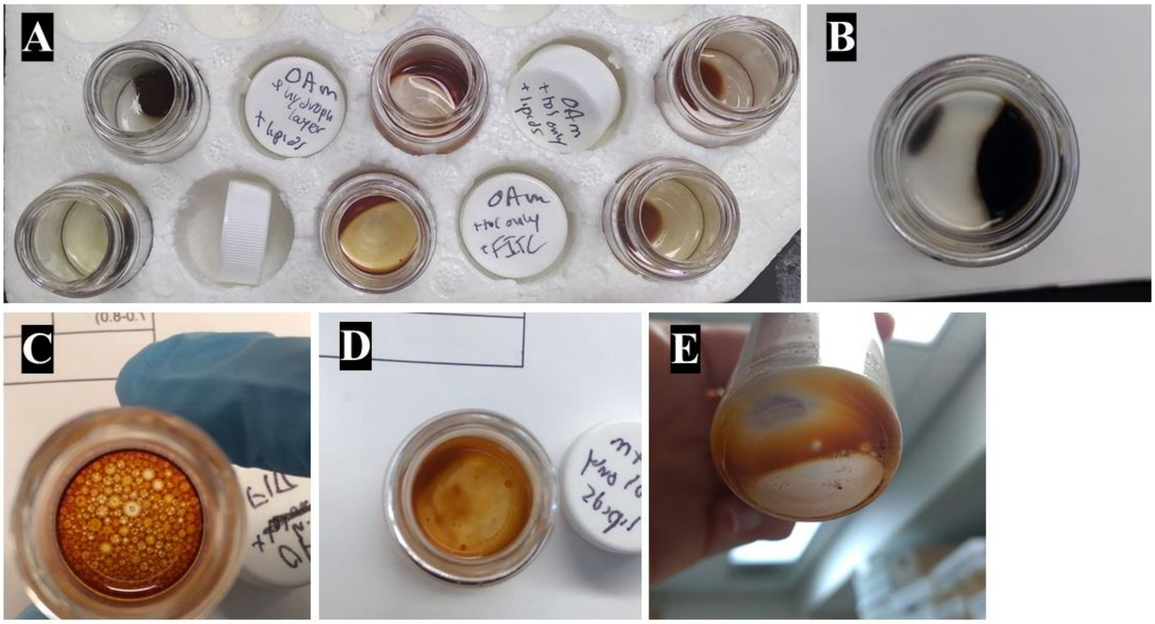

Figure 29: SPION-OA and SPION-OAm were dispersed in chloroform and toluene, respectively, and then gently mixed with hydrophilic lipid layer in 4% ethanol in DI water. A) Samples before mixing. Left to right: SPIONs-OA in chloroform with hydrophilic lipids, SPIONs-OAm in SLNP hydrophobic layer (section 2.1.3) with hydrophilic lipids, SPIONs-OAm in toluene with FITC-labeled hydrophilic lipids. B) SPIONs-OA in chloroform with hydrophilic lipids after mixing. C) SPIONs-OAm in hydrophobic layer with hydrophilic lipids after mixing. D) SPIONs-OAm in toluene with hydrophilic lipids (and FITC) after mixing. E) SPION-OAm precipitation and gravitational accumulation in prepared hydrophobic layer of SLNPs.

	Components	**Fig. 29B**	**Fig. 29C**	**Fig. 29D/E**
Hydrophobic	SPIONs-OA	✓		
	SPIONs-OAm		✓	✓
	Toluene		✓	✓
	Chloroform	✓	✓	
	OAm		✓	
Hydrophilic	Lipids	✓	✓	✓

Table 11: Hydrophobic and hydrophilic components used to test SPION-lipid surfactant interaction for three samples imaged in Fig. 29.

SPIONs-OA in chloroform remained separate from the lipid layer, indicating very limited interaction between the hydrophobic and hydrophilic components (Fig. 29B). However, SPIONs-OAm in the hydrophobic SLNP layer and toluene both displayed increased interaction at the hydrophobic/hydrophilic layer interface, creating a more mixed sample (Fig. 29C and D). Additionally, SPIONs-OAm precipitated out of the hydrophobic solvent it had been dispersed in, suggesting low OAm coating efficacy and poor dispersion. Based on this simple test, SPIONs-OAm interact with the hydrophobic-hydrophilic interface more than SPIONs-OA. This suggests oleic acid may be a better SPION coating as it is less susceptible to interacting with hydrophilic components during SLNP synthesis, thus keeping SPIONs hydrophobic and promoting their incorporation in the SLNP core.

Incorporation of SPIONs in the SLNP core was also explored by formulating simpler SLNPs. Polystyrene nanoparticles (PS-NPs) without PEG- and fluorophore-lipids were synthesized according to section 2.1.4 as a simpler version of SLNPs (Fig. 30). By examining simpler SLNP structures, sequential synthesis methods can be explored where SPIONs are first encapsulated by PtC shell and PEG- and fluorophore-lipids are subsequently added to reduce SPION-lipid surfactant interaction. Hydrodynamic diameter and zeta potential were collected for all batches of PS-NPs made, and results indicate SPIONs-OA (with added OA) are stable and negatively charged at the slipping plane and OAm addition increases zeta potential (Tbl. 12). Negative zeta potential > 30 mV in magnitude indicates stable particles and likely less cytotoxic particles. For the remainder of the thesis, SPIONs-OA are used due to their lower potential cytotoxic effects.

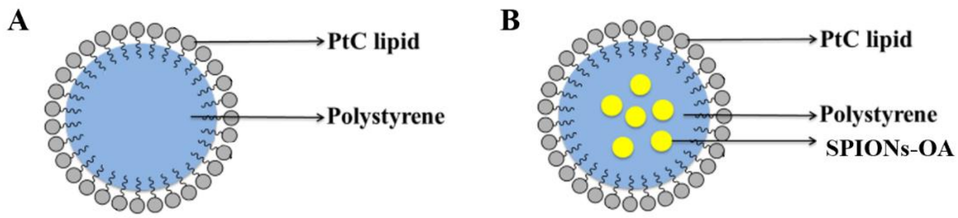

Fig. 30: Schematic of simple PtC-shelled, PS core NPs. A) No SPIONs are incorporated, B) SPIONs-OA are incorporated into SLNP core. Additional OAm or OA was added to certain batches to improve dispersion of SPIONs and formation of PS-NPs.

NP Type	D_h (nm)	pdi	ZP (mV)
PS-NPs (no OAm)	200.7± 4.6	0.149 ± 0.030	+45.95 ± 4.27
PS-NPs (+ OAm)	226.1± 5.4	0.207 ± 0.043	+57.60 ± 2.49
PS-NPs/SPIONs-OA + OAm	309.7±43.0	0.156 ± 0.131	+46.53 ± 2.24
PS-NPs/SPIONs-OA + OA	183.7±3.5	0.195 ± 0.011	-35.65 ± 3.99

Table 12: Hydrodynamic diameter (nm) and zeta potential of PS-NP batches.

SPION-free PS-NPs were synthesized according to section 2.1.4.ii. A small volume of OAm was added to promote nanoparticle formation (Mourdikoudis & Liz-Marzan). TEM images were captured to verify PS-NP morphology. PS-NPs with OAm demonstrated a similar round morphology to SLNPs in Fig. 27, indicating successful synthesis of PS core/PtC shell NPs.

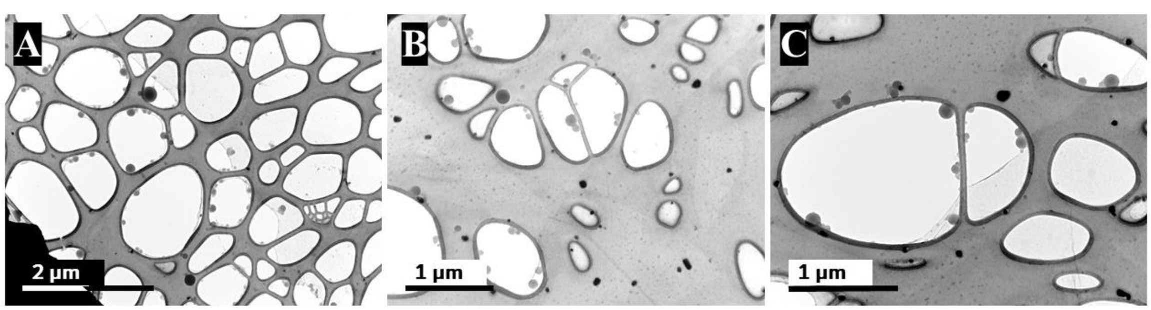

Figure 31: TEM images of PS NPs with added OAm synthesized according to section 2.1.4.

After confirming PS-NPs produce viable NPs, PS-NPs with SPIONs-OA were synthesized according to section 2.1.4.iii and imaged with TEM. For both formulations (added OAm or added OA), free SPION-OA concentration is lower than SLNPs in Figs.

27 and 29. SPIONs in the PS/SPIONs-OA with added OAm appear to have less free SPIONs present and some incorporation of SPIONs within PS-NP cores. SPIONs in the PS/SPIONs-OA with added OA batch appear to aggregate just under or near the surface of nanoparticles, potentially indicating an improved SPION coating/polymer pair and/or reduced hydrophilic surfactant interaction. These images are consistent with previous literature documenting TEM images of successful SPION-OA incorporation into polymeric NPs (Sommertune et al.). However, TEM images cannot distinguish between internalized and free SPIONs, and these results should be validated with quantitative analysis.

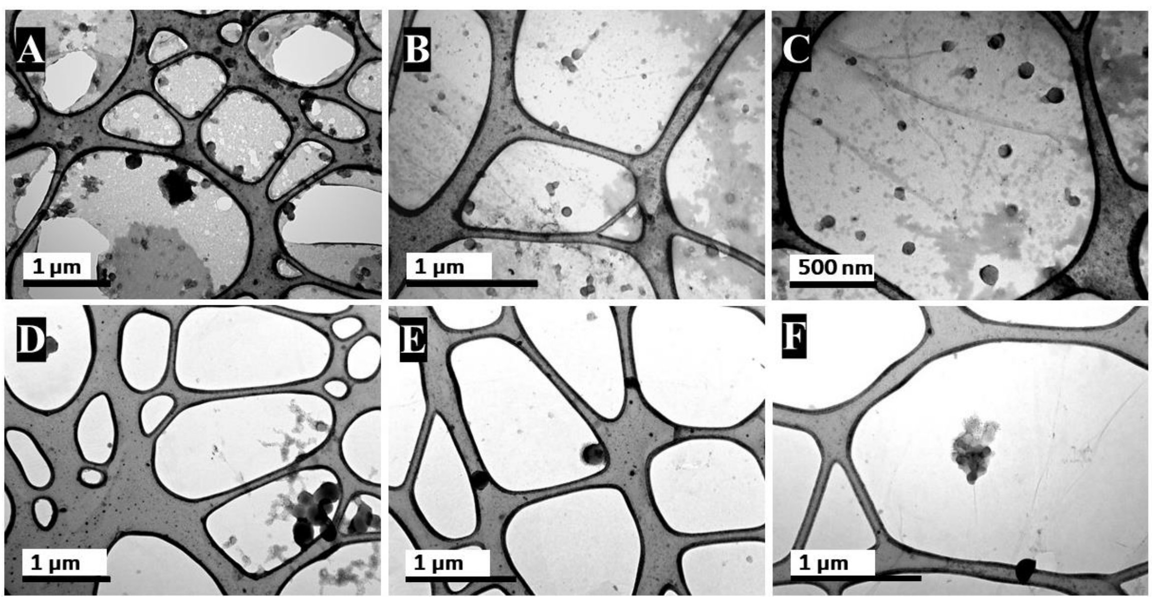

Figure 32: TEM images of PS/SPION-OA NPs synthesized using additional A-C) OA or D-F) OAm.

Based on these findings, OA is a better SPION coating than OAm due to its negative charge and reduced interaction with hydrophilic surfactants of the current SLNP formulation. Future work should focus on using SPIONs-OA instead of SPIONs-OAm as resulting particles have improved SPION incorporation and a negative zeta potential, likely reducing a cause of SLNP cytotoxicity seen in this work. Further optimization of the SPION/lipid surfactant content to maximize SPION incorporation into SLNP core, reduce free SPION content, and produce fewer non-magnetic SLNPs should be completed in future work.

CHAPTER 4:

FUTURE WORK

4.1 SPION and SLNP Characterization Techniques

This study focused on modifying SLNP formulations for improved SLNP tracking batch consistency, and improved cell-SLNP interactions, with goals of minimizing cytotoxicity and maximizing phagocytosis. Thorough characterization of both SPIONs and SLNPs is essential for determining particle stability, morphology, concentration, and other properties. Characterization techniques used in this thesis provided information about each modified formulation, establishing standards for future SLNP syntheses and cell studies.

Method	Function	Pro(s)	Con(s)
DLS	Determine hydrodynamic diameter of colloidal dispersion	Simple method of determining size and stability	Estimate of aggregation size, not single particle size
ZP	Determine electrokinetic potential of colloidal dispersion	Simple method of determining stability and charge at solid/liquid interface	Cuvette/electrode fit; solvent pH influence on charge
TEM	Capture detailed images of SLNPs and SPIONs	Determine single particle size and morphology of both colloids; Can visually separate SPIONs and SLNPs	Cannot distinguish when SPIONs are inside or outside SLNPs (no Z stack available)
Fluorescent microscopy	Capture fluorescent images of SLNPs	Confirm fluorescence can be activated via pH-dependent conditions; Determine particle morphology and size	Low resolution; Brownian motion of SLNPs can make imaging difficult
STED	Capture high resolution images of SLNPs	Super-resolution; Confirm fluorescence can be activated via pH-dependent conditions; Determine particle morphology and size	Brownian motion; Fluorophore selection

Table 13: Pros and cons of various NP characterization methods.

DLS was useful in collecting estimated hydrodynamic diameter of SPIONs and SLNPs. SPIONs-OAm were found to be relatively stable over 2 hours, with aggregate hydrodynamic diameter changing by 2-3 SPIONs at most. Many SLNP samples were characterized with DLS, including different AF488-PE:lipid molar ratio formulations, different purification techniques, sterilization techniques, short and long term stability, and different fluorophore combinations. DLS measurements were used primarily as an estimate of NP aggregate size and stability, though data for the sample formulation often fluctuated batch-to-batch. Future work should include zeta potential to supplement stability assessments using DLS. Zeta potential sign and magnitude provides insight regarding potential cytotoxicity and NP stability. Additional analysis of PS-NP particles, which only contain PtC shells and PS cores (in chloroform), should be further characterized to determine the source of positive ZP measurements seen in this study.

Future short and long-term SLNP stability studies would benefit from also adding more time points, collecting both hydrodynamic diameter and zeta potential data, and focusing on phenol-free, HI-FBS-containing RPMI 1640 media (cell incubation condition) and pH balanced DI water as storage solvents (Meisel et al.). Lyophilization of SLNPs can also provide a viable storage alternative and should be assessed in future storage and stability assays (section A.1). Additionally, future work should consider pH of storage solvent and influence on zeta potential of SPION and SLNP samples.

TEM provided high magnification imaging of SPION and SLNP samples, allowing for single particle sizing and qualitative morphology exploration. SPION and SLNP morphology and size remained consistent for all batches imaged: 7-8 nm and 100 ± 35 nm in single particle diameter, respectively. Because TEM was able to distinguish between the two types of particles, we discovered substantial free SPION content present in SLNP samples imaged with TEM, an issue with SPION incorporation not previously known. However, TEM is unable to distinguish between intra-SLNP and surface bound SPIONs, which limits our ability to qualitatively assess SPION incorporation into the SLNP core. Free SPION content varied between samples depending on purification method used and particle composition, with SPION-OA containing PS-NPs demonstrating the lowest free SPIONs present. In the future, TEM should be used to quantify single particle diameter and qualitatively assess free SPION content in SLNP samples. These observations should be supplemented with quantitative assessments of SPION encapsulation by thermogravimetric analysis (TGA) and/or atomic absorption spectrometry (AAS) (Hamzian et al., Omwoyo et al.).

Fluorescence and STED microscopy provided useful information regarding particle fluorescence and morphology. pH-dependent and pH-independent fluorescence was confirmed with fluorescence microscopy, and single particle diameter was calculated to be 114.4 ± 75.8 nm. STED microscopy allowed for super-resolution imaging of SLNPs, revealing organization of lipid-conjugated fluorophores in the lipid shell of each SLNP. Future work with these techniques should be limited to confirming expected fluorescence of SLNPs prior to and after incubation with cells. Implementing solid mounting media to reduce motion of SLNPs in solution can simplify imaging. Alternatively, STED microscopy can be used with mobile samples to track Brownian motion of SLNPs or even phagocytosis of SLNPs by J774 cells.

4.2 SLNP Synthesis, Purification, and Preparation for Cell Studies

This thesis work established the importance of qualitative assessment of free SPION content. TEM images revealed significant amounts of free SPION content outside SLNs, an issue not previously known or explored. As discussed in section 3.5, free SPIONs-OAm were likely present due to insufficient SLNP washing and purification and/or low SPION-OAm incorporation into SLNP core. Centrifugal filtration removed free SPIONs-OAm from SLNP samples better than dialysis, though free SPIONs-OAm were still present (Bartoš et al.). Duration, yield, and quality of SLNP synthesis and purification need to be balanced to optimize a scalable protocol. Further investigation into SLNP purification methods, potentially through a combination of centrifugation and dialysis techniques, must be examined and implemented to remove free SPIONs from SLNP samples (Mihaila et al.). If purification techniques are lengthy timewise, they should be executed in a cold room (4 ºC) to maintain SLNP stability. Additionally, molecular weight cut off should be examined to ensure only SLNPs are retained post-purification (Fadel et al.). Low SPIONs-OAm incorporation in SLNP cores could be due to excessive SPIONs-OAm, excessive lipid surfactant, or a SPION-coating/polymer pair that is not preferred (Sommertune et al.). Tailoring SPION/surfactant ratio to minimize excess SPIONs and SPION-surfactant interaction due to high lipid content would improve SPION incorporation in SLNP cores. Additionally, utilizing OA as a SPION coating instead of OAm may also reduce SPION-surfactant interactions as seen in Fig. 29 and negative, less cytotoxic zeta potential in Table 12. Other polymers (such as poly(vinyl pyridine), poly(methyl methacrylate), poly(lactic acid), and poly(caprolactone)) may further improve

SPION-OA incorporation into SLNP core (Bartoš et al., Horechyy et al., Sommertune et al.). Future work must focus on developing an optimized SLNP formulation and purification method to maximize SPION incorporation in SLNP core (and thus, maximize magnetic strength), reduce free SPION content, and scale reproducibly. Future studies must prioritize the assessment of SPION encapsulation both qualitatively through TEM and quantitatively via TGA or AAS.

TEM also revealed morphological differences in magnetic SLNPs and non-magnetic SLNPs. Further characterization (DLS, ZP) can be completed to determine other differences in morphologies or NP properties exist between magnetic and non-magnetic SLNPs. Though optimizing the formulation using aforementioned strategies can potentially maximize SPION incorporation into SLNP core, increasing the magnetic population of SLNPs should be prioritized. Additionally, separating any non-magnetic SLNPs from magnetic SLNPs should be consistently implemented to reduce cell exposure to non-magnetic particles and should continue to be used as standard practice in future phagocytosis and magnetic isolation assays.

Ultimately, this work revised design criteria and solutions established by Dr. Wong, Dr. Zhong, and Dr. Yu in Table 1 (Yu). Importantly, the addition of pH-insensitive fluorophore, maximizing SPION encapsulation, and zeta potential criteria were added due to findings presented in this work. This revised table of SLNP design criteria should be used as the standard for the future SLNP formulations and guide revisions based on expected characterization and cell-SLNP interactions.

	Design Criteria	Design Solution
SLNP core	Highly magnetically responsive compared to existing magnetic beads	Clustered SPIONs (Yu) Maximize encapsulation of clustered SPIONs
SLNP coating	Prevent aggregation and protein binding Efficiently target NIMPAB cells in < 6 hours	PEG lipid PtC-lipid coating
SLNP stability	Stable for 3 days during cell experiments	Polymer in core to provide structural integrity
SLNP size	Does not trigger non-specific endocytosis	Size should be ≥ 200nm (Vo et al., Yameen et al.)
Verify targeting abilities	Track location of SLNPs using fluorescence	pHrodo-red marker pH insensitive (AF488 or FITC) marker
SLNP ZP	Reduce cytotoxicity Prevent aggregation	Negative ZP with absolute magnitude > 10 mV Oleic acid coating/surfactant

Table 14: Revised SLNP criteria and potential solutions. Updated from Table 1.

4.3 SLNP Cytotoxicity Studies

An *in vitro* model was designed to test iterations of SLNP formulations using a phagocytosing monocyte cell line. We demonstrated limited phagocytosis of SLNPs by J774 cells in Figs. 23 and 24, but surprisingly, MTT and FACS revealed SLNPs were very cytotoxic at concentrations as low as 20 ug/mL. Positive zeta potential values and mass concentration of SLNPs added to cells were explored as potential cause of cytotoxicity. Oleylamine, with a pKa of 10.7, likely contributed to positive zeta potential values of high magnitude, especially with excess free SPIONs-OAm present in SLNP samples (Fahmi & Chang, Kanicky & Shah). Validation of SPIONs-OAm cytotoxicity should be examined to confirm this hypothesis. Comparative cytotoxicity studies should be conducted with SPIONs-OA based PS-NPs and/or lipid nanoparticles to confirm NPs with negative zeta potential and improved SPION incorporation are less cytotoxic than the original SLNP formulation.

FACS studies should also be repeated to confirm cell viability and SLNP uptake observed in this thesis. Unfixed cell samples should be used to limit pHrodo-red fluorescence reversal. Additionally, cell viability markers should be added to distinguish live and dead cells more easily during data collection and analysis. Previous literature has noted autofluorescence of trypan blue can be detected at 585-600 nm in fixed cell samples, potentially disrupting fluorescence readout. This autofluorescence should be taken into consideration before using trypan blue-mediated quenching of extracellular fluorophores and cell fixing in quantification assays like FACS (Shilova et al.). Obtaining FACS results for SLNP phagocytosis studies was challenging, as cytotoxicity was high and multiple populations with abnormal morphologies were present. J774 cells are semi-adherent, meaning the cell line has both adherent (majority) and suspension (minority) cells present. It was challenging to identify which population of cells we needed to further analyze, and it is possible that due to the different morphologies of adherent and suspension cells, there were multiple distinct cell-SLNP interactions. Future studies can be simplified by only studying adherent J774 cell interactions with SLNPs or switching to an alternative adherent monocyte or macrophage cell line.

To investigate the optimal SLNP-to-cell ratio and reduce potential high concentration-induced cytotoxicity, mass concentration curves were established and standardized for both centrifugation and dialysis purification techniques. Previous work calculated number concentration of SLNPs with Nanoparticle Tracking Analysis, adding

SLNPs to cells in a number ratio (Yu). Establishing a relationship between mass concentration and number concentration of SLNPs (or a molar concentration) would allow for more reproducible cell assays regardless of equipment access and reduce potential concentration-related cytotoxicity (Shang & Gao). Using a combination of TEM to determine single particle size, Small Angle X-ray Scattering (SAXS) to measure nanoscale densities, DLS to estimate aggregate size, absorbance to estimate mass, and subsequent elemental analysis, SLNP samples can be better quantified by weight concentration (Toufanian et al.). These SLNP concentrations should be used to replicate previous cytotoxicity studies with the same and lower concentrations (particularly less than 20 ug/mL).

Though not explored, insufficient sterilization may also impact SLNP cytotoxicity. UV radiation was used as an alternative sterilization technique after unsuccessful sterilization using 0.45 μm filters (Tapia-Guerrero, Bernal-Chavez et al.). Future studies should be completed to validate changes in SLNP size and zeta potential after UV radiation, as well as determining optimal exposure time to reduce SLNP cytotoxicity. Additionally, UV light sterilization was conducted with a biosafety cabinet, which is difficult to control and evaluate the intensity of UV exposure. Using a consistent source of UV light can better standardize the SLNP sterilization procedure.

4.4 Validating PtC-specific Phagocytosis of SLNPs

The long-term goal of isolating NIMPAB cells with magnetic SLNPs is challenging to test *in vitro* as the target cell type is rare and difficult to study. Developing a model with non-discriminating monocyte cell type like J774A.1 monocyte cells allows for simpler assessment of cell-SLNP interactions while the SLNP formulation and related procedures are still being manipulated. This model should continue to be used and developed to optimize the SLNP formulation. Once cytotoxicity is manageable and phagocytosis of SLNPs is sufficient, magnetic isolation steps should be executed with the *in vitro* model to assess efficacy of SLNP-mediated phagocytotic cell enrichment. Inclusion of a non-phagocytosing control population to mimic the target rare cell population *in vitro* may also help iterate and improve upon the SLNP formulation (section A.2). Once the SLNP formulation has been finalized, *ex vivo* studies using mouse peritoneal cavity washout cells, containing both phagocytes and lymphocytes, must be conducted to verify discriminatory phagocytosis of SLNPs by NIMPAB cells (Yu).

4.5 Summary

Overall, future investigations should prioritize scalable synthesis of SPION-incorporating SLNPs using methods and suggestions outlined in this thesis work as the starting point. Rigorous characterization of SLNP formulations using techniques detailed in Table 13 and others discussed in this work should drive changes to NP synthesis, formulation, and cell assay preparation. Additionally, observed (and undesired) cell-SLNP interactions should influence future changes made to the SLNP formulation. The characterization techniques and *in vitro* model described in this thesis should be used to assess scalability and efficacy of SLNP batches and to continue tailoring the SLNP formulation for the long-term goal of NIMPAB cell enrichment.

CHAPTER 5:

CONCLUSION

In this thesis work, we aimed to optimize a magnetic SLNP formulation designed to isolate NIMPAB cells and develop an experimental *in vitro* model to assess cell-SLNP interactions. We began by modifying SLNP formulations with pH-insensitive fluorophore(s) for improved location tracking, verifying fluorescence output, observing SLNP morphology, and determining particle size with multiple microscopy techniques. We characterized SLNP formulation size, stability, and charge using hydrodynamic diameter and ZP, noting changes in these parameters over time, in different storage solvents, at different storage temperatures, and after different sterilization techniques. An *in vitro* model using J774 monocyte cells as our interim phagocytosing target cell type was designed to examine cell-SLNP interactions, aiming to minimize cytotoxicity and maximize phagocytosis. Cytotoxicity and phagocytosis assays demonstrated current SLNP formulations could be phagocytosed by J774 cells but killed many cells in each study. These results were used to assess flaws in the current SLNP formulation, identifying high free SPION-OAm content in SLNP samples likely due to an excess of SPIONs-OAm in the formulation and ineffective incorporation of SPIONs in SLNP core. We returned to the SLNP formulation, synthesized simplified particles, and exchanged SPIONs-OAs for SPIONs-OA. These changes improved SPION incorporation in SLNP core and produced particles with a negative zeta potential, hypothesized to reduced cytotoxic effects. Though only one round of cytotoxicity and phagocytosis assays was executed in this work, we obtained significant insight from the results to influence design criteria and essential characterization techniques for the next SLNP formulation. Ultimately, this thesis established a workflow to synthesize, characterize, and assess cell-SLNP interaction to optimize SLNP formulation for the long-term goal of isolating NIMPAB cells for immuno-therapeutic study (Ill. 5). Future work should use this experimental framework to continue iterating and improving the current SLNP formulation.

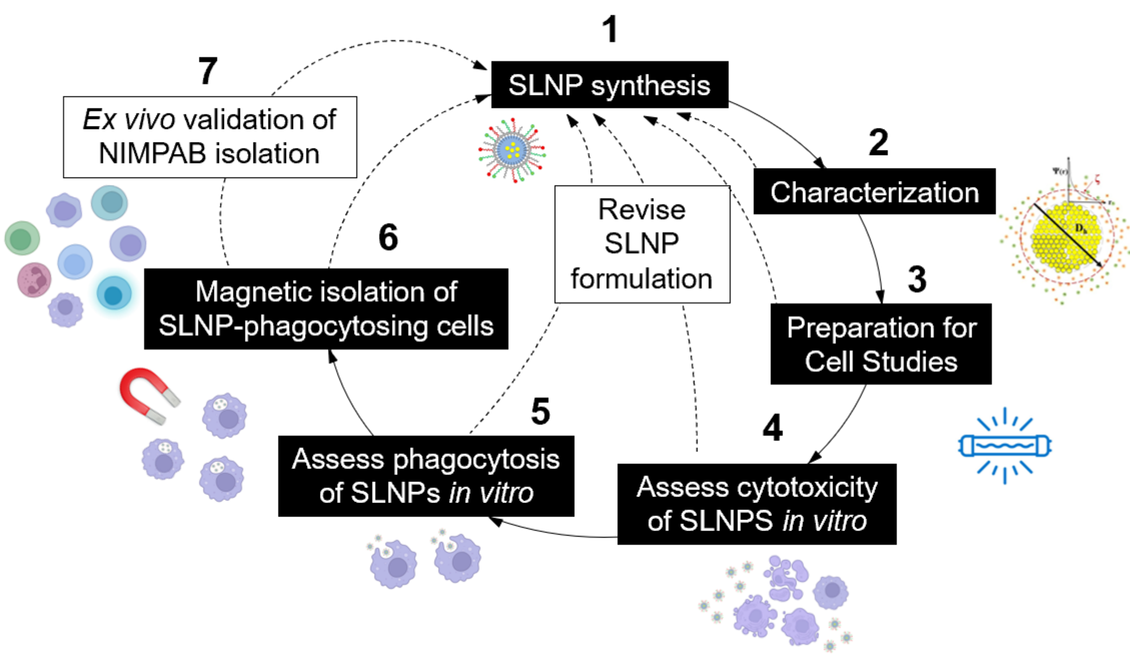

Illustration 5: Cycle of optimization. An established experimental workflow established to test, refine, and optimize SLNP formulations and characterization methods to improve cell-SLNP interaction with *in vitro* model.

APPENDIX

A.1 Lyophilization of SLNPs for Storage

Lyophilization is an established method of both storing and delivering NPs and has not yet been rigorously explored for this project. To lyophilize SLNPs for storage, known volumes of SLNPs were diluted 1:1 with 4% sucrose (Sigma Life Sciences, CAS 57-50-1, Burlington, MA) in DI water (pH 7.5–8.0) to prevent particle aggregation. SLNP/sucrose volumes were transferred to Eppendorf tubes covered with Kim wipes secured to the tube by an elastic band and were submerged in liquid nitrogen to flash freeze. Samples were lyophilized overnight and dialyzed for 24 hours to remove sucrose according to section 2.1.3.ii.

A.2 Cytochalasin D Cytotoxicity

A.2.1 Motivation and Background

While developing an *in vitro* model, we discussed using a phagocytosis-inhibiting agent to create a non-phagocytosing J774 population. This control cell population would be used to dilute the natively phagocytosing J774 cells to mimic cellular concentration of target NIMPAB cells *in vivo*, thus creating an *in vitro* model of a rare cell population to validate SLNP-mediated magnetic isolation. Cytochalasin D is an actin polymerization inhibitor that has demonstrated >90% reduction of phagocytosis in mouse microglial cells (Ribes et al.). For our rare cell model, we decided to explore cytochalasin D-mediated phagocytosis inhibition to create a non-phagocytosing control cell population. Both the dose required and time until phagocytotic behavior recurs need to be determined to establish a non-phagocytosing control population.

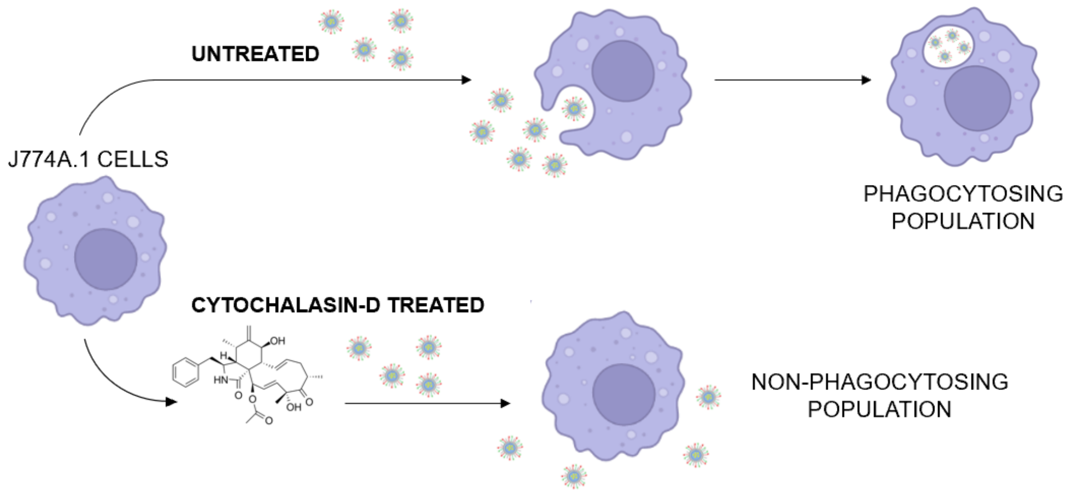

Illustration A1: Schematic of developing cytochalasin D-treated, non-phagocytosing J774A.1 cell population *in vitro*.

A.2.2 Methods

A dose-dependent cytochalasin D study was conducted by Dr. Xuemei Zhong at Antagen Biosciences, Inc. to determine the optimal concentration of cytochalasin D to add to J774 cells to minimize cell death. Prior studies use 10 µM of cytochalasin D, an actin polymerization inhibitor, to prevent phagocytosis in primary mouse microglial cells, though lower concentrations have induced cytotoxicity (Ribes et al., Wakatsuki et al.). CellTox™ Green Cytotoxicity Assay (Promega, Cat#G8741, Madison, WI) was purchased and used according to manufacturer's protocol. J774 cells were cultured 2-4 days prior to the experiment and then plated in a black/clear bottom TC-treated 96 well-plate at $5*10^3$ and $1*10^4$ cells/well in 50 uL of R10 media (Gibco, Waltham, MA). Serial dilutions (1 µM to 0.001953 µM) of cytochalasin D (Sigma Aldrich, CAS 22144-77-0, St. Louis) were added in duplicate of both cell concentrations in 50 uL. Positive control (lysed cells), negative control (PBS-treated viable cells), and vehicle control (cells treated highest concentration of DMSO in experimental wells) were plated in triplicate in 50 uL volumes Moisture control wells with 200 uL of PBS were also plated in edge wells. CellTox Green Reagent (2x) was added to a final volume of 200 uL in all wells according to manufacturer's protocol. The plate was imaged 15 minutes after the addition of CellTox Green Reagent using 485-510 excitation laser and 520-530 emission filter with Keyence All-in-One Fluorescent Microscope at Antagen Biosciences, Inc..

A.2.3 Results

Based on qualitative observations from 15-minute imaging in Figure A1, increased cytochalasin D concentration increases cytotoxicity. Unfortunately, quantitative fluorescence readout data was unable to be collected to verify this observation. Future work must include spectrometer readings to quantify fluorescence output as well as microscopy imaging. Additionally, Dr. Zhong indicated that CellTox green dye concentration can be reduced as 100 uL was more than sufficient. In the future, additional time points, especially the expected duration of SLNP phagocytosis (2- 6 hours) and full duration of the magnetic isolation experiment (24 hours), should be included to determine how long cytotoxic effects of cytochalasin D persist.

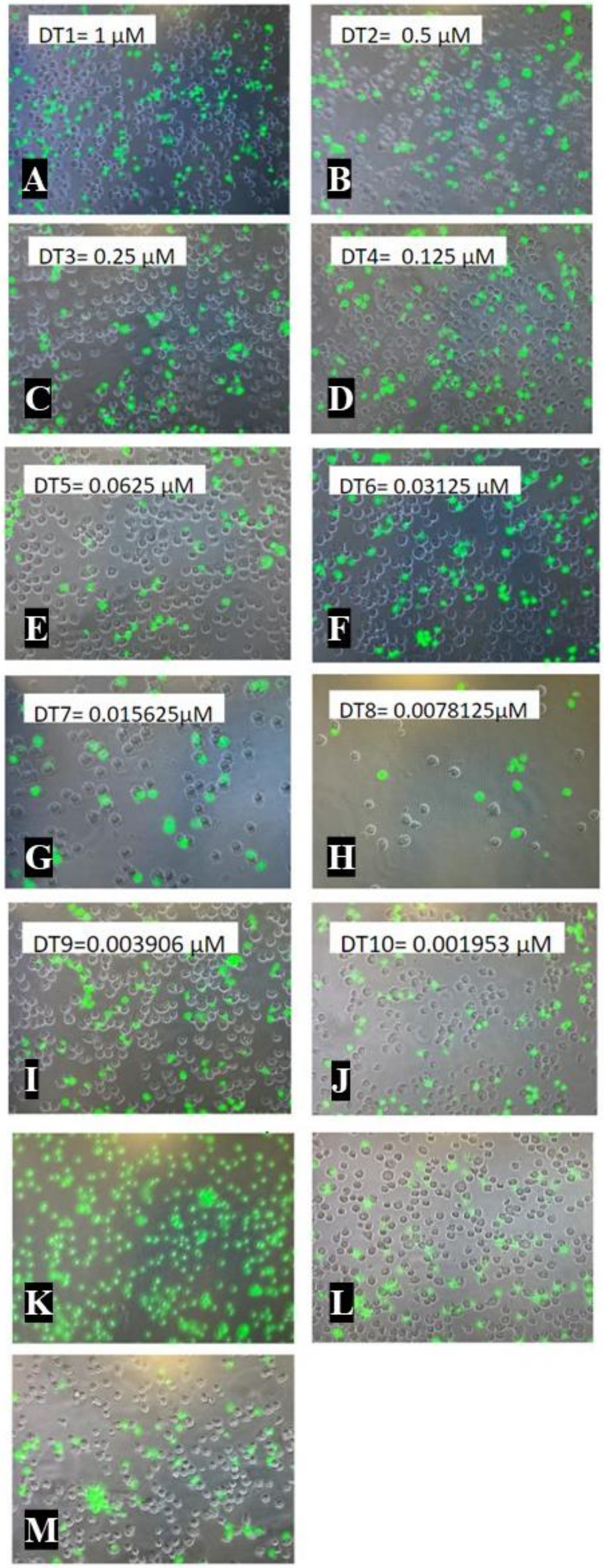

Figure A1: Dose-dependent cytotoxicity of cytochalasin D. J774 cells fluorescing green are not viable. A) 1 µm; B) 0.5 µm; C) 0.25 µm; D) 0.125 µm; E) 0.0625 µm; F) 0.03125 µm; G) 0.015625 µm; H) 0.0078125µm; I) 0.003906 µm; J) 0.001953 µm; K) lysed cells; L) vehicle control (DMSO); M) PBS-treated cells.

A.3 Additional Imaging of SLNPs

Additional fluorescent imaging of SLNPs contributed to fluorescent marker observation. Another successful batch of AF488/pHrodo-red labeled SLNPs is shown in Figure A2.

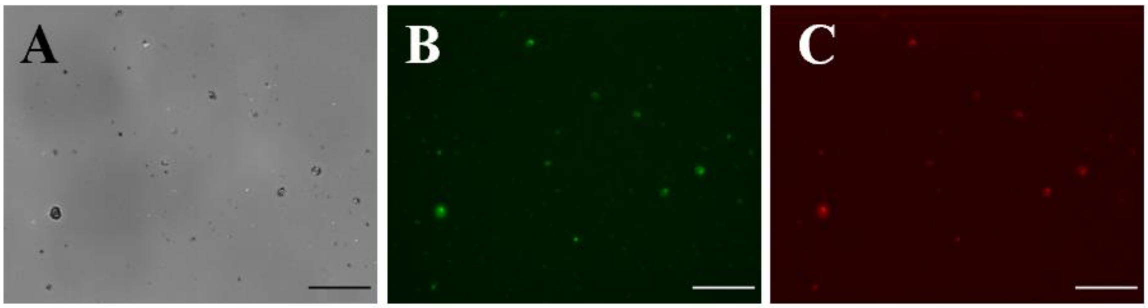

Figure A2: A) Brightfield and fluorescent microscopy using B) FITC cube/filter and C) TRITC cube/filter confirms pH-insensitive and pH-sensitive markers fluoresce as expected in acidic storage conditions. Scale bars: 5 μm.

Additional fluorescent imaging of cells incubated with SLNPs during a phagocytosis assay (section 3.4.2) demonstrate the lack of AF488 fluorescence and limited pHrodo-red fluorescence (Fig. A2). Most likely this sample used was a few weeks old, potentially contributing to weaker fluorescence output. These images, including Fig. 23, suggest that there may also be a variation in fluorescence intensity between particles that can affect how well they can be imaged. Using a fresher SLNP sample and/or potentially choosing a more robust fluorophore can improve reliability and increase intensity of fluorophore markers.

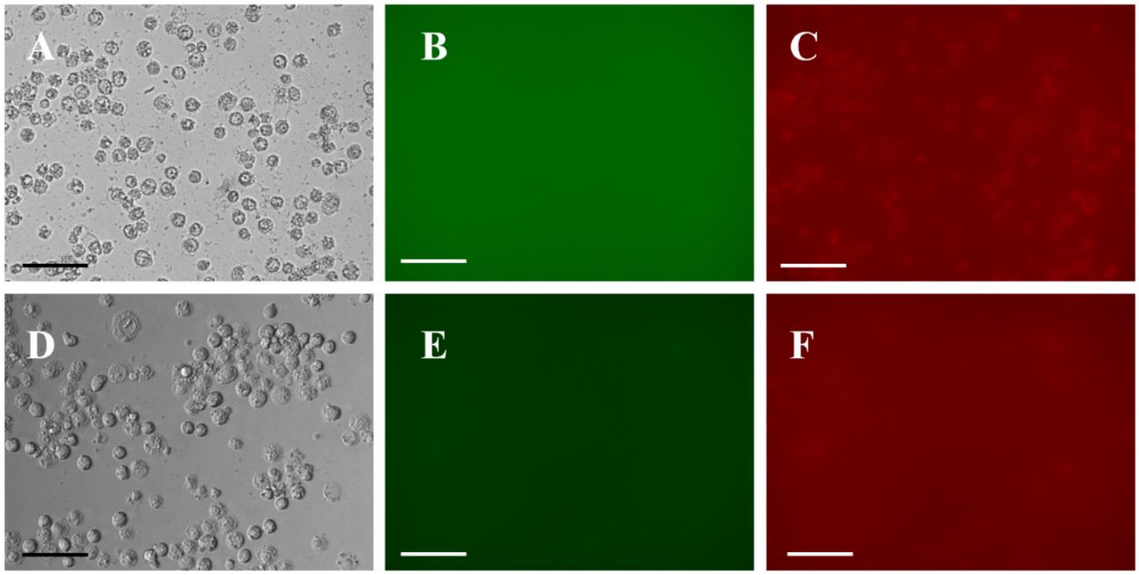

Figure A3: Fluorescent microscopy images of J774 cells incubated with SLNPs for 2 hours. A, D) Brightfield, B, E) FITC laser/ filter cube, and C, F) TRITC laser/ filter cube were used to detect cells and AF488/pHrodo-red fluorophore labeling. Fluorescence output was weak, indicating these particles were not labeled well or the fluorophores were weak.

BIBLIOGRAPHY

Arruebo, Manuel, et al. (2011). "Assessment of the Evolution of Cancer Treatment Therapies." C*ancers*, *3*(3), 3279–3330. PubMed Central, https://doi.org/10.3390/cancers3033279.

Adapted from *"Immune and Blood Cells"*, *"Eppendorf Tube (2/3 liquid, closed)"* and *"Metastasis"*, by BioRender.com (2022). Retrieved from https://app.biorender.com/illustrations

Alcantara, D., & Josephson, L. (2012). Chapter 11. Magnetic Nanoparticles for Application in Biomedical Sensing. *Frontiers of Nanoscience*, *4*, 269–289. https://doi.org/10.1016/B978-0-12-415769-9.00011-X

Baranov, D., Lynch, M. J., Curtis, A. C., Carollo, A. R., Douglass, C. R., Mateo-Tejada, A. M., & Jonas, D. M. (2019). Purification of Oleylamine for Materials Synthesis and Spectroscopic Diagnostics for trans Isomers. *Chemistry of Materials*, *31*(4), 1223–1230. https://doi.org/10.1021/acs.chemmater.8b04198

Bartoš, D., Wang, L., Anker, A. S., Rewers, M., Aalling-Frederiksen, O., Jensen, K. M. Ø., & Sørensen, T. J. (2021). *A Reproducible and Scalable Method for Producing Fluorescent Polystyrene Nanoparticles*. https://doi.org/10.26434/chemrxiv-2021-3blgm

Berg, E.G. Making antibodies minus the cells. (2017). *Chemical & Engineering News*, *95*(20). https://cen.acs.org/articles/95/i20aking-antibodies-minus-cells.html

Bernal-Chávez, S. A., Del Prado-Audelo, M. L., Caballero-Florán, I. H., Giraldo-Gomez, D. M., Figueroa-Gonzalez, G., Reyes-Hernandez, O. D., González-Del Carmen, M., González-Torres, M., Cortés, H., & Leyva-Gómez, G. (2021). Insights into Terminal Sterilization Processes of Nanoparticles for Biomedical Applications. *Molecules*, *26*(7), 2068. https://doi.org/10.3390/molecules26072068

Chan, J. M., Zhang, L., Yuet, K. P., Liao, G., Dhee, J.-W., Langer, R., & Farokhzad, O. C. (2009). PLGA-lecithin-PEG core-shell nanoparticles for controlled drug delivery. *Biomaterials*, *30*(8), 1627–1634. https://doi.org/10.1016/j.biomaterials.2008.12.013

Chen, A. K., Cheng, Z., Behlke, M. A., & Tsourkas, A. (2008). Assessing the Sensitivity of Commercially Available Fluorophores to the Intracellular Environment. *Analytical Chemistry*, *80*(19), 7437–7444. https://doi.org/10.1021/ac8011347

Chinen, A. B., Guan, C. M., Ko, C. H., & Mirkin, C. A. (2017). The Impact of Protein Corona Formation on the Macrophage Cellular Uptake and Biodistribution of Spherical Nucleic Acids. *Small*, *13*(16), 10.1002/smll.201603847. https://doi.org/10.1002/smll.201603847

Chiu, J. (2020). Development of a Lipid-Coated Calcium Phosphate Nanoparticle for SiRNA Delivery to the Brain (Ph.D. dissertation). Boston University Theses & Dissertations. https://open.bu.edu/handle/2144/39368

Christine Kemmer, G., Ammitzbøll Bogh, S., Urban, M., G. Palmgren, M., Vosch, T., Schiller, J., & Pomorski, T. G. (2015). Lipid-conjugated fluorescent pH sensors for monitoring pH changes in reconstituted membrane systems. *Analyst*, *140*(18), 6313–6320. https://doi.org/10.1039/C5AN01180A

Clogston, J. D., & Patri, A. K. (2011). Zeta potential measurement. *Methods in Molecular Biology*, *697*, 63–70. https://doi.org/10.1007/978-1-60327-198-1_6

Commonly Used Fluorochromes and Their Properties. (n.d.). University of Mississippi Medical Center. Retrieved June 13, 2022, from https://www.umc.edu/cancerinstitute/Cancer-Research/Core-Facilities/Flow Cytometry Core/Resources/Commonly-Used-Fluorochromes-and-Properties.html

Esfahani, K., Roudaia, L., Buhlaiga, N., Del Rincon, S. V., Papneja, N., & Miller, W. H. (2020). A review of cancer immunotherapy: From the past, to the present, to the future. *Current Oncology*, *27*(Suppl 2), S87–S97. https://doi.org/10.3747/co.27.5223

Fadel, M., Wyart, Y., & Moulin, P. (2020). An Efficient Method to Determine Membrane Molecular Weight Cut-Off Using Fluorescent Silica Nanoparticles. *Membranes*, *10*(10), 271. https://doi.org/10.3390/membranes10100271

Fröhlich, E. (2012). The role of surface charge in cellular uptake and cytotoxicity of medical nanoparticles. *International Journal of Nanomedicine*, *7*, 5577–5591. https://doi.org/10.2147/IJN.S36111

Gaspar, A. S., Santos, P. H. C., Borges, O., Costa, B. F. O., & Durães, L. (2019). Biocompatible and high-magnetically responsive iron oxide nanoparticles for protein loading. *Journal of Physics and Chemistry of Solids*, *134*, 273–285. https://doi.org/10.1016/j.jpcs.2019.06.016

Gill, K. K., Kaddoumi, A., & Nazzal, S. (2015). PEG-lipid micelles as drug carriers: Physiochemical attributes, formulation principles and biological implication. *Journal of Drug Targeting*, *23*(3), 222–231. https://doi.org/10.3109/1061186X.2014.997735

Hamzian, N., Hashemi, M., Ghorbani, M., Bahreyni Toosi, M. H., & Ramezani, M. (2017). Preparation, Optimization and Toxicity Evaluation of (SPION-PLGA) ±PEG Nanoparticles Loaded with Gemcitabine as a Multifunctional Nanoparticle for Therapeutic and Diagnostic Applications. *Iranian Journal of Pharmaceutical Research : IJPR*, *16*(1), 8–21.

Handbook of Media for Clinical Microbiology—2nd Edition—James W. (n.d.). Retrieved June 13, 2022, from https://www.routledge.com/Handbook-of-Media-for-Clinical-Microbiology/Snyder-Atlas/p/book/9780367453602

Herzenberg, L. A., Tung, J., Moore, W. A., Herzenberg, L. A., & Parks, D. R. (2006). Interpreting flow cytometry data: A guide for the perplexed. *Nature Immunology*, *7*(7), 681–685. https://doi.org/10.1038/ni0706-681

Horechyy, A., E. Zafeiropoulos, N., Nandan, B., Formanek, P., Simon, F., Kiriy, A., & Stamm, M. (2010). Highly ordered arrays of magnetic nanoparticles prepared via block copolymer assembly. *Journal of Materials Chemistry*, *20*(36), 7734–7741. https://doi.org/10.1039/C0JM01103G

Hybridoma Fusion Partners Cell Lines. (n.d.). Retrieved June 23, 2022, from https://www.sigmaaldrich.com/US/en/technical-documents/technical-article/cell-culture-and-cell-culture-analysis/mammalian-cell-culture/hybridoma-fusion

Kanicky, J.R. & Shah D.O. (2002). Effect of Degree, Type, and Position of Unsaturation on the pKa of Long-Chain Fatty Acids. *Journal of Colloid and Interface Science*, *256*(1), 201–207. https://doi.org/10.1006/jcis.2001.8009

Kim, S. K., & Cho, S. W. (2022). The Evasion Mechanisms of Cancer Immunity and Drug Intervention in the Tumor Microenvironment. *Frontiers in Pharmacology*, *13*. https://www.frontiersin.org/article/10.3389/fphar.2022.868695

Krøigård, Anne Bruun, et al. (2018). “Identification of Metastasis Driver Genes by Massive Parallel Sequencing of Successive Steps of Breast Cancer Progression.” *PLoS ONE*, *13*(1), e0189887. PubMed Central, https://doi.org/10.1371/journal.pone.0189887.

Lai, C.W., F.W. Low, M.F. Tai, S.B.A. Hamid. (2018). Iron oxide nanoparticles decorated oleic acid for high colloidal stability. *Advanced Polymer Technology*. https://doi.org/10.1002/adv.21829

Lee, B., Yoon, S., Lee, J. W., Kim, Y., Chang, J., Yun, J., Ro, J. C., Lee, J.-S., & Lee, J. H. (2020). Statistical Characterization of the Morphologies of Nanoparticles through Machine Learning Based Electron Microscopy Image Analysis. *ACS Nano*, *14*(12), 17125–17133. https://doi.org/10.1021/acsnano.0c06809

Lee, J., Kim, S., & Kim, S. (2008). Biochemical and Antibacterial Properties of Lysozyme Purified from the Viscera of Scallops (patinopecten Yessoensis). *Journal of Food Biochemistry*, *32*(4), 474–489. https://doi.org/10.1111/j.1745-4514.2008.00177.x

Limitations of TEM. (2018, January 3). News-Medical.Net. https://www.news-medical.net/life-sciences/Limitations-of-TEM.aspx

Lu, Y., Jiang, J., Park, S., Wang, D., Piao, L., & Kim, J. (2020). Wet-Spinning Fabrication of Flexible Conductive Composite Fibers from Silver Nanowires and Fibroin. *Bulletin of the Korean Chemical Society*, *41*(2), 162–169. https://doi.org/10.1002/bkcs.11945

Luangtana-anan, M., Limmatvapirat, S., Nunthanid, J., Chalongsuk, R., & Yamamoto, K. (2010). Polyethylene Glycol on Stability of Chitosan Microparticulate Carrier for Protein. *AAPS PharmSciTech*, *11*(3), 1376–1382. https://doi.org/10.1208/s12249-010-9512-y

Meisel, C. L., Bainbridge, P., Mitsouras, D., & Wong, J. Y. (2018). Targeted Nanoparticle Binding to Hydroxyapatite in a High Serum Environment for Early Detection of Heart Disease. *ACS Applied Nano Materials*, *1*(9), 4927–4939. https://doi.org/10.1021/acsanm.8b01099

Mihaila, R., Chang, S., Wei, A. T., Hu, Z. Y., Ruhela, D., Shadel, T. R., Duenwald, S., Payson, E., Cunningham, J. J., Kuklin, N., & Mathre, D. J. (2011). Lipid nanoparticle purification by spin centrifugation-dialysis (SCD): A facile and high-throughput approach for small scale preparation of siRNA-lipid complexes. *International Journal of Pharmaceutics*, *420*(1), 118–121. https://doi.org/10.1016/j.ijpharm.2011.08.017

Mourdikoudis, S., & Liz-Marzán, L. (2013). Oleylamine in Nanoparticle Synthesis. *Chemistry of Materials*, *25*. https://doi.org/10.1021/cm4000476

Müller, T., Schumann, C., & Kraegeloh, A. (2012). STED Microscopy and its Applications: New Insights into Cellular Processes on the Nanoscale. *ChemPhysChem*, *13*(8), 1986–2000. https://doi.org/10.1002/cphc.201100986

Omwoyo, W. N., Ogutu, B., Oloo, F., Swai, H., Kalombo, L., Melariri, P., Mahanga, G. M., & Gathirwa, J. W. (2014). Preparation, characterization, and optimization of primaquine-loaded solid lipid nanoparticles. *International Journal of Nanomedicine*, *9*, 3865–3874. https://doi.org/10.2147/IJN.S62630

PHrodo^{TM} Red Phagocytosis Particle Labeling Kit for Flow Cytometry. (n.d.). Retrieved June 13, 2022, from https://www.thermofisher.com/order/catalog/product/A10026

Potential Application of Oleylamine-encapsulated AgInS2-ZnS Quantum Dots for Cancer Cell Labeling—ScienceDirect. (n.d.). Retrieved June 13, 2022, from https://www.sciencedirect.com/science/article/pii/S187661961600019X

Ribes, S., Ebert, S., Regen, T., Agarwal, A., Tauber, S. C., Czesnik, D., Spreer, A., Bunkowski, S., Eiffert, H., Hanisch, U.-K., Hammerschmidt, S., & Nau, R. (2010). Toll-Like Receptor Stimulation Enhances Phagocytosis and Intracellular Killing of Nonencapsulated and Encapsulated Streptococcus pneumoniae by Murine Microglia. *Infection and Immunity*, *78*(2), 865–871. https://doi.org/10.1128/IAI.01110-09

Shang, J., & Gao, X. (2014). Nanoparticle Counting: Towards Accurate Determination of the Molar Concentration. *Chemical Society Reviews*, *43*(21), 7267–7278. https://doi.org/10.1039/c4cs00128a

Shao, X.-R., Wei, X.-Q., Song, X., Hao, L.-Y., Cai, X.-X., Zhang, Z.-R., Peng, Q., & Lin, Y.-F. (2015). Independent effect of polymeric nanoparticle zeta potential/surface charge, on their cytotoxicity and affinity to cells. *Cell Proliferation*, *48*(4), 465–474. https://doi.org/10.1111/cpr.12192

Sheth, T., Seshadri, S., Prileszky, T., & Helgeson, M. E. (2020). Multiple nanoemulsions. *Nature Reviews. Materials*, *5*(3), 214–228. https://doi.org/10.1038/s41578-019-0161-9

Shi, J., Kantoff, P. W., Wooster, R., & Farokhzad, O. C. (2017). Cancer nanomedicine: Progress, challenges and opportunities. *Nature Reviews. Cancer*, *17*(1), 20–37. https://doi.org/10.1038/nrc.2016.108

Shibad, V., Bootwala, A., Mao, C., Bader, H., Vo, H., Landesman-Bollag, E., Guo, C., Rubio, A., Near, R., Gao, W., Challa, S., Chukka, V., Gao, J., Kelly, A., Landesman, T., VanHelene, T., & Zhong, X. (2021). L2pB1 Cells Contribute to Tumor Growth Inhibition. *Frontiers in Immunology*, *12*, 3754. https://doi.org/10.3389/fimmu.2021.722451

Shilova, O. N., Shilov, E. S., & Deyev, S. M. (2017). The effect of trypan blue treatment on autofluorescence of fixed cells. *Cytometry Part A*, *91*(9), 917–925. https://doi.org/10.1002/cyto.a.23199

Sommertune, J., Sugunan, A., Ahniyaz, A., Bejhed, R. S., Sarwe, A., Johansson, C., Balceris, C., Ludwig, F., Posth, O., & Fornara, A. (2015). Polymer/Iron Oxide Nanoparticle Composites—A Straight Forward and Scalable Synthesis Approach. *International Journal of Molecular Sciences*, *16*(8), 19752–19768. https://doi.org/10.3390/ijms160819752

STED. (n.d.). Retrieved June 13, 2022, from https://abberior-instruments.com/knowledge/microscopy-tutorials/sted/

Stetefeld, J., McKenna, S. A., & Patel, T. R. (2016). Dynamic light scattering: A practical guide and applications in biomedical sciences. *Biophysical Reviews*, *8*(4), 409–427. https://doi.org/10.1007/s12551-016-0218-6

Stillwell, W. (Ed.). (2016). Front Matter. In *An Introduction to Biological Membranes (2nd Edition)* (p. iii). Elsevier. https://doi.org/10.1016/B978-0-444-63772-7.01001-0

Study of Protein Hydrodynamics with Light Scattering: Size and Charge of Lysozyme—Brookhaven Instruments. (n.d.). Retrieved June 23, 2022, from https://www.brookhaveninstruments.com/study-of-protein-hydrodynamics-with-light-scattering-size-and-charge-of-lysozyme/

Sukhanova, A., Bozrova, S., Sokolov, P., Berestovoy, M., Karaulov, A., & Nabiev, I. (2018). Dependence of Nanoparticle Toxicity on Their Physical and Chemical Properties. *Nanoscale Research Letters*, *13*, 44. https://doi.org/10.1186/s11671-018-2457-x

Sun, S. Zeng. H. (2002. Size-Controlled Synthesis of Magnetite Nanoparticles | *Journal of the American Chemical Society*, *124*(28), 8204–8205. Retrieved March 5, 2021, from https://pubs.acs.org/doi/10.1021/ja026501x

Tapia-Guerrero, Y. S., Del Prado-Audelo, M. L., Borbolla-Jiménez, F. V., Giraldo Gomez, D. M., García-Aguirre, I., Colín-Castro, C. A., Morales-González, J. A., Leyva-Gómez, G., & Magaña, J. J. (2020). Effect of UV and Gamma Irradiation Sterilization Processes in the Properties of Different Polymeric Nanoparticles for Biomedical Applications. *Materials*, *13*(5), 1090. https://doi.org/10.3390/ma13051090

Toufanian R, Zhong X, Kays J, Saeboe A, Dennis A. Correlating ZnSe Quantum Dot Absorption with Particle Size and Concentration. ChemRxiv. Cambridge: Cambridge Open Engage; 2021; This content is a preprint and has not been peer-reviewed.

Vo, H., Chiu, J., Allaimo, D., Mao, C., Wang, Y., Gong, Y., Ow, H., Porter, T., & Zhong, X. (2014). High fat diet deviates PtC-specific B1 B cell phagocytosis in obese mice. *Immunity, Inflammation and Disease*, *2*(4), 254–261. https://doi.org/10.1002/iid3.41

Wahajuddin, null, & Arora, S. (2012). Superparamagnetic iron oxide nanoparticles: Magnetic nanoplatforms as drug carriers. *International Journal of Nanomedicine*, *7*, 3445–3471. https://doi.org/10.2147/IJN.S30320

Wakatsuki, T., Schwab, B., Thompson, N. C., & Elson, E. L. (2001). Effects of cytochalasin D and latrunculin B on mechanical properties of cells. *Journal of Cell Science*, *114*(Pt 5), 1025–1036. https://doi.org/10.1242/jcs.114.5.1025

Weng, Jingwen & Tong, Henry & Chow, Shing. (2020). In Vitro Release Study of the Polymeric Drug Nanoparticles: Development and Validation of a Novel Method. *Pharmaceutics*, *12*, 732. 10.3390/pharmaceutics12080732.

Wesierska-Gadek, J., Schreiner, T., Maurer, M., Waringer, A., & Ranftler, C. (2007). Phenol red in the culture medium strongly affects the susceptibility of human MCF-7 cells to roscovitine. *Cellular & Molecular Biology Letters*, *12*(2), 280–293. https://doi.org/10.2478/s11658-007-0002-5

Wiogo, H. T. R., Lim, M., Bulmus, V., Yun, J., & Amal, R. (2011). Stabilization of magnetic iron oxide nanoparticles in biological media by fetal bovine serum (FBS). *Langmuir*, *27*(2), 843–850. https://doi.org/10.1021/la104278m

Wulandari, A. D., Sutriyo, S., & Rahmasari, R. (2022). Synthesis conditions and characterization of superparamagnetic iron oxide nanoparticles with oleic acid stabilizer. *Journal of Advanced Pharmaceutical Technology & Research*, *13*(2), 89–94. https://doi.org/10.4103/japtr.japtr_246_21

Xu, Z., Shen, C., Hou, Y., Gao, H., & Sun, S. (2009). Oleylamine as Both Reducing Agent and Stabilizer in a Facile Synthesis of Magnetite Nanoparticles. *Chemistry of Materials*, *21*(9), 1778–1780. https://doi.org/10.1021/cm802978z

Yameen, B., Choi, W. I., Vilos, C., Swami, A., Shi, J., & Farokhzad, O. C. (2014). Insight into nanoparticle cellular uptake and intracellular targeting. *Journal of Controlled Release*, *190*, 485–499. https://doi.org/10.1016/j.jconrel.2014.06.038

Yu, J. (2020). *Developing superparamagnetic nanoparticle (SPION) systems with tunable colloidal stability and magnetic properties* (Ph.D. dissertation). Boston University Theses & Dissertations. https://open.bu.edu/handle/2144/41041

Zanetti-Domingues, L. C., Tynan, C. J., Rolfe, D. J., Clarke, D. T., & Martin-Fernandez, M. (2013). Hydrophobic Fluorescent Probes Introduce Artifacts into Single Molecule Tracking Experiments Due to Non-Specific Binding. *PLoS ONE*, *8*(9), e74200. https://doi.org/10.1371/journal.pone.0074200

Zhong, Xuemei, et al. (2009). “A Novel Subpopulation of B-1 Cells Is Enriched with Autoreactivity in Normal and Lupus-Prone Mice.” *Arthritis & Rheumatism*, 60(12), 3734–3743. https://doi.org/10.1002/art.25015.

Zhong, Xuemei. Development of a Novel Cell-Based Immune Therapy Using Nanoparticles and Natural IgM-Producing Phagocytic B Cells. grantome.com, https://grantome.com/grant/NIH/R21-CA205415-01. Accessed 18 Feb. 2021.

CURRICULUM VITAE

[redacted]

[redacted]

[redacted]